JOHANNES GUTENBERG UNIVERSITY
MAINZ

DOCTORAL THESIS

Improving Ultracold Neutron Density and Storage: Applications to Neutron Lifetime and Electric Dipole Moment Experiments

Author:
Noah Gabriel
YAZDANDOOST
KHOSRAVI

Place of birth:
Wiesbaden,
Germany

A thesis submitted in fulfillment of the requirements for the degree of doctor rerum naturalium in chemistry

in the

UCN Group
Department of Chemistry - TRIGA site
Faculty of Chemistry, Pharmaceutical Sciences,
Geography and Geosciences

Mainz, August 6, 2024

Dean:
Prof. Dr. Eva RENTSCHLER
Supervisor:
Dr. Dieter RIES
Second Supervisor:
Prof. Dr. Martin FERTL

Day of the oral exam:

"Die Arbeit, die tüchtige, intensive Arbeit, die einen ganz in Anspuch nimmt mit Hirn und Nerven, ist doch der größte Genuß im Leben."

Rosa Luxemburg

JOHANNES GUTENBERG UNIVERSITY MAINZ

Abstract

Department of Chemistry - TRIGA site

doctor rerum naturalium

Improving Ultracold Neutron Density and Storage: Applications to Neutron Lifetime and Electric Dipole Moment Experiments

by Noah Gabriel YAZDANDOOST KHOSRAVI

This thesis presents a comprehensive study on ultracold neutron (UCN) storage measurements for the n2EDM experiment, which searches for a property of the neutron called "electric dipole moment", and the τSPECT experiment, which measures the free neutron lifetime. Both experiments are situated at the Paul Scherrer Institute in Villigen, Switzerland. Additionally, this thesis includes studies on the UCN source at the research reactor TRIGA Mainz, Germany, and a comparison to the UCN source at Paul Scherrer Institute in Villigen, Switzerland.

Ultracold neutron sources

An optimization of the UCN source at the research reactor TRIGA Mainz is described, achieved by increasing the temperature of the deuterium and hydrogen crystals, which are the central component of the UCN source where neutrons are moderated and then converted to UCNs. This optimization increases the UCN densities available for experiments.

A comparison of the UCN source at the research reactor TRIGA Mainz, Germany, and the one at the Paul Scherrer Institute is made for a storage volume mimicking the conditions of the τSPECT experiment.

τSPECT

The τSPECT experiment aims to measure the neutron lifetime by storing UCNs in a magnetic field gradient trap and counting the UCNs reaming after a storage period. The first storage curves after the relocation of the τSPECT experiment from the research reactor TRIGA Mainz, Germany, to the Paul Scherrer Institute were measured.

n2EDM

The n2EDM experiment aims to measure the neutron's electric dipole moment. This work describes the manufacturing and characterization of the insulating rings and the first UCN storage measurements for the n2EDM experiment. Furthermore, a new method to investigate the UCN energy spectrum in the n2EDM experiment was developed.

JOHANNES GUTENBERG UNIVERSITY MAINZ

Zusammenfassung

Department of Chemistry - TRIGA site

doctor rerum naturalium

Verbesserung von ultrakalten Neutronendichten und -speicherung: Anwendung auf Neutronenlebensdauer- und elektrisches Dipolmomentexperimente

von Noah Gabriel YAZDANDOOST KHOSRAVI

Diese Arbeit präsentiert eine umfassende Studie über die Speicherung von Ultrakalten Neutronen (UCNs) für das n2EDM-Experiment, das nach einem elektrischen Dipolmoment des Neutrons sucht, und das τSPECT-Experiment, das die freie Neutronenlebensdauer misst. Beide Experimente befinden sich am Paul Scherrer Institut in Villigen, Schweiz. Zusätzlich umfasst diese Arbeit Studien über die UCN-Quelle am Forschungsreaktor TRIGA Mainz, Deutschland, und einen Vergleich mit der UCN-Quelle am Paul Scherrer Institut in Villigen, Schweiz.

Ultrakalte Neutronquellen

Eine Optimierung der UCN-Quelle am Forschungsreaktor TRIGA Mainz wird beschrieben, die durch eine Erhöhung der Temperatur der Deuterium- und Wasserstoffkristalle erreicht wird, welche die zentralen Komponenten der UCN-Quelle sind, in denen Neutronen moderiert und dann in UCNs umgewandelt werden. Diese Optimierung erhöht die für Experimente verfügbaren Ultrakalten Neutronendichten.

Ein Vergleich der UCN-Quelle am Forschungsreaktor TRIGA Mainz und der am Paul Scherrer Institut, Villigen, Schweiz, wurde für ein Speichervolumen durchgeführt, das die Bedingungen des τSPECT-Experiments nachahmt.

τSPECT

Das τSPECT-Experiment misst die Neutronenlebensdauer, indem UCN in einer magnetischen Feldgradientenfalle gespeichert werden. Die ersten Speicherkurven nach dem Umzug des τSPECT-Experiments vom Forschungsreaktor TRIGA Mainz zum Paul Scherrer Institut wurden gemessen.

n2EDM

Das Ziel des n2EDM Experiments ist es das elektrische Dipolmoment vom Neutron zu messen. Diese Arbeit beschreibt die Herstellung und Charakterisierung der Isolierringe sowie die ersten Speicherungsmessungen von UCN für das n2EDM-Experiment. Darüber hinaus wurde eine neue Methode zur Untersuchung des Energiespektrums der UCN im n2EDM-Experiment entwickelt.

Contents

List of Figures

List of Tables

List of Abbreviations

BBN	**B**ig **B**ang **N**ucleosynthesis
BMSR-2	**B**erlin **M**agnetically **S**hielded **R**oom-2
CKM matrix	**C**abibbo-**K**obayashi -**M**askawa-matrix
C.L.	**C**onfidence **L**evel
CPT symmetry	**C**harge-**P**arity-**T**ime symmetry
dPE	**d**euterated **P**oly**E**thylene
dPS	**d**euterated **P**oly**S**tyrene
EDM	**E**lectric **D**ipole **M**oment
HFS	neutron in the **H**igh **F**ield **S**eeking state
HV	**H**igh **V**oltage
JGU	**J**ohannes **G**utenberg **U**niversity Mainz
LFS	neutron in the **L**ow **F**ield **S**eeking state
MSR	**M**agnetically **S**hielded **R**oom
nEDM	**n**eutron **E**lectric **D**ipole **M**oment
PE	**P**oly**E**thylene
PS	**P**oly**S**tyrene
PSI	**P**aul-**S**cherrer **I**nstitute
SCM	**S**uper**C**onducting **M**agnet
SQUID	**S**uperconducting **Q**uantum **I**nterference **D**evice
TRIGA	**T**raining **R**esearch **I**sotopes **G**eneral **A**tomics
UCN	**U**ltracold **N**eutron
UCNs	**U**ltracold **N**eutrons
USSA	**U**-shaped **s**imultaneous **S**pin state **A**nalyser
UV	**U**ltra **V**iolet

Chapter 1

Introduction

Scientific progress is a tale of human curiosity and ingenuity, starting with observation using the naked eye and evolving into increasingly sophisticated methods to study and describe nature.

Early science began with direct observations of natural phenomena such as the patterns cycles of the moon, and changing seasons were all noted without any instruments by our ancestors. These observations led to the development of the first calendars and weather predictions, greatly aiding daily life and agricultural practices.

For example, the ancient Egyptians noticed that the annual flooding of the Nile river was correlated with the heliacal rising of the star we know today as Sirius. This knowledge allowed them to anticipate the floods and plan their farming activities accordingly, demonstrating practical applications of astronomical observations and science, described in Ref. [SA17].

As time progressed, scientific observations were made with instruments. For example, Galileo Galilei's use of the telescope in the early 17th century, summarized in Ref. [Str09]. His discovery of the moons of Jupiter and the phases of Venus with a telescope provided strong evidence for the heliocentric model of our solar system, fundamentally altering our understanding of our place in the universe and humbling humanity by challenging long-held geocentric views. As scientific tools became more advanced, so did our ability to explore the intricacies of nature.

In the 20th century, the development of particle accelerators and detectors enabled scientists to investigate the smallest building blocks of matter, described in Ref. [Bis08]. For example, the discovery of the neutron by James Chadwick in 1932 reported in Ref. [Cha32] expanded our understanding of atomic structure and led to the emergence of modern nuclear physics. Other groundbreaking discoveries summarized in Ref. [Fra13] include the uncovering of subatomic particles such as quarks, leptons, and bosons, which have furthered our understanding of the universe.

While we believe today that we have identified the fundamental building blocks of the universe that can be discovered directly, our quest to understand the universe continues with an emphasis on precision. Modern physics aims to measure the properties of particles and forces with incredible accuracy, often requiring collaboration among different nations and hundreds of researchers to construct elaborate experimental setups.

By comparing the results of these measurements with the theory predictions, scientists can identify discrepancies that may point to new physics beyond our current theories and understanding of nature.

The study of ultracold neutrons is a prime example of measurements with high precision to discover new aspects of the universe. Measuring the properties of the neutron, such as the neutron lifetime or the neutron electric dipole moment, and comparing the results with theoretical predictions, allows us to challenge and refine our understanding of the universe.

Building on the foundations laid centuries ago by observations with the naked eye or simple instruments, nowadays, the main tool in physics to reveal the mysteries of the universe is precision.

Chapter 2

Theoretical and experimental foundations

2.1 Ultracold neutrons

The most accurate experiments dedicated to measuring the free neutron lifetime and the neutron's electric dipole moment (nEDM), as described in Refs. [Abe+20] and [UCN+21], rely on neutrons with kinetic energies (E_{kin}) in the neV range, known as ultracold neutrons (UCNs). UCNs can reflect off material walls or be contained by magnetic field gradients or gravity. The unique storability of UCNs is particularly beneficial for precision measurements, as it allows for extended observation periods of the interaction of the UCNs with the fundamental forces.

All four fundamental forces, which are described in the following subsections, play a significant role in the characterization and behavior of UCNs.

2.1.1 Weak interaction

Free neutrons n^0 decay into protons p^+ via the weak interaction after a lifetime of approximately 15 min. In this process, a down-quark is converted into an up-quark under the emission of a W^- boson, which then decays into an electron e^-, and electron antineutrino $\bar{\nu}_e$. The full process can be described by equation (2.1):

$$n^0 \rightarrow p^+ + e^- + \bar{\nu}_e + 782\,\text{keV} \tag{2.1}$$

2.1.2 Electromagnetic interaction

Neutrons have an intrinsic angular momentum, called spin and represented as $\vec{S}$, with a spin quantum number of $\frac{1}{2}$. This spin is linked to an antiparallel oriented magnetic dipole moment, $\vec{\mu}_n$. The magnitude of a neutron's magnetic moment is approximately $-60.3\,\text{neV/T}$ (compare to Ref. [Gol91]). While this value is known with greater precision, for the purposes of the energy discussion of UCNs in this work, the level of precision is sufficient. In an external magnetic field, the orientation of a neutron's spin influences its potential energy: Comparing the potential energy of two neutrons in an external magnetic field, where one neutron's spin is aligned with the field and

one is anti-aligned, one observes a difference in their potential energies due to their spin orientations relative to the magnetic field. The neutron with its spin aligned antiparallel to the magnetic field will be in a lower energy state compared to the neutron whose spin is aligned parallel to the field. Consequently, a neutron with its spin anti-aligned to the magnetic field direction, known as a neutron in the low-field-seeking state (LFS), experiences deceleration by an increasing magnetic field gradient. Conversely, a neutron with its spin aligned with the magnetic field, referred to as a neutron in the high-field-seeking state (HFS), undergoes acceleration by an increasing magnetic field gradient.

2.1.3 Gravitational interaction

Like all particles which possess mass, neutrons with their mass m_n are subject to gravitational forces. On Earth, this means that neutrons are affected by the gravitational potential of the planet. Consequently, the potential energy of neutrons at the surface of the Earth changes by approximately 102 neV/m with their movement along the axis of gravity according to Ref. [Gol91].

2.1.4 Strong interaction

Given that neutrons are composed of quarks, they are subject to the strong interaction, which governs their interactions with atomic nuclei. The wave function of a neutron ψ_na, involved in the coherent scattering of an atomic nucleus with the coherent scattering length a, can be described at position vectors r_a exceeding the atomic radius R by Equation (2.2):

$$\psi_\mathrm{na} = e^{ikr_\mathrm{a}} \left(1 + \frac{-a}{r_\mathrm{a}}\right) \tag{2.2}$$

This description is valid for neutrons with sufficiently large wavelengths, specifically when $\lambda_\mathrm{n} \gg R$ as shown in Ref. [Gol91]. Here λ_n is the de Broglie wavelength and v the velocity, defined in Equation (2.3) (compare to Ref. [Bro24]):

$$\lambda_\mathrm{n} = \frac{h}{m_\mathrm{n} v} \tag{2.3}$$

2.1.5 Fermi pseudo-potential

When the neutron's momentum towards a material boundary is sufficiently low and its dynamic de Broglie wavelength is large, see Equation (2.3), a single atomic nucleus's scattering description as in Subsection 2.1.4 becomes inadequate. Instead, the scattering must be understood as an interaction with a collection of atomic nuclei. This collection of atomic nuclei and their coherent scattering lengths a forms a potential for the UCN, as described in Ref. [Fer+46]. The potential also known as Fermi pseudo-potential V_f can be

TABLE 2.1: Fermi pseudo-potential values for selected materials. These values, which can vary by a few neV due to differences in material density and composition, are sourced from Refs. [Kuz08], [Ass09], and [Gol91].

material	density $\frac{g}{cm^3}$	coherent scattering length fm	Fermi pseudo-potential neV
Al	2.7	3.5	54
B	2.34	5.3	180
^{10}B	2.34	-0.2	-7
Cu	8.8	7.7	169
H_{solid}	0.1	-3.7	-58
D_{solid}	0.2	6.7	104
PE	-0.3	0.95	-9
dPE	6.7	1.1	210
PS	1.5	1.1	36
dPS	6.7	1.2	165
Ni	8.8	10.6	261
^{58}Ni	8.8	14.4	335
SiO_2	3.22	5.3	95
Ti	4.54	-3.4	-50

described by Equation (2.4) with the sum of coherent scattering length a and the number density N of the elements i of the wall material.

$$V_f = \frac{2\pi\hbar^2}{m_n \sum_i N_i a_i} \tag{2.4}$$

The Fermi pseudo-potential of materials important for UCN physics are summarized in Table 2.1.

Loss per bounce

When an UCN is reflected off a Fermi pseudo-potential, there exists a non-zero probability for the neutron, and its derivative to penetrate this potential. This probability exits because the wavefunction of the UCN is continuous and does not abruptly halt at the vacuum-material boundaries. Interactions within the material can be categorized as follows:

1. Upscattering: This process involves scattering that increases the neutron's energy beyond the storable range, rendering it no longer classifiable as a UCN. It is important to note that upscattering is temperature-dependent.

2. Absorption: This is when the neutron is absorbed by an atomic nucleus within the wall material, a phenomenon also referred to as neutron capture. After absorption, the neutron is no longer considered a free neutron.

The loss factor η_l for UCN reflection on a material surface can be quantified using the material-dependent total cross section for such events σ_{tot}, the wavelength of the neutron λ_n and the coherent scattering length a. The loss per bounce factor can also be expressed as the quotient of the imaginary part of the Fermi pseudo-potential W divided by the real part of the Fermi pseudo-potential. This formulation is justified by the fact that at the very low energies of UCNs the scattering process can be described using S-wave scattering, as higher-order partial waves are negligible due to the absence of significant angular momentum, allowing the interactions to be approximated as isotropic and spherically symmetric.

$$\eta_l = \frac{\sigma_{tot}}{2\lambda_n a} = \frac{W}{V_f} \tag{2.5}$$

Equation (2.5) facilitates the formulation of Equation (2.6), which establishes a kinetic-energy-dependent loss per bounce factor, denoted as μ_l, for UCNs with random trajectories.

$$\mu_l\left(E_{kin}\right) = \frac{2\eta_l V_f}{E_{kin}} \sin^{-1}\left(\sqrt{\frac{E_{kin}}{V_f}} - \sqrt{\frac{V_f}{E_{kin}} - 1}\right) \tag{2.6}$$

The description of neutron interactions with a collection of atoms is based on the theory outlined in Ref. [Gol91].

2.1.6 Interactions of ultracold neutrons in traps

The interactions of UCNs within traps extend beyond mere reflection on the trap walls. As a result, several additional loss channels contribute to reducing the storage time τ_s of UCNs as shown in Equation (2.7). All loss channels, aside from beta decay, are energy-dependent and therefore influenced by the stored energy spectrum, which can change over the storage period.

$$\tau_s^{-1} = \tau_\beta^{-1} + \tau_{abs}^{-1} + \tau_{up}^{-1} + \tau_{slit}^{-1} + \tau_{marg}^{-1} + \tau_{gas}^{-1} \ldots \tag{2.7}$$

- τ_β: Free neutrons undergo β^--decay as described in Subsection 2.1.1. Following the decay, the neutron effectively disappears from the trap, resulting in its loss from the system.

- τ_{abs} & τ_{up}: The interaction between UCNs and wall atoms within material traps can result in the neutron being absorbed or receiving an energy transfer that renders it non-storable. These phenomena are detailed in Subsection 2.1.5.

- τ_{slit}: Since UCN traps using material surfaces to store UCNs, are mechanically constructed, they inherently possess imperfections, creating the possibility for slits through which neutrons can either escape from the trap or experience numerous reflections in a brief period. Neutrons that undergo numerous reflections are more likely to be lost from the trap due to the increased probability of upscattering and absorption.

- τ_{marg}: After filling a UCN trap, some UCNs within the trap may possess total kinetic energies higher than the trap's potential. Their kinetic energy is typically distributed among three components of momentum. The component of momentum directed perpendicular to the wall may be too small to initially overcome the wall's potential, even if their total momentum is sufficient to surpass the potential barrier. These neutrons can have orbits that take a considerable amount of time to reach a point where their momentum perpendicular to a wall is sufficient to overcome the trap's potential barrier. As time progresses, more of these neutrons eventually exit the trap, leading to a reduction in their number. This phenomenon introduces an additional loss channel within the trap, particularly if the energy spectrum of UCNs is not carefully manipulated before the storage period.

- τ_{gas}: Neutrons can be absorbed or scattered off residual gas atoms inside the trap volume, rendering them no longer storable as UCNs.

2.1.7 Production of ultracold neutrons

The techniques for reducing neutron energies to the UCN regime primarily encompass two approaches: the Doppler effect and the superthermal process, as described in Ref. [GB83]. While sources based on the Doppler effect, particularly the one detailed in Ref. [Ste+86], were historically pivotal, modern UCN sources predominantly employ the superthermal method.

The cooling process of neutrons can be conceptualized in three stages. Initially, neutrons generated through spallation or fission are moderated to thermal neutrons through elastic collisions, typically with water. This process reduces the energy of the neutrons from megaelectronvolts to tens of millielectronvolts. Subsequently, these thermal neutrons are further cooled to cold neutrons, possessing kinetic energies in the lower millielectronvolts range, by further elastic scattering with hydrogen or hydrogen-rich compounds at low temperatures typically 20 K – 30 K. To diminish neutron absorption deuterium-enriched moderators are often used. The hydrogen nucleus consists of a single proton, whereas the deuterium nucleus consists of a neutron and a proton. This composition reduces the neutron absorption cross-section of deuterium compared to hydrogen. Finally, these cold neutrons undergo inelastic scattering in a deuterium crystal or superfluid helium, a process that effectively converts them into UCNs.

2.2 Free neutron lifetime

The mean free lifetime of a neutron is the average time it takes until a neutron decays. The only known decay process for a neutron so far is into a proton, an electron, and an electron anti-neutrino. The neutron decay is important in various physics domains:

The neutron-to-proton ratio, essential in determining the light elements formed during Big Bang nucleosynthesis (BBN), is directly influenced by the neutron lifetime. A longer neutron lifetime would result in a higher neutron-to-proton ratio, leading to the formation of more neutron-rich elements during the BBN. Conversely, a shorter neutron lifetime would yield a lower neutron-to-proton ratio, resulting in the creation of more proton-rich elements described in Ref. [Cyb+16].

The neutron lifetime in combination with other measurements can also be used to probe the standard model of particle physics. The Cabibbo-Kobayashi-Maskawa (CKM) matrix, as represented in Equation (2.8) and published in Reference [KM73], describes the mixing of the different quark flavors into each other. This mixing occurs because the mass eigenstates of quarks d_q, s_q, b_q, which are the states with definite mass, are not aligned with the flavor eigenstates d'_q, s'_q, b'_q, which are the states that participate in weak interactions. As a result, when quarks undergo weak decays, they transition between different flavors.

$$\begin{bmatrix} d'_q \\ s'_q \\ b'_q \end{bmatrix} = \begin{bmatrix} V_{ud} & V_{us} & V_{ub} \\ V_{cd} & V_{cs} & V_{cb} \\ V_{td} & V_{ts} & V_{tb} \end{bmatrix} \begin{bmatrix} d_q \\ s_q \\ b_q \end{bmatrix} \tag{2.8}$$

From the decay of the neutron, the mixing between the up and down quarks can be determined by measuring the mean lifetime and the weak axial-vector coupling constant. This allows for the extraction of the matrix element V_{ud} of the CKM matrix.

The Standard Model of Particle Physics predicts the unitarity of the CKM matrix. Therefore, the sum of the relative transition probabilities for the down quark, obtained by adding the squares of the matrix elements in the first row of the CKM matrix, is expected to be equal to one. A beyond the Standard Model mixing of the down quark would lead to a sum of the relative transition probabilities which differs from one. If one combines the most accurate measurements of V_{ud} from superallowed $0^+ \rightarrow 0^+$ nuclear beta decays, V_{us} from Kaon and Pion decays, and V_{ub} from B mesons decays, to test the unitarity predicted by the Standard Model of Particle Physics the result is an approximately 2 σ deviation from 1 for the first row. This calculation is summarized in Equation (2.9) with values from Reference [Par+22] with their total uncertainties in brackets.

$$V_{ud}^2 + V_{us}^2 + V_{ub}^2 = 0.9482(3) + 0.0503(4) + 0.000015(2) = 0.9985(7) \tag{2.9}$$

Note that because V_{ub}^2 is so small, it has no significant influence on the result at the current level of precision.

To scrutinize prior measurements of V_{ud} and measure V_{ud} without the need for nuclear corrections, free neutron β decay can be utilized. V_{ud} can be extracted from free neutron β decay by considering the axial vector coupling, λ_g which can be extracted from the neutron decay correlation coefficients a_n or A_n and the mean neutron lifetime. It is important to include radiative corrections Δ_R^V in this calculations, as it is done in Equation (2.10).

$$V_{ud}^2 = \frac{5024.7\,\mathrm{s}}{\tau_n \left(1 + 3\lambda_g^2\right)\left(1 + \Delta_R^V\right)} \tag{2.10}$$

Taking the average for the neutron lifetime τ_{PDG} and the axial vector coupling λ_{PDG} from the PDG [Par+22] and Δ_R^V from Ref. [Sen+18], V_{ud}^2 can be calculated as show in Equation (2.10).

$$\begin{aligned} V_{ud}^2 &= \frac{5024.7\,\mathrm{s}}{879.4(6)\,\mathrm{s}\,(1 + 31.27641(56)^2)\,(1 + 0.024567(22))} \\ &= 0.97370(33)_\tau(35)_\lambda(10)_{RC} \end{aligned} \tag{2.11}$$

To be competitive with superallowed $0^+ \to 0^+$ nuclear β decays and in the future with values extracted by Pion decay described in Ref. [Col+22], a more precise measurement of the neutron decay coefficient a_n or A_n, as planned by the PERC experiment described in Ref.[Wan+19], and the neutron lifetime is needed. Additionally, it is important to note that the theoretical framework for extracting V_{ud} from superallowed $0^+ \to 0^+$ nuclear β decays is evolving. This evolution in the theoretical understanding suggests that the current nuclear uncertainties used to extract V_{ud} might be underestimated as described in Ref. [GS24].

2.2.1 Measuring the free neutron lifetime

Historically, two different types of experiments have been developed to measure the lifetimes of exponential decay processes. One is known as the beam method and the other one is known as the bottle method, and in the following they are described for measurements of the free neutron lifetime. A schematic comparison of both methods is shown in Figure 2.1.

The first type are beam experiments, where a cold neutron beam travels through a decay volume. The neutrons are counted after traversing this volume using a neutron detector. Within the decay volume, the decays are monitored; specifically, the protons or electrons resulting from the decay of neutrons are counted. The neutron lifetime can be extracted by combining the counting rates from the neutron detector R_n and the electron/proton detector R_{pe}, taking into account their respective efficiencies ϵ_n and ϵ_{pe}. The primary systematic uncertainty lies in accurately determining the absolute efficiency of the neutron and electron/proton detectors.

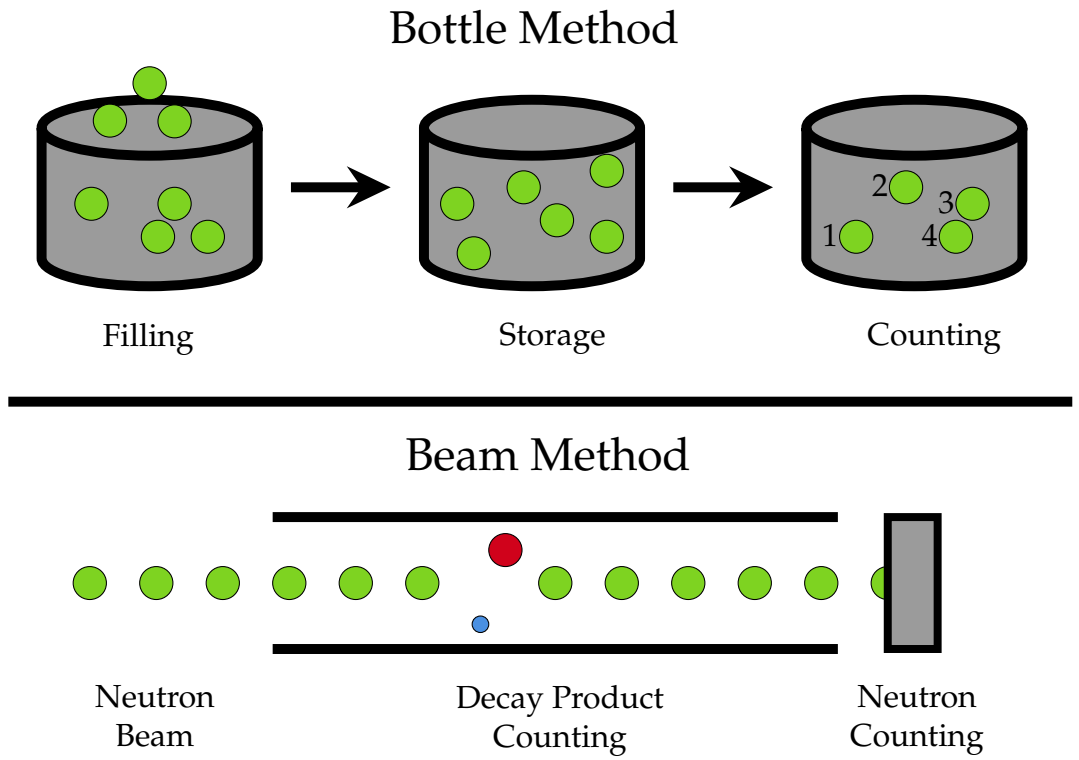

FIGURE 2.1: Schematic drawing of neutron lifetime measurements using the bottle and beam methods, illustrating the two different concepts of neutron lifetime measurement.

In bottle-type experiments, UCNs are filled into and stored within a trap. The neutrons are counted destructively after various storage periods to determine the exponential decay constant, which is then used to calculate the neutron lifetime. A significant source of uncertainty in this method is the interaction between the neutrons and the wall atoms as described in subsection 2.1.6.

These two methods, bottle and beam experiments, yield differing results for the neutron lifetime ($\tau_{\text{bottle}} = 878.4(5)\,\text{s}$ (Ref. [UCN+21]) and $\tau_{\text{beam}} = 887.7(22)\,\text{s}$ (Ref. [Yue+13]) summarized in Ref. [Tan23]), with a discrepancy of approximately 4 σ. This discrepancy has led to speculation about phenomena such as dark neutron decays and oscillations into sterile neutrons, as described in Ref. [Pau09]. However, it has not been ruled out that one of the methods might be affected by an unidentified systematic error that has yet to be accounted for. Therefore, future efforts should focus on developing more reliable methods for measuring the free neutron lifetime. The current generation of neutron lifetime experiments will focus on bottle experiments designed to eliminate the main systematic error associated with material bottle type experiments by avoiding wall contact of UCNs during storage. This is achieved by confining the neutrons with magnetic field gradients and/or gravity, leading to measurements of the neutron lifetime with lower corrections and less systematic uncertainties.

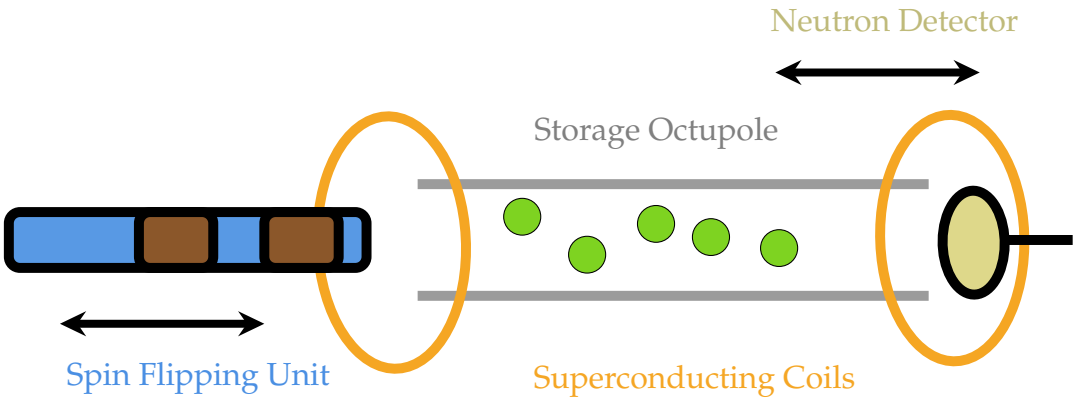

FIGURE 2.2: Schematic diagram of the τSPECT experiment used to measure the neutron lifetime.

2.2.2 τSPECT

τSPECT represents a cutting-edge approach in the next generation of neutron lifetime experiments. In this setup, UCNs are confined entirely through electromagnetic interactions as described in Ref. [Aul+23]. The confining magnetic field configuration is formed from a cylindrical arrangement, utilizing a permanent Halbach octupole (Ref. [Hal80]) with an inner diameter of 54 mm and a length of 1.38 m and a minimum magnetic field of 780 mT at 26.75 mm radius from the center axis of the cylinder. The ends of this cylindrical volume are magnetically sealed by magnetic fields generated by superconducting coils. To store neutrons in the storage region, their spins have to be manipulated by an electromagnetic field generated by a device called the spin flipping unit at the entrance of the trap. This manipulation of the spin state is necessary because the magentic fields reflect storable LFS, allowing only HFS within the storable energy range to enter the trapping region. After a predetermined storage period, the neutrons are counted by a movable UCN detector located at the opposite end of the cylinder from the spin flipping unit, where the neutrons are initially fed into the experiment. By conducting measurements after various storage periods, an exponential decay curve can be fitted to the detected neutrons after different storage periods. The decay constant of this fit is the storage time constant of the trap. In the ideal case, by understanding and applying corrections and considerations of systematic uncertainties, this storage time, along with other relevant measurements, is used to determine the free neutron lifetime.

A single measurement cycle can be summarized as follows:

1. The spin flipping unit, positioned inside the storage volume in the filling position, generates a rotating electromagnetic field to flip the spin of incoming neutrons, allowing them to be storable.

2. Once the filling time is over, the spin flipping unit ceases electromagnetic field emission and is mechanically retracted from the storage volume.

3. The neutron detector slightly enters the storage volume to detect and thus remove only the highest-energy neutrons. This step ensures the removal of neutrons that are not permanently storable and might exit the trap during the storage period by means other than β decay.

4. The detector is withdrawn from the storage volume, marking the start of the storage period.

5. Following the storage period, the detector fully enters the storage volume to count the remaining neutrons in the trap. Subsequently, the detector stays in position to also measure the background.

6. Finally, the detector is removed from the storage volume, and the spin flipping unit is moved from its storage position back to the filling position inside the storage volume for the next cycle.

2.3 Electric dipole moment of the neutron

Over the years, a series of satellites, including COBE, WMAP, and Planck, have progressively enhanced our measurement precision of the cosmic microwave background radiation. These measurements have established that the observable universe, consists of 4.9 % ordinary matter, 26.8 % dark matter, and 68.3 % dark energy as described in Ref. [Ade+16]. This non-observation of antimatter presents a conundrum when juxtaposed with predictions from the Standard Model of Particle Physics, which predicts that the Big Bang should have generated equal quantities of matter and antimatter. Consequently, the Standard Model faces a significant challenge in explaining the observed dominance of ordinary matter in the universe.

Andrei Sakharov identified in Ref. [Sak67] three essential criteria that any theoretical model must satisfy to account for the observed imbalance between matter and antimatter. These criteria are: violation of baryon number, occurrence of interactions outside thermal equilibrium, and violation of charge-parity (CP) symmetry. Although the Standard Model of Particle Physics incorporates CP violation, the extent of this violation is insufficient to explain the significant disparity between matter and antimatter. Therefore, scientists worldwide are actively searching for evidence of a more substantial CP violation. One promising avenue of investigation is the potential existence of a permanent electric dipole moment (EDM) in particles.

As illustrated in Figure 2.3, a permanent EDM of a particle would violate T-symmetry, as reversing the direction of time would change the direction of the EDM, while the direction of an external electric field would remain unchanged, leading to a violation of energy conservation. Assuming that CPT-symmetry is intact, a permanent EDM of a particle also implies a violation of CP-symmetry.

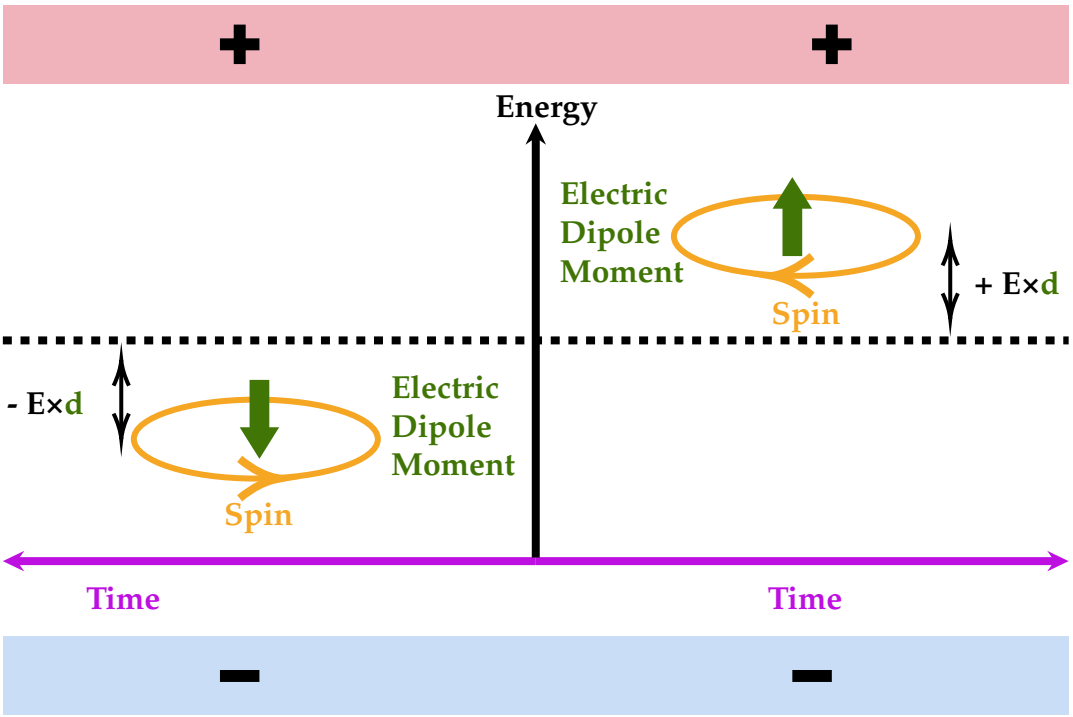

FIGURE 2.3: Schematic drawing of a particle with a permanent EDM in an electric field breaking T-symmetry.

To date, research has only managed to establish upper limits for the magnitude of electric dipole moments of particles, with no definitive measurements confirming their existence. Specifically, efforts are underway to measure the neutron's electric dipole moment (nEDM) with the utmost precision, as summarized in Ref. [Mar20]. The lowest upper limit (90 % C.L.) to date for the neutron's electric dipole moment has been reported as 1.8×10^{-26} e cm, as detailed in Ref. [Abe+20]. These measurements are crucial for advancing our understanding of the universe.

2.3.1 Ramsey's method of separated oscillating fields

Over the last decades, the most precise measurements of the nEDM have been conducted using the Ramsey method of separated oscillating fields, as described in Ref. [Ram50]. The measurement setups evolved from utilizing neutron beams to trapping neutrons.

Polarized UCNs are stored in a trap where an electric field E_0 and a magnetic field B_0 are applied either parallel or antiparallel to each other. At the start of the storage period, the projection of the neutrons' spin on the Bloch sphere is flipped from the z-axis to the $x-y$-plane using an electromagnetic pulse. The neutrons then undergo free precession for a duration T_f, also known as the free precession time. At the end of this period, the spin of the neutrons is flipped to the opposite direction on the z-axis compared to its initial orientation, using a second electromagnetic pulse that is in phase with the first one. The spin flip is in resonance, and thus most efficient, when the

frequency of the electromagnetic pulse matches the precession frequency of the neutrons, denoted as ω_n as detailed in Equation (2.12):

$$\omega_n = \frac{-2\mu_n B_0 \pm 2d_n E_0}{\hbar} \tag{2.12}$$

Here, B_0 represents the applied magnetic field and E_0 the electric field, while μ_n and d_n are the magnetic and electric dipole moments of the neutron, respectively. This relationship allows the measurement of the neutron electric dipole moment by assessing the spin flip efficiency and the magnetic field. The statistical sensitivity in measuring the electric dipole moment of the neutron $\sigma(d_n)$, is detailed in Equation (2.13), assuming a constant magnetic field and electromagnetic pulses of constant frequency:

$$\sigma(d_n) \propto \frac{\hbar}{2E_0 T_f \alpha \sqrt{N_n}} \tag{2.13}$$

The statistical sensitivity is inversely proportional to the strength of the applied electric field, the duration of the free precession time, and the square root of the number of neutrons detected N_n, as well as the contrast between the two spin states α.

2.3.2 Description of the n2EDM experiment

By utilizing Ramsey's method of separated oscillating fields simultaneously in two chambers under extremely well controlled magnetic field conditions, the n2EDM experiment is build to attain the most accurate measurement of the neutron's electric dipole moment ever achieved, detailed in Ref. [Ayr+21].

Neutrons are guided from the UCN source located at the Paul Scherrer Institute (PSI) to the experiment using glass guides coated with NiMo (85:15)[3] On their path to the experiment, the neutrons pass through a guide surrounded by a superconducting magnet (SCM), which produces a magnetic field of up to 5 T. This creates a potential hill of approximately 300 neV for LFS, and correspondingly, a potential well of the same magnitude for HFS. Next, the neutrons proceed to a section of movable neutron guides, referred to as the switch. This switch can direct the neutrons either from the source to the precession chamber or to the U-shaped simultaneous spin state analyser (USSA), the latter path being known as 'direct shots'. Additionally, the switch has a third position that connects the precession chamber to the USSA. The neutrons are guided into the precession chamber through holes in a magnetically shielded room, referred to as the MSR. The MSR, in combination with an active magnetic shield surrounding the entire experimental area, shields the inner precession chamber from external magnetic fields and variations of the magnetic fields over time. This setup ensures that the

[3] NiMo (85:15) is an alloy consisting of 85 % nickel and 15 % molybdenum. It is chosen because it is non-magnetic compared to pure Nickel, and therefore does not have a neutron spin-dependent pseudo Fermi potential, which can lead to varying transmission values based on the spin state of the neutrons.

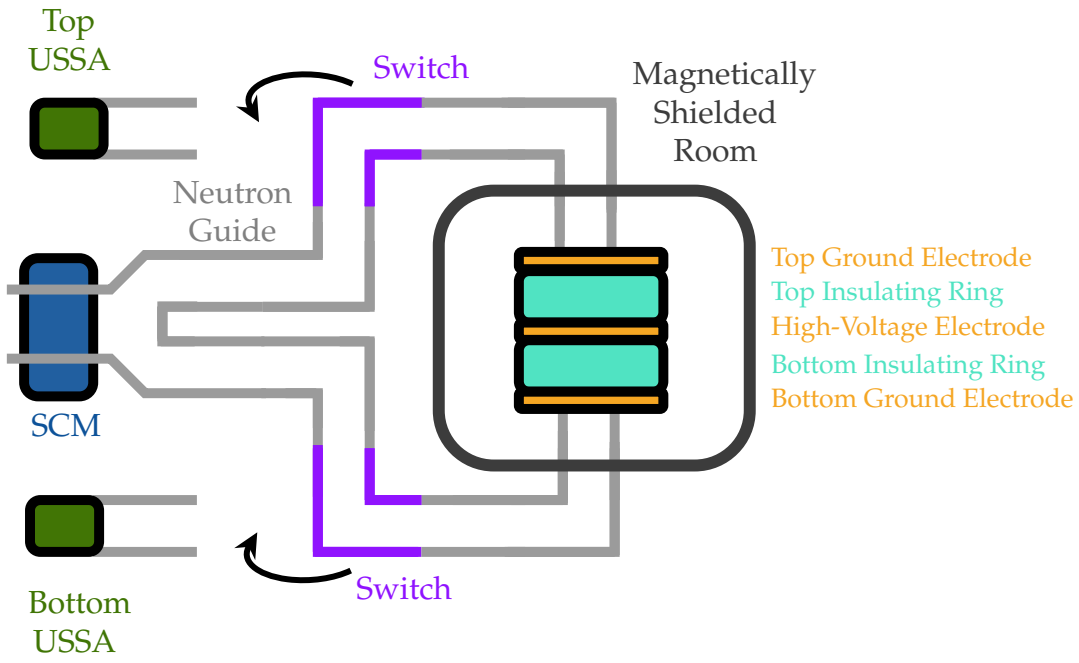

FIGURE 2.4: Schematic drawing of the n2EDM experimental setup used to measure the neutron's electric dipole moment. The movement of the switch is indicated by the arrows.

applied magnetic field inside the precession chamber is as homogeneous as possible. A stable, homogeneous magnetic field is crucial since any variation in the magnetic field would alter the precession frequency of the neutrons, as detailed in Equation (2.13). Such variations would introduce systematic uncertainties into the measurement of the neutron's electric dipole moment. To monitor variations in the magnetic field, two types of magnetometers are used. One consists of an array of cesium magnetometers housed in small glass cells placed above and below the precession chamber. The other is a mercury-based magnetometer, where the mercury atoms occupy almost the same volume in the precession chamber as the neutrons.

The precession chamber itself consists of two separate chambers, within which the direction of the electric field is pointing in opposite directions. The high voltage electrode separate these cylindrical chambers. The lateral surface of the cylinders features an insulating ring made of Rexolite 1422, coated with deuterated polystyrene. Each insulating ring features two holes to facilitate the laser readout of the mercury magnetometer, accommodating UV-transparent windows made of fused silica also known as UV windows. These windows are coated with deuterated polyethylene (dPE). The chambers are sealed by the ground electrodes, which, like the high voltage electrode, are made of aluminum and are coated with diamond-like carbon. The precession chamber is closed off after the filling time for the storage period by shutters located in the middle of the ground electrodes. After the free precession time and the second electromagnetic pulse, the neutrons are directed from the precession chamber to the USSA to analyze their spin state. A schematic overview of the setup is shown in Figure 2.4.

Chapter 3

The insulating rings for the n2EDM precession chamber

The precession chamber of the n2EDM experiment, which the insulating rings are part of, is described in Subsection 2.3.2. This chapter focuses on the manufacturing, coating, and testing of these insulating rings.

3.1 The insulating rings of the precession chambers in nEDM experiments at PSI

The insulating rings are a crucial component of the nEDM experiments conducted at PSI. They are one of the four parts in contact with the neutrons during the free precession time, alongside the UV windows described in Subsection 2.3.2, the electrodes, and the shutters that open or close the precession chamber for neutrons and mercury atoms. As such, there are numerous and stringent requirements for both the materials of the rings and the coatings used. The required properties of the coating and the insulating rings include:

- **Ring**
  - Bulk material for mechanical machining is readily available and possesses good mechanical machining properties
  - Good mechanical stability, as the weight of several hundred kilograms of the electrodes rests on the insulating rings
- **Coating**
  - (High) Fermi pseudo-potential adequate to confine the UCN energy spectrum guided to the experiment
  - Low loss per bounce factor for neutrons
  - At least 1 µm of layer thickness to ensure the coating is not penetrated by UCNs as UCN transmission probability drops below 10^{-6} for coatings in the 100 nm–300 nm range. This transmission probability is significantly lower than the typical material loss probability, which is on the order of 10^{-4} according to Ref.[Kuz08]
  - Non-depolarizing for neutrons and mercury atoms

  - Chemically compatible with the mercury vapor and UV fluorescence light

- **Ring and Coating**
  - Good adhesion between the coating and the ring material
  - Low outgassing (vapor pressure $< 1 \times 10^{-3}\,\mathrm{N\,m^{-2}}$) and compatible with vacuum requirements in the experiment ($< 1 \times 10^{-4}\,\mathrm{mbar}$)
  - Insulating for high voltage (180 kV Ref. [Ayr+21]) due to their position between the high voltage and ground electrode
  - Non-magnetic and no magnetic dipoles with strengths of $> 5\,\mathrm{nA\,m^2}$ derived from Ref. [Ayr+21] which results in a systematic uncertainty of $3 \times 10^{-29}\,\mathrm{e\,cm}$ for the measured nEDM

First tests of different materials for the coating and the ring itself have been conducted in Ref. [Kuz08] by Marcin Kuźniak. A suitable combination of materials was found to be Rexolite 1422 for the ring itself and deuterated polystyrene (dPS, $V_\mathrm{f} = 165\,\mathrm{neV}$) for the coating. Further analysis of other materials and the used coatings was done in Ref. [Yaz20]. Deuterated long-chain alkanes on a Rexolite 1422 ring were promising candidates for a coating with a higher Fermi pseudo-potential, which would allow the storage of neutrons with higher energy for the PSI UCN source energy spectrum and fewer losses per bounce and therefore more neutrons in the apparatus. This, in turn, increases the statistical sensitivity for an nEDM per measurement cycle, as shown in Equation (2.13). However, after further investigation during my work for this thesis, it was not possible to achieve a reproducible procedure for applying a uniform and thin coating of deuterated long-chain alkanes on a Rexolite 1422 ring by melting the deuterated long-chain alkanes with a local heating element. Therefore, the first insulating rings for the n2EDM experiment were produced with a dPS coating on Rexolite 1422.

The technical drawing created by Dieter Ries and Michael Meier for the Rexolite 1422 rings is in Appendix B. The rings were cut from a Rexolite 1422 block by "POLYTRON Kunststofftechnik". The key dimensions for the Rexolite 1422 rings are an inner diameter of $840.0^{+0.2}_{+0.4}$ mm, an outer diameter of $800.0^{+0.2}_{+0.4}$ mm, and a height of $150.0(1)$ mm with two opposing holes in the center of the lateral surface for the UV windows. The used nomenclature for the ring surfaces in this Thesis is shown in Figure 3.1. The uncertainties were chosen to ensure the mechanical fit of the insulating rings with the other components of the experiments.

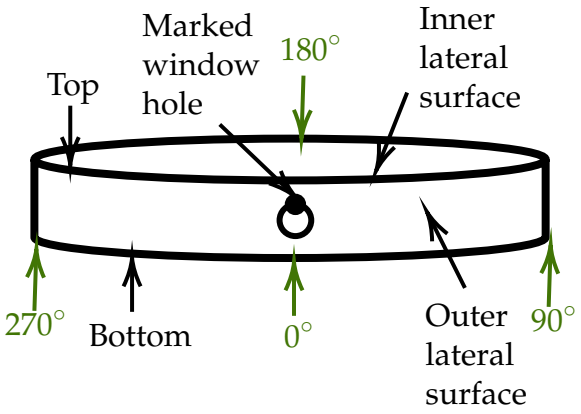

FIGURE 3.1: Schematic sketch of one Rexolite 1422 insulating rings for the n2EDM precession chamber and the nomenclature used in this thesis for the different surfaces and positions of the ring.

3.2 Mechanical dimensions of the first set of Rexolite 1422 rings for the n2EDM precession chamber

The mechanical dimensions of the uncoated rings were measured at the Physikalisch Technische Bundesanstalt (PTB) Braunschweig with the help of Konrad Hierse and Jürgen Hirsch. The measurements were performed on a calibrated coordinate measuring machine called LEITZ Infinity, with a maximum length probing deviation $E_{0,\mathrm{MPE}}$ below $0.3\,\mu\mathrm{m} + \frac{l}{1000\,\mathrm{mm}\,\mu\mathrm{m}^{-1}}$ with the measured length l in mm. A picture of the setup is shown in Figure 3.2 This machine uses a mechanical probe to measure the points of contact between the probe and the object within the machine's coordinate system.

The window holes on the lateral surface were measured with a probe of 33 mm length and a sphere diameter of 3 mm, while all other measurements were conducted using a probe of 180 mm length and a sphere diameter of 10 mm. The lateral surface was measured with 72 contact points at each distance of 130 mm, 110 mm, 90 mm, 70 mm, 50 mm, 30 mm and 5 mm from the bottom frontal surface (surface laying on the measurement table in Figure 3.2), each point was measured five times. The window holes were measured with 16 contact points, each point was measured five times. The measurements were taken at 20.2 °C and were corrected to 20.0 °C using a thermal expansion coefficient of $70.0 \times 10^{-6}\,\mathrm{K}^{-1}$. The uncertainties are provided for a 95 % confidence interval and were calculated following the Guide to the Expression of Uncertainty in Measurement (GUM), Supplement 1 (JCGM 101:2008) and ISO/TS 15530-4:2008 "Evaluating task-specific measurement uncertainty using simulation" by employing the Virtual Coordinate Measuring Machine (VCMM) method. The documentation of the measurements, created by Konrad Hierse and Jürgen Hirsch, can be found in Appendix B.

The most important mechanical parameters for the n2EDM experiment are summarized in Table 3.1. The inner and outer diameter at different

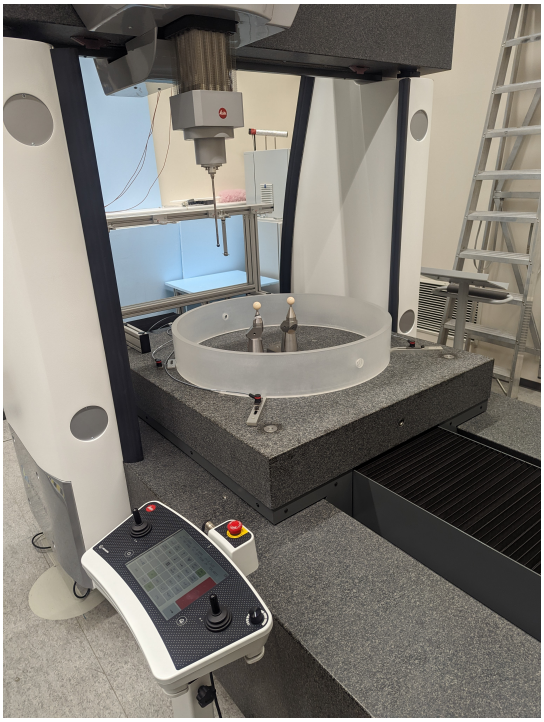

FIGURE 3.2: One of the Rexolite 1422 insulating rings for the n2EDM precession chamber mounted in the coordinate machine at PTB Braunschweig to measure its mechanical dimensions, ensuring the ring is suitable for the n2EDM experiment.

heights is plotted in Figure 3.3.

While the inner diameter of the rings decreases at higher heights, the outer diameter increases. These changes are represented in the concentricity parameter. On that scale, the change in diameter at different heights will not introduce relevant systematic uncertainties on the measurement of the neutron electric dipole moment at the aimed sensitivity (private communication with Dieter Ries), nor will it affect the assembly of the experiment. The height of the rings $150.001(1)$ mm and $150.004(1)$ mm is within the range specified in the technical drawing $150.0(1)$ mm. The flatness and parallelism of the end faces are excellent, allowing for proper alignment of the entire precession chamber. This ensures that the electric and magnetic fields can be well-aligned in the frame of gravity, avoiding additional systematic uncertainties due to misalignment caused by the rings. Therefore, the mechanical dimensions are adequate for the experimental use of the insulating rings in the n2EDM experiment.

3.3 Magnetic properties of the first set of Rexolite 1422 rings for the n2EDM precession chamber

The uncoated insulator rings were measured in Berlin magnetically shielded room-2 (*BMSR-2*), a magnetic shielded room at PTB Berlin, for magnetic contamination above $1\,\mathrm{nA\,m^2}$ after production. The room is described in

TABLE 3.1: The most relevant measurements and calculations of the mechanical dimensions of the first set of Rexolite 1422 rings for the n2EDM experiment at PSI.

Parameter	Insulating ring I mm	Insulating ring II mm
height	150.001(1)	150.004(1)
average inner diameter	800.022(5)	800.070(5)
average outer diameter	840.019(6)	840.211(6)
flatness	0.045(2)	0.049(2)
non-parallelity end faces	0.000	0.001
concentricity	0.074(3)	0.047(3)

Ref. [Bor00] and a picture is shown in Figure 3.4. An array of 304 superconducting quantum interference device (SQUID) probes structured in 19 modules was used as magnetic sensors for this measurement. The noises of the SQUID probes are below, $2\,\mathrm{pT}/\sqrt{\mathrm{Hz}}$ at 0.01 Hz described in Ref. [Bur+04]. One module (Z3L) was not working properly during the measurements. Additionally, the end stop in one direction (x-direction in *BMSR-2* coordinates) used to fix the SQUID array over the measured parts was broken at the time, resulting in an uncertainty of 4 mm in that direction.

Before the measurements were conducted, the rings were magnetized by close contact with a 30 mT magnet wrapped in plastic foil (to prevent magnetic contamination by the magnet itself). The insulator rings were either rotated by hand for the lateral surface measurement or using a non-magnetic contraption driven by pressurized air for measuring the top and bottom side of the insulating rings. The measurements were supervised by Allard Schnabel and Jens Voigt, and carried out with the help of Martin Engler. The analysis was done with the assistance of Allard Schnabel and Anastasio Fratangelo. The magnetic contamination detected is summarized in Table 3.2. The measured magnetic contamination is below the required limit of $5\,\mathrm{nA\,m^2}$ set in Ref. [Ayr+21], and therefore, the magnetic properties of the uncoated rings meet the requirements for the n2EDM experiment.

3.4 dPS coating of the first set of Rexolite 1422 rings for the n2EDM precession chamber

The coating for the set of Rexolite 1422 rings for the n2EDM experiment at PSI was done similarly as described in Ref. [Kuz08]. The comparison between the Fermi pseudo-potential values, as shown in Table 2.1, for deuterated and non-deuterated polystyrene highlights the advantages of using deuterated polystyrene. The significantly higher Fermi pseudo-potential of deuterated

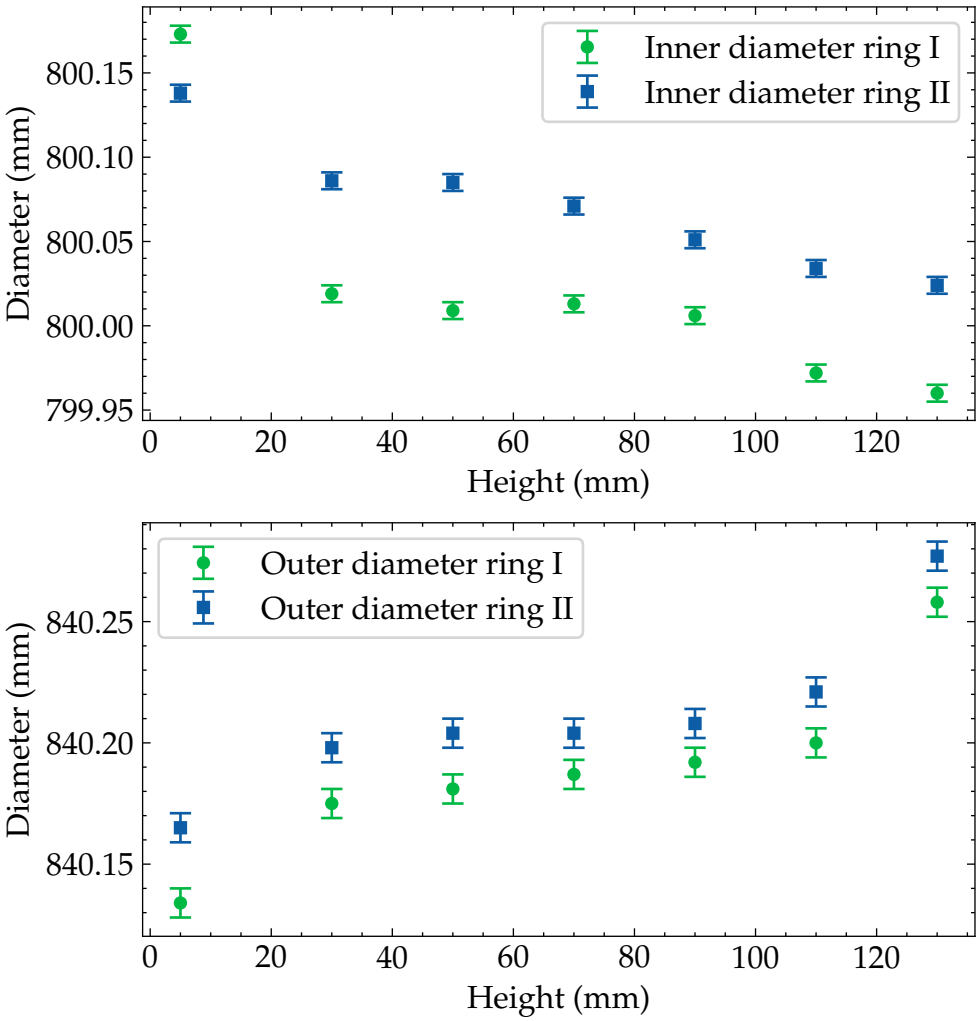

FIGURE 3.3: Average inner and outer diameter of the Rexolite 1422 rings for the n2EDM precession chamber at different heights measured at PTB Braunschweig.

polystyrene, resulting from the replacement of hydrogen atoms with deuterium atoms, makes it a much better coating material. All used chemicals are specified in Appendix C. A picture of the setup used for this thesis is shown in Figure 3.5. The dPS (>98 % degree of deuteration for measurments see Ref. [Yaz20]) used for the coating was from the same manufacturer (*ARMAR*), as the one used in Ref. [Kuz08]. The rings are rotated along their inner lateral sides, filled with a "lake" of dissolved coating material (dPS) in a solvent (deuterated/non-deuterated toluene or benzene). One UV window per hole was mounted during the coating process, to seal the holes on the lateral surface of the insulator ring and prevent the solution from dripping out. As the ring rotates, the solution consistently covers the bottom part of the inner surface, with the covered part changing as the ring rotates. The solvent evaporates over time, leaving a thin layer of the coating material on the ring's inner surface. If the solvent evaporates slowly enough, this process ensures that the entire inner surface of the rings is evenly coated. For the insulator

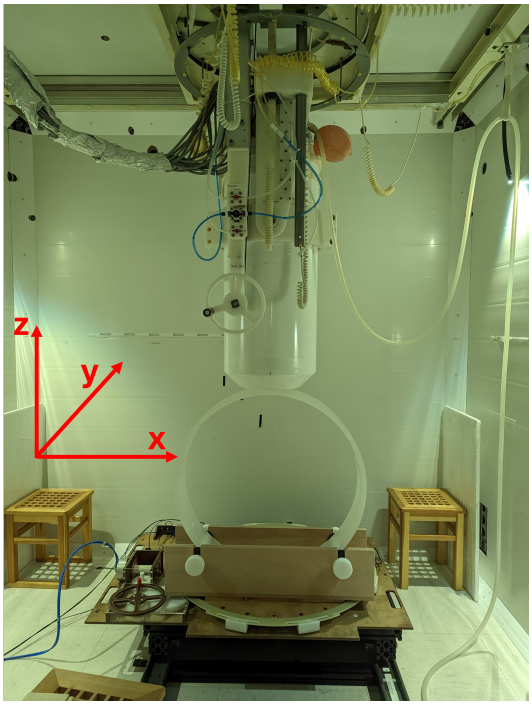

FIGURE 3.4: One of the Rexolite 1422 insulating rings for the n2EDM precession chamber in the *BMSR-2*, ready to be checked for magnetic contamination to ensure it can be used in the n2EDM experiment. The direction of the axis of the coordination system of the *BMSR-2* are shown in red.

rings of the n2EDM experiment, a 1 µm coating, which is more than the penetration depth of UCNs in material, would require approximately 0.9 g of dPS evenly spread on the whole inner surface.

Surface preparation

Before the coating was applied using the described technique, the rings were cleaned with clean room tissues and isopropanol to remove any dust and contamination from their surfaces. After cleaning, the rings were allowed to dry for at least 24 h. After the drying period, the insulating rings were mounted between two aluminum rings and then installed in the coating setup, which rotates the ring inside a box made of acrylic glass in a fume hood to maintain a clean atmosphere. No o-rings were used to exclude contamination from the o-ring material.

Coating solution preparation

Small chips of dPS were dissolved at room temperature in the solvent overnight while stirring with a Teflon-coated stirring bar in an airtight glass container with a chemical-proof screw-on plastic lid.

TABLE 3.2: Overview of the magnetic signals of the magnetized uncoated insulator rings for the n2EDM experiment detected at *BMSR-2*.

Insulator ring	Distance ring to SQUID mm	Surface	Magnetic signal nAm^2	Position °
I	410(5)	top	1.4(5) nAm^2	270(5)
I	410(4)	bottom	1.8(5) nAm^2	175(5)
I	75(4)	outer lateral	1.2(5) nAm^2	280(5)
II	410(4)	top	none	-
II	410(4)	bottom	1.9(5) nAm^2	315(5)
II	75(4)	outer lateral	none	-

Coating process

The first coating attempts were done with deuterated benzene instead of deuterated toluene as deuterated benzene has a higher vapor pressure than deuterated toluene and will therefore leave fewer traces in the coating as described in Ref. [Yaz20]. Additionally, deuterated benzene is significantly cheaper than deuterated toluene. Due to the high toxicity of benzene and to keep the rings free from contamination, clean room overalls, special gloves, gas masks, and safety goggles were used during the coating process. The insulator rings were also constantly discharged by grounding the aluminum plates holding it and using an anti-static gun every 20 min. The first coating attempt was done with ring II.

2.5 g of dPS was dissolved in 200 mL of deuterated benzene overnight. It was originally planned to apply four layers, with 50 mL of the solution for each layer. The ring was rotated with a stepper motor at a speed of 3 rpm for the ring. The first 50 mL of the solution evaporated in less than a minute. Therefore, it was decided to apply the remaining 150 mL of the solution at once. It took 7 min for the 150 mL of the solution to evaporate, but the distribution on the inner surface of the ring was very uneven. The evaporation rate of benzene was too fast to achieve good coatings, so benzene was replaced with toluene. To spread the already applied dPS more evenly, 200 mL of non-deuterated toluene was added to the slowly rotating ring (0.85 rpm). The expectation was that the toluene would dissolve the dPS and spread it more evenly on the surface of the ring. The toluene evaporated after 40 min. On top of this layer, 1 g of dPS dissolved in 100 mL deuterated toluene was applied.

It was planned to use the expensive deuterated solvents for the top layer only, while using the less expensive non-deuterated solvents for the layers below, as the quality of the top layer is the most critical for the UCNs. In theory, and according to Ref. [Yaz20], a marginal amount of the solvent would remain in the coating anyway.

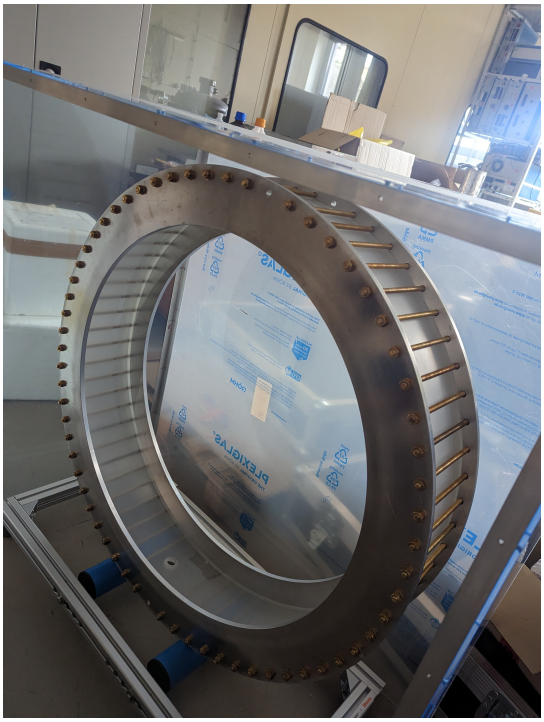

FIGURE 3.5: One of the Rexolite 1422 insulating rings mounted in the coating setup between the two aluminum plates.

For insulator ring I, which was coated after insulator ring II, the procedure was adjusted. First, 2.5 g of dPS dissolved in 400 mL of non-deuterated toluene was applied while the ring was rotated at 0.85 rpm. On top of this, a second layer with 1 g of dPS dissolved in 100 mL deuterated toluene was applied. The result for both insulator rings I and II was a surface with a shinier finish compared to the results reported in Ref. [Kuz08], but no visible air bubbles or major defects were observed.

3.5 Fermi pseudo-potential of the first set of insulating rings for the n2EDM precession chamber

The rings themselves are not suitable test objects due to their bulkiness and insufficient flatness, to measure the Fermi pseudo-potential of the coating on the insulating rings by cold neutron reflectometry. Any curvature in the rings poses a significant challenge in data analysis, as discussed in Ref. [CF20]. However, the UV windows, which were placed inside the UV window holes to seal them during the coating process, should have a similar coating on one side as the rest of the insulator ring's inner surfaces. These windows are flat and small enough to be used in cold neutron reflectometry measurements to determine the Fermi pseudo-potential of the coating. The only difference is that the UV windows were longer submerged in the coating solution, as

they are positioned lower than the inner surface of the ring. Consequently, the coating on them is predicted to be more regular and thicker than on the lateral inner surface of the insulating rings.

The Fermi pseudo-potential of the dPS-coated UV windows was measured at the polarized neutron reflectometer *NARZISS* at the Swiss Spallation Neutron Source *SINQ* using cold neutrons with a wavelength of 500(8) pm (from Ref. [PP12]). The given error represents the wavelength spread for the full width at half maximum. A detailed description of the apparatus can be found in Ref. [NAR] and a picture of the setup is shown in Figure 3.6. The measurements were conducted under the guidance of Bernhard Lauss.

FIGURE 3.6: The cold neutron beam line NARZISS which was used to measure the Fermi pseudo-potential of the coating of the insulating rings for the n2EDM experiment.

Cold neutrons were reflected at small angles from the dPS-coated UV windows. The angle was gradually increased until the cold neutrons were no longer reflected, as their kinetic energy perpendicular to the surface $E_{\text{kin}\perp}$ became too high. The angle at which the reflection stops is also known as the critical angle (θ_{crit}). Using Equation (3.1), the Fermi pseudo-potential can be calculated by measuring the critical angle and knowing the kinetic energy of the cold neutron beam perpendicular to the sample surface.

$$V_{\text{f}} = \sin^2(\theta_{\text{crit}}) E_{\text{kin}\perp} \tag{3.1}$$

For the measurements, the horizontal slits were set to 0.8 mm, 0.8 mm, 1.0 mm and 2.0 mm, and the vertical slits were set to 50 mm, 20 mm, 20 mm and 20 mm. The beam was adjusted using an uncoated window, and both sides of the windows (coated and uncoated) were measured, as well as a polished part of the Rexolite 1422 from the same block of material used to make the rings. The data can be fitted using Equation (3.2) with R for the reflectivity to extract the critical angle/Fermi pseudo-potential as shown for a single

UV window in Figure 3.7.

$$R(E_{\mathrm{kin}\perp}, V_{\mathrm{f}}) = \frac{\sqrt{\frac{2m_{\mathrm{n}}E_{\mathrm{kin}\perp}}{\hbar^2}} - \sqrt{\left(\sqrt{\frac{2m_{\mathrm{n}}E_{\mathrm{kin}\perp}}{\hbar^2}}\right)^2 - \left(\sqrt{\frac{2m_{\mathrm{n}}V_{\mathrm{f}}}{\hbar^2}}\right)^2}}{\sqrt{\frac{2m_{\mathrm{n}}E_{\mathrm{kin}\perp}}{\hbar^2}} + \sqrt{\left(\sqrt{\frac{2m_{\mathrm{n}}E_{\mathrm{kin}\perp}}{\hbar^2}}\right)^2 - \left(\sqrt{\frac{2m_{\mathrm{n}}V_{\mathrm{f}}}{\hbar^2}}\right)^2}} \tag{3.2}$$

The analysis was done with the help of Cornelis Doorenbos. The measured Fermi pseudo-potential are listed in Table 3.3, and they are consistent with the findings in Ref. [Kuz08], indicating that the windows, and consequently the insulating rings, were successfully coated with dPS. To differentiate the UV windows and to know the orientation of the insulating ring, one window holder was marked with a dot using a permanent marker which was tested to be non-magnetic at the PTB-Berlin.

TABLE 3.3: Overview of the Fermi pseudo-potential of the dPS coated UV windows, which were mounted during the coating of the insulator ring, measured at NARZISS.

Window	Fermi pseudo-potential neV
Ring I not marked	170(20)
Ring I marked	170(20)
Uncoated side	90(20)
Rexolite 1422	30(20)

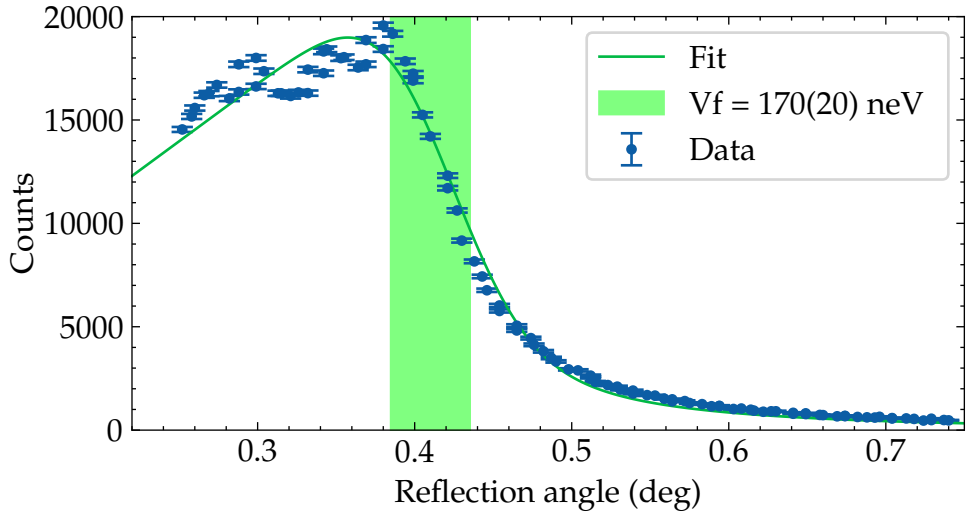

FIGURE 3.7: Data of the Fermi pseudo-potential measurement of the dPS coated UV window for the n2EDM precession chamber installed during the coating process of the Rexolite 1422 insulating ring I (side of the ring without marking).

3.6 Magnetic properties of the first coating of the first set of insulating rings for the n2EDM precession chamber

After the coating, the marked window on insulator ring I was scanned for magnetic contamination using the magnetic gradiometer at PSI, with the guidance of Victoria Kletz. A picture of the setup is shown in Figure 3.8.

The magnetic gradiometer at the PSI is a device, that measures the magnetic signature of different parts by moving them over an array of optical magnetometers in a magnetically shielded environment. No significant

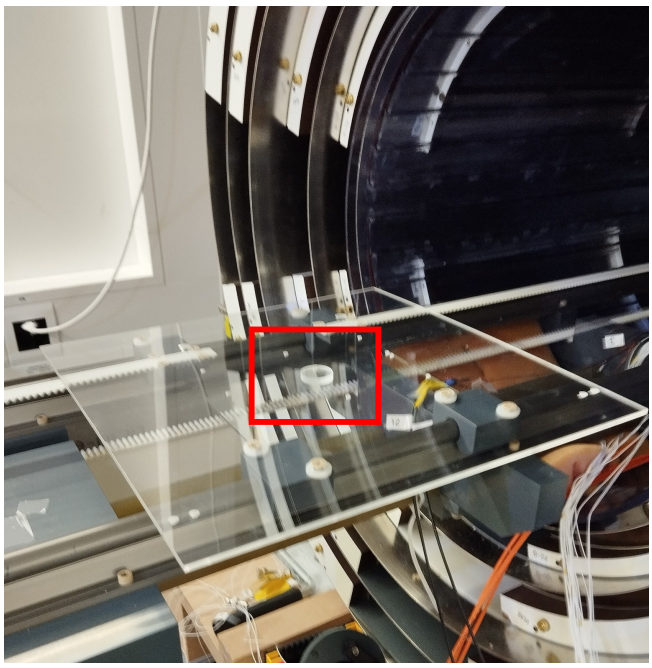

FIGURE 3.8: One of the dPS coated UV windows for the n2EDM precession chamber on the gradiometer cart (highlighted by the red rectangle), ready to be checked for magnetic properties.

magnetic signal from the coated UV window was detected in the magnetic gradiometer at the PSI which is sensitive to surface dipoles with a strength 0.1 nA m^2 measured at a distance of 25 mm (private communication with Victoria Kletz). Due to the need for the insulating rings at PSI for measurements with the n2EDM experiment and the availability constraints of the *BMSR-2*, it was not possible to allocate time to remeasure the full insulator rings for magnetic contamination at the *BMSR-2*. This will be done in the future when time permits.

3.7 First set of UV windows for the n2EDM precession chamber

There are two window holes in the lateral surface of the ring in which UV windows can be installed (see Appendix B). These UV windows are needed to read out the mercury magnetometer by a strong UV laser at 254 nm wavelength. The UV windows, which fit in the holes of the insulator rings, are $5.0^{+0.0}_{-0.2}$ mm thick and have a diameter of 25.4(3) mm. They are made out of fused silica and were bought from *THORLABS*.[4]

Fused silica is not UV sensitive, but its Fermi pseudo-potenital of 90 neV is significant lower than that of the rest of the insulator rings as shown in Table 2.1. Therefore, the windows need a coating on the side facing the neutrons which has a high Fermi pseudo-potential. dPS, which is used for the inner lateral surface of the insulating rings, is not a suitable coating, as it absorbs UV light and degrades over time. The coating for the previous experiment was done with dPE dissolved in deuterated xylene applied with spin coating as described in Ref. [Kuz08]. Spin coating is a technique, where on a spinning target droplets of a solution with coating material and solvent are disposed. Due to the spinning, the coating will be pushed away from the center of the spinning target to the outside. During the spread out of the solution, the solvent is evaporating and leaves a layer of the coating material behind. Described in Ref. [Kuz08] is the deposition of 8 mL of a solution with 0.75 % dPE (>98 % degree of deuteration from *AMAR* for more details see Appendix C) in deuterated ortho-xylene with 1300 rpm at 130 °C. Resulting in 75 nm thick coatings for windows with a diameter of 50 mm and 57 mm. The dPE used for the coating of the UV windows was from the same manufacturer as the one used in Ref. [Kuz08]. For the spin coating, the setup shown in Figure 3.9 was used.

3.7.1 Coating of the first set of UV windows for the n2EDM precession chamber

The windows for the n2EDM experiment have a diameter of 25.4 mm and therefore the amount of solution was adjusted to 4 mL to obtain a 75 nm thick coating as described in Ref. [Kuz08]. The windows were preheated on a hot plate to 140 °C and then mounted on the spin coater. The dPE-xylene-solution was kept at 140 °C and applied with a preheated glass syringe. As the first coating was not transparent, adjustments to the coating process were made. The adjustments and the result of the coatings are summarized in Table 3.4. The first four windows were used to dial in the coating process and then windows 5, 6, 7 and 8 were produced in the same way to have four windows for the rings which could also be tested for reproducibility of the coating process.

[4] https://www.thorlabs.com/thorproduct.cfm?partnumber=WG41050

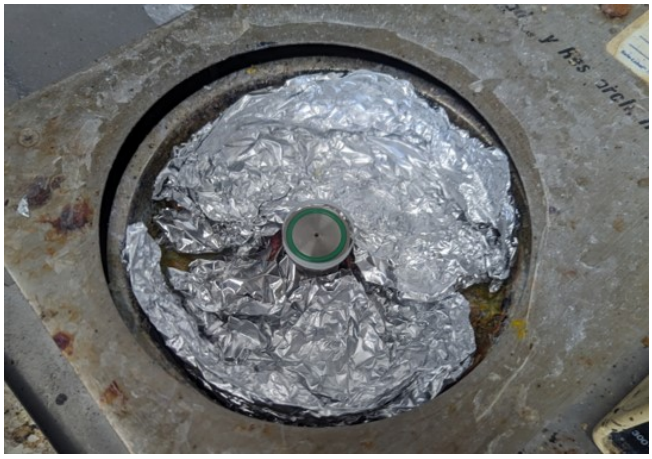

FIGURE 3.9: One of the UV windows for the n2EDM precession chamber mounted in the spin coater to coat them with dPE to increase the Fermi pseudo-potential.

TABLE 3.4: Overview of the coating process for the dPE coated UV windows for the n2EDM precession chamber.

Number	result	comment
1	opaque	as described in Ref. [Kuz08]
2	thin	1 mL solution
3	thick	2 mL solution
4	irregular	2 mL solution at 1500 rpm
5	thin	1 mL solution at 850 rpm
6	thin	1 mL solution at 850 rpm
7	thin	1 mL solution at 850 rpm
8	thin	1 mL solution at 850 rpm
9	no coating	control window

3.7.2 UV transmission properties of the first set of UV windows for the n2EDM precession chamber

An important property of the UV windows for the n2EDM experiment is the transmission of UV light with the wavelength of 254 nm for the readout of the mercury magnetometer. This was measured and analyzed with Wenting Chen and Lukas Kostal. The setup to measure the indirect transmission of the UV windows is shown in Figure 3.10.

The UV laser light is split by a beamsplitter. One part of the beam is guided to the photodiode I to monitor the power of the UV laser, while the other part is transmitted through the UV window. The power of the laser light transmitted through the UV window is then measured using photodiode II. The transmission is calculated with the measurements of the power

at photodiode II without a UV window. From Table 3.5, it is evident that the

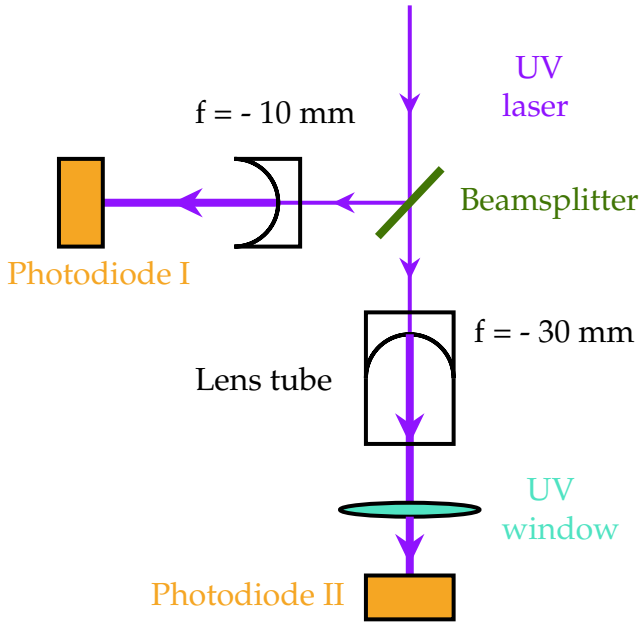

FIGURE 3.10: Schematic drawing of the setup used to test the 254 nm laser light transmission of the dPE-coated UV windows, ensuring their suitability for the n2EDM experiment.

coating of the windows slightly reduces the transmission of UV light compared to the uncoated window (number 9). However, the reduction in transmission measured with the setup shown in Figure 3.10 is not large enough to pose a problem for the n2EDM experiment.

TABLE 3.5: Overview of indirect measured laser light transmission of the dPE coated UV windows for the n2EDM precession chamber at at a wavelength of 254 nm using the setup shown in Figure 3.10.

Number	Power at photodiode I μW	Transmission %
1	86(6)	88(7)
2	84(6)	87(7)
3	83(6)	85(7)
4	86(6)	80(7)
5	79(6)	85(7)
6	85(6)	92(7)
7	86(6)	94(7)
8	87(6)	92(7)
9	83(6)	99(7)

3.7.3 Magnetic properties of the first set of UV windows for the n2EDM precession chamber

The same way the UV windows inserted during the coating process were measured for their magnetic properties, the dPE coated windows, which are compatible with the UV laser of the mercury magnetometer, were tested for magnetic contamination. This was done and analyzed with the help of Vic-

TABLE 3.6: Overview of the magnetic properties of the UV windows for the n2EDM precession chamber after coating measured with the gradiometer at PSI.

Number	Magnetized ΔB pT	Demagnetized ΔB pT	Fitted magnetic dipole strength nAm^2
1	3(1)	6(1)	none
2	15(1)	5(1)	2.3(3)
3	11(1)	5(1)	1.2(2)
4	6(1)	4(1)	none
5	4(1)	4(1)	none
6	4(1)	3(1)	none
7	4(1)	3(1)	none
8	3(1)	3(1)	none
9	7(1)	3(1)	none

toria Kletzl and Eliza Kukowka. The results are summarized in Table 3.6. The UV windows are non-magnetic enough to use them in the n2EDM experiment, as no magnetic dipoles larger than the $5\,nA\,m^2$ limit set in Ref. [Ayr+21] were measured.

3.7.4 Fermi pseudo-potential of the first set of UV windows for the n2EDM precession chamber

To verify that the dPE-coated UV windows are also compatible with UCNs, the Fermi pseudo-potential was measured in the same way as for the dPS-coated windows, as described in Section 3.5. The results are summarized in Table 3.7. The Fermi pseudo-potential is consistent and in agreement with Ref. [Kuz08], leading to the conclusion that the windows can be used for the n2EDM experiment.

TABLE 3.7: Overview of the measured Fermi pseudo-potential using cold neutron reflectometry on the dPE coated UV windows for the n2EDM precession chamber at NARZISS.

Number	Result	Fermi pseudo-potential neV
1	opaque	no fit possible
2	thin	210(20)
3	thick	no fit possible
4	irregular	210(10)
5	thin	230(20)
6	thin	190(20)
7	thin	200(20)
8	thin	210(10)
9	no coating	90(20)

Chapter 4

Ultracold neutron storage in the n2EDM experiment

4.1 First storage curve

As described in Subsection 2.3.2, measuring the electric dipole moment of the neutron with the n2EDM experiment involves first guiding and then storing the neutrons in the precession chamber. After the storage period, the neutrons are guided to the detectors. The number of neutrons counted by the detectors depends on the transmission efficiency of the neutrons to and from the precession chamber, as well as the storage efficiency of the precession chamber itself. To quantify the storage properties of the precession chamber and separate them from the transmission efficiency of the neutron guides, measurements with different storage periods can be performed. By combining these measurements and fitting the counts of UCNs after different storage times, a storage time constant for the precession chamber can be extracted. Since the loss probabilities for a single UCN are energy-dependent, as shown in Equation (2.6), the fit can result in multiple storage time constants for an ensemble of UCNs with a range of energies.

Measurement campaigns are divided into runs for the n2EDM experiment. A run typically consists of multiple measurements. At the time the data was taken, the person operating the n2EDM experiment usually decided when to start a new run and end the previous one.

The first results of such storage measurements for polarized UCNs (runs 2785-2788) are shown in Figure 4.1. The precession chamber was opened for 50 s after start of the UCN production (filling time). This filling time of 50 s was optimized for storage measurements of 120 s. The data points for the top and bottom chambers were fitted using a double exponential fit according to Equation (4.1). The fit parameters are summarized in Table 4.1. The double exponential fit is not chosen for any specific physical motivation; it is selected because it requires the fewest parameters to fit the data points, with a reduced χ^2 close to 1. A consequence of choosing the double exponential fit is that the neutrons are split into two energy groups. The lower energy group has a longer storage time because they interact with the walls of the experiment less frequently, resulting in a lower probability of losses.

$$N(t) = N_1 \exp\left(-t/\tau_1\right) + N_2 \exp\left(-t/\tau_2\right) \tag{4.1}$$

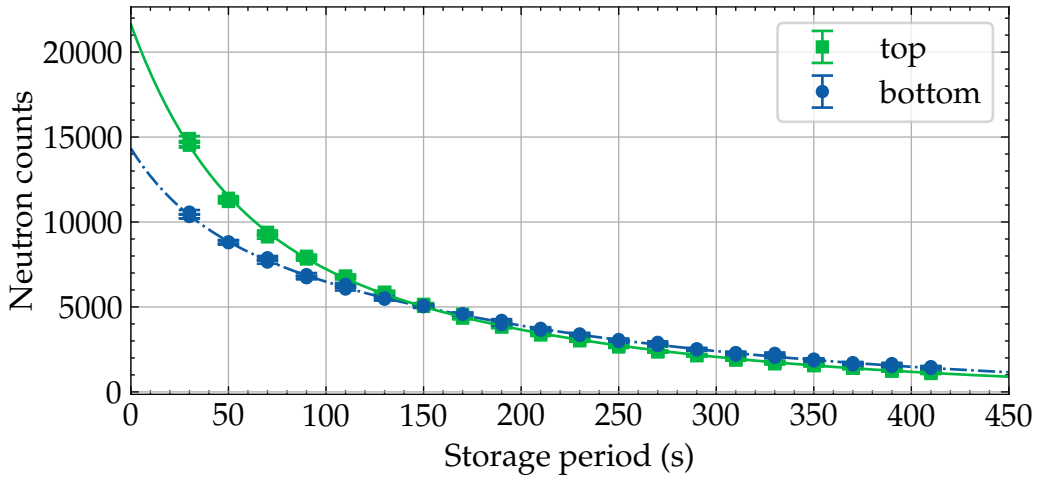

FIGURE 4.1: Storage curve for the top and bottom precession chambers with polarized UCNs. Data from runs 2785 – 2788 of the n2EDM experiment were used. The lines indicate the double exponential fits of the data with the parameters summarized in Table 4.1.

TABLE 4.1: Overview of the parameters used to fit the n2EDM storage curve simulation shown in Figure 4.1 using Equation (4.1).

Chamber	N_1	τ_1 s	N_2	τ_2 s	χ^2/ndf
top	10 900(300)	43(2)	10 800(300)	181(3)	1.7
bottom	4000(400)	30(4)	10 300(100)	206(2)	1.6

The difference in storage performance between the top and bottom chambers is primarily due to the height difference to the beamport of the chambers, which leads to variations in the energy spectrum of the UCNs filled into the precession chambers, as UCNs are affected by gravity (described in Section 2.1.3). This hypothesis was confirmed by measuring UCN storage characteristics of insulating rings at the same height.

In Figure 4.2, the measured storage curve is compared to the Monte Carlo simulations of the n2EDM experiment as described in Ref [Ayr+21]. The simulation data was provided by Geza Zsigmond and Guillaume Pignol. Both the simulated and experimental data were fitted using the same equation (Equation 4.1), with the results summarized in Table 4.2. The χ^2/ndf values, which are higher than 1, suggest that this may not have been the optimal fit for the data, but it facilitates a straightforward comparison between the experimental and simulated data. For the uncertainties in the simulated data, only the standard error was considered. Systematic errors were not accounted for. According to Ref. [Ayr+21], the typical deviation from measurement for UCN Monte Carlo simulations is approximately 15 %. However, as the inputs for UCN Monte Carlo simulations are adjusted over time to align

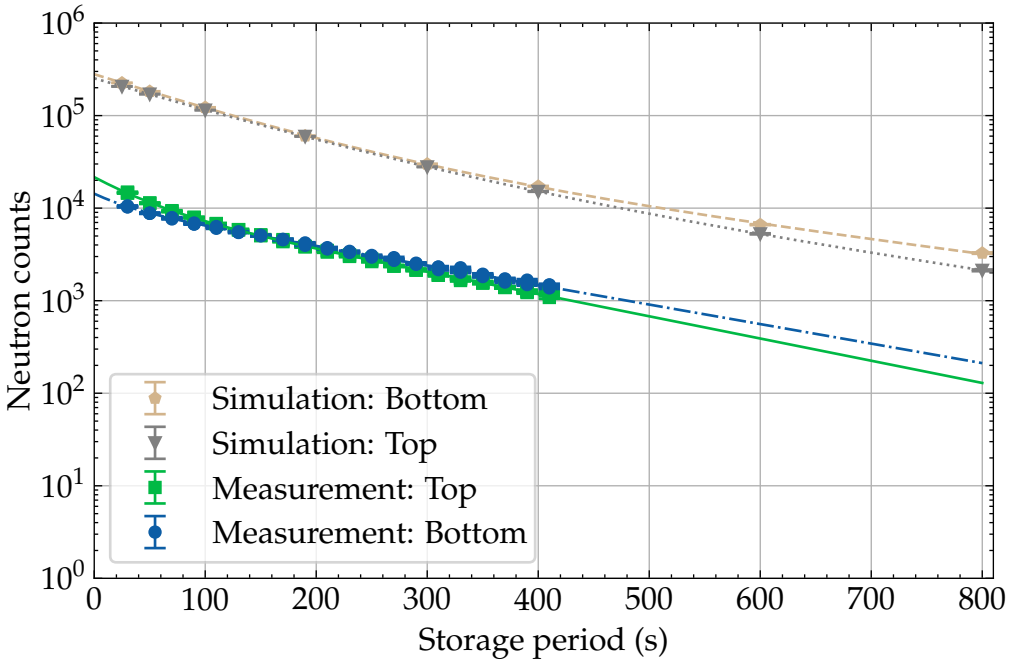

FIGURE 4.2: Storage curve for combined counts of top and bottom precession chambers with polarized UCNs. Data from runs 2785 – 2788 of the n2EDM experiment were used. For the simulations, the data from Ref. [Ayr+21] split for bottom and top chamber which was simulated with MCUCN was used. The lines indicate the double exponential fits of the data using the Equation 4.1 with the parameters summarized in Table 4.2.

with measurement results, and since the simulations have not yet been adjusted for the new n2EDM experiment (these being the first measurements), the uncertainties in the simulations might be larger. What we can deduce from this comparison is that the measured counts are about a factor of 10 lower than the simulated UCN counts. Additionally, the distribution of the UCNs with long and short storage times and the values of the long and short from the measurements τ_1 and τ_2 differ from the simulation results.

The first experimental results differ substantially from simulated predictions, underscoring the necessity for further investigation into factors affecting neutron storage performance. The discrepancies in storage time constants and UCN distributions are less significant than the differences in neutron counts at short storage times. Additionally, the uncertainties for simulated storage time constants and distributions are typically higher than for count rates at short storage times, as the material properties of the n2EDM precession chamber, which are less precisely known than the UCN source performance, become more important with longer storage times. Therefore, the primary focus of the investigation was to increase neutron counts in the chamber.

TABLE 4.2: Overview of the parameters used to fit the first n2EDM storage curve data from Ref. [Ayr+21] shown in Figure 4.2 using Equation (4.1).

Chamber	N_1	τ_1 s	N_2	τ_2 s	χ^2/ndf
Simulation Top	209 000(9000)	111(4)	44 000(9000)	260(20)	3.0
Simulation Bottom	230 000(9000)	102(4)	50 000(10000)	290(30)	11.5

4.2 Energy spectrum of stored UCNs

To investigate the reasons for the lower number of UCN counts compared to simulations, a method was developed to isolate specific parts of the UCN energy spectrum within the chamber and measure the amount of stored UCNs for those energy ranges. This was achieved by using the SCM as an energy filter for one spin state. As the required kinetic energy for LFS to pass the magnetic field potential increases with an increased magnetic field (60 neV T^{-1}), lower portions of the energy spectrum can be filtered out by increasing the magnetic field. The energy acceptance of the n2EDM experiment is also influenced by a foil located at the center of the SCM. This foil, made of aluminum with 3 % magnesium (yielding a Fermi pseudo-potential of approximately 54 neV), acts as an additional potential barrier for the neutrons. Furthermore, the energy acceptance is modified by gravity due to the height difference from the SCM to the precession chamber. This height variation affects the neutrons' potential energy, further refining the spectrum of UCNs that can be stored and measured in the chambers.

By changing the magnetic field produced by the SCM, the storage efficiency for different segments of the UCN energy spectrum can be systematically examined, thereby determining if there are specific energy ranges where discrepancies between experimental results and simulations are most pronounced. A similar measurement technique was recently employed to characterize the UCN beamline at Los Alamos National Laboratory, as described in Ref. [Won+23]. In Figure 4.3, the results of the measurements are summarized, and two calculations for different maximum storable UCN energies are indicated.

The calculated polarization P_i for a magnetic field strength of the SCM B_i and the maximum storable UCN energy in the precession chamber $E_{\text{storable, max}}$ is given by Equation (4.2):

$$P_\mathrm{i} = \frac{N_\mathrm{HFS} - N_\mathrm{LFS}}{N_\mathrm{HFS} + N_\mathrm{LFS}} = \frac{\int_{0\,\mathrm{T}}^{\frac{E_{\text{storable, max}}}{\mu_\mathrm{N}}} (\mu_\mathrm{N} \cdot B)^{2.5}\, dB - \int_{B_\mathrm{i}}^{\frac{E_{\text{storable, max}}}{\mu_\mathrm{N}}} (\mu_\mathrm{N} \cdot B)^{2.5}\, dB}{\int_{0\,\mathrm{T}}^{\frac{E_{\text{storable, max}}}{\mu_\mathrm{N}}} (\mu_\mathrm{N} \cdot B)^{2.5}\, dB + \int_{B_\mathrm{i}}^{\frac{E_{\text{storable, max}}}{\mu_\mathrm{N}}} (\mu_\mathrm{N} \cdot B)^{2.5}\, dB} \tag{4.2}$$

It is assumed that the number of neutrons at a given energy is proportional to the energy raised to the power of 2.5, as described in Ref. [Gol91].

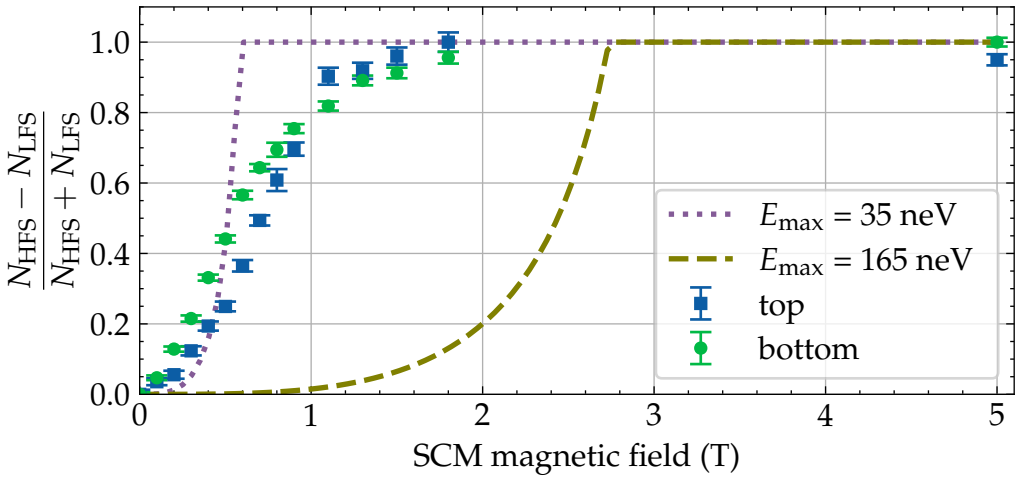

FIGURE 4.3: Measurements were conducted with a storage period of 120 s, varying the field strength of the SCM. Data from runs 2904 – 2944 of the n2EDM experiment, with a filling time of 50 s, were used. The counts were scaled such that the minimum corresponds to an asymmetry of 0 and the maximum to an asymmetry of 1. The two lines indicate the calculated asymmetry for a UCN source spectrum scaling with $N(E) \propto E^{2.5}$, assuming the momenta of the UCNs are perpendicular to the magnetic field of the SCM and without considering the effects of gravity.

Since the calculations do not consider effects such as gravity, the momentum distribution of the UCNs, or transmission changes for high-field seeking (HFS) neutrons due to acceleration in a high magnetic field, UCN energy-depended storage losses or the presence of UCNs with slightly higher energies than the Fermi pseudo-potential, they do not align very well with the experimental data. Additionally, the spin transport for the UCNs and the spin analyzing efficiency of the USSA at the time the data were taken might have fluctuated with the different field strengths of the SCM.

Nevertheless, it is visible that the maximum storable energy in the chamber is closer to 35 neV (the calculated Fermi pseudo-potential for uncoated Rexolite 1422) than to 165 neV (Fermi pseudo-potential of dPS).

These findings were later confirmed by Monte Carlo UCN simulations for this setup, performed by Geza Zsigmond, which included the effects of gravity, energy-dependent loss channels, and the momentum distribution of the UCNs. The reason for a maximum storable energy well below 165 neV is likely due to exposed surfaces of either the aluminum (V_f = 54 neV) of the electrodes or the Rexolite 1422 (V_f = 37 neV) of the insulating rings, or both.

4.3 Investigation of potential low Fermi pseudo-potential surfaces in the n2EDM precession chamber

To determine the cause of the differing performances compared to the simulations in Ref. [Ayr+21] a new measurement series was conducted. The

inner surface of the insulating ring was covered with a thin sheet of copper (V_f = 169 neV) as show in Figure 4.4. By measuring with this setup, both

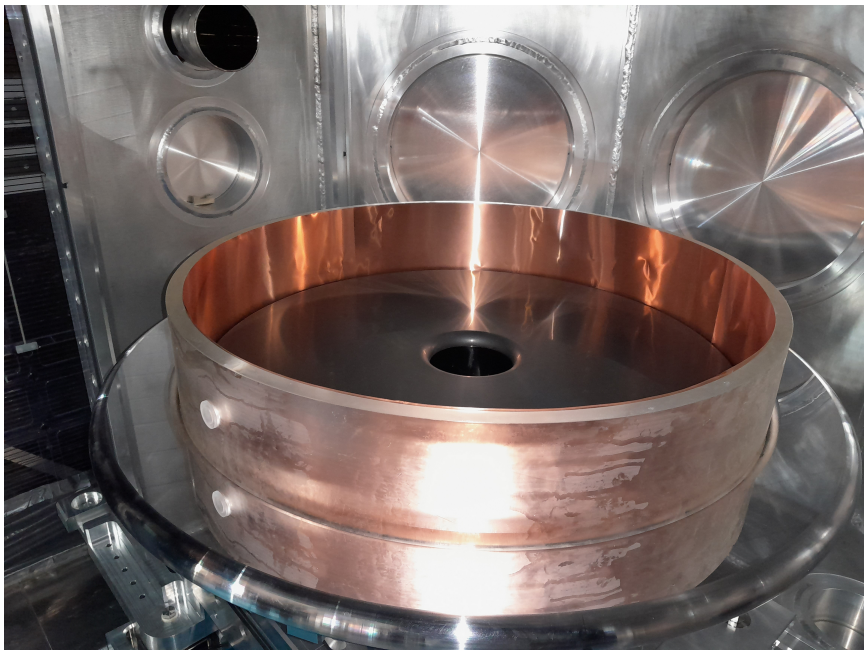

FIGURE 4.4: The inner surface of dPS-coated insulating ring I of the n2EDM precession chamber covered with a thin sheet of copper. Details about the copper sheet can be found in Appendix D.

with and without the copper sheet, and comparing the results, it can be determined if there is an issue with the coating of the rings. A good dPS coating (V_f = 165 neV) should have a storage performance, similar to the copper foil, although small discrepancies are expected. If the dPS coating performs slightly worse, it could be due to the slightly lower Fermi pseudo-potential. Conversely, if it performs slightly better, it might be because there are fewer gaps in the setup with the rings compared to the copper foil. However, these measurements do not rule out potential problems with the coating of the electrodes. If the electrodes limit the storage performance, no significant difference in the storage measurements with and without the copper sheet will be visible. The copper sheet (> 99.8 % Cu) used was manufactured by thyssenkrupp the material number is EN 13599-CW004A it was cold rolled and the delivery condition is specified as R240 further information about the material can be found in Appendix D.

To quickly test the insulating rings without having to remount the heavy and fragile HV-electrode, the HV-electrode was replaced with a copper plate (V_f = 169 neV)[5], as shown in Figure 4.5. By performing storage measurements for the insulating ring and the insulating ring covered with the copper sheet using the setup shown in Figure 4.4, the storage curves shown in Figure 4.6 were obtained. The variation in the number of measurement points is due

[5]Diameter = 900 mm, thickness = 2 mm, cut by Merki + Hitz AG, Cu > 99.8 %, specified as btp half hard. Merki + Hitz AG could not trace the exact manufacturer, but it is either Promethan or Häuselmann Metall GmBH.

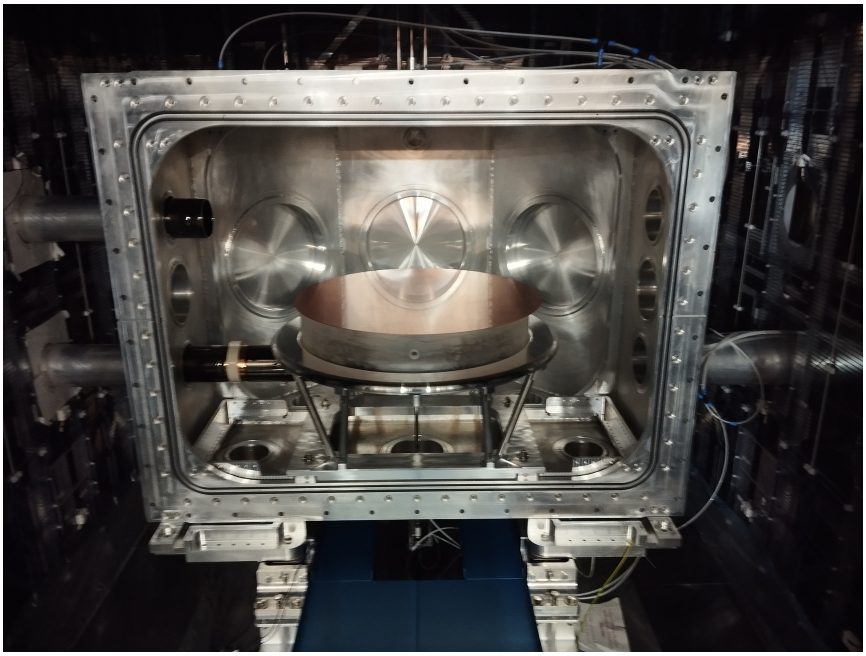

FIGURE 4.5: Test setup for the insulating rings for the n2EDM precession chamber with the HV-electrode replaced by a copper plate for easier transition between setups. More information about the copper in Footnote 5.

to different production cycles of the UCN source, causing the data taken for the insulating ring without the copper sheet during longer storage times to be contaminated by background counts and not usable. Additionally, the amount of measurement points was determined by the individuals responsible for the measurements, resulting in variations across different measurements. The parameters for the exponential fits in Figure 4.6 are shown in Table 4.3. The copper sheet, which has only a slightly higher Fermi pseudo-

TABLE 4.3: Overview of the parameters for fitting the n2EDM storage curve data shown in Figure 4.6 using Equation (4.1) to compare the storage performance of the dPS coatings of the insulating rings for the n2EDM precession chamber with a copper sheet.

Ring	lateral surface	N_1	τ_1 s	N_2	τ_2 s	χ^2/ndf
I	coating	15 000(1000)	16(8)	22 000(200)	150(20)	1.6
I	copper sheet	180 000(4000)	53(2)	52 000(2000)	150(5)	2.0

potential than dPS, performs significantly better in storage measurements than the insulating rings. The copper sheet allows a considerably higher number of UCNs to be stored. The similar storage time constant is likely due to surface imperfections, gaps, and the higher mean energy stored. While the copper sheet is not an ideal surface and there are gaps between the electrode and the copper sheets, it still stores more UCNs (especially at short storage

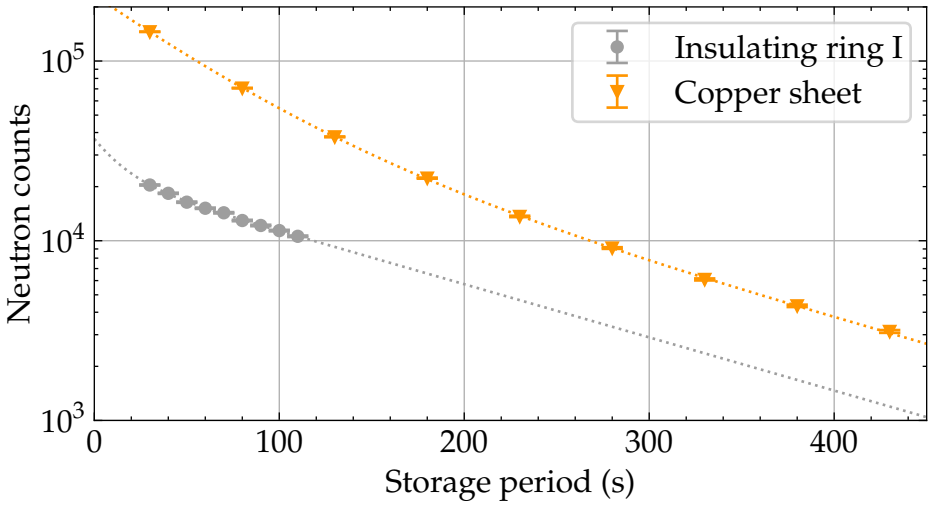

FIGURE 4.6: Comparison of polarized UCN storage performance of the insulating ring I (Run 3198, grey) and the inner surface of the insulating ring covered with a thin sheet of copper (Run 3251, orange). The dotted lines indicate the double exponential fit. Fit results are shown in Table 4.3.

periods). This indicates that the dPS coating of the ring has worse UCN storage properties than predicted in Ref. [Ayr+21].

4.4 Recoated insulating rings of the n2EDM precession chamber

Since there is potential for improvement with the coating of the rings, as shown in Subsection 4.3, and there is no reasonable expectation of lowering the Fermi pseudo-potential with another layer of coating, it was decided to enhance the storage performance of the n2EDM experiment by recoating the insulating rings and reducing uncoated spots on their surface.

As it was unclear why the "rotating lake" technique described in Section 3.4 did not yield the expected results, the decision was made to apply the dPS coating to the inner surface of the insulating rings using a "brushing" technique. This "brushing" technique, where a clean room tissue[6] soaked in a solution of toluene and dPS is used to apply the coating to a surface, had already been tested on smaller scales (private communication with Bernhard Lauss).

The used chemicals in the following paragraph are specified in Appendix C. For the recoating of the insulating ring II, 2.65 g of dPS (>98 % degree of deuteration, measurements are shown in Ref. [Yaz20]) was dissolved in 200 mL of deuterated toluene. Approximately 20 % of the solution was applied in multiple steps using a pipette on the inner surface of the ring. For each step, the solution was transferred with the pipette to the lowest point

[6]Manufacture: Dynoclean, product code: 2014011, type: heavyWipe, Polyester, 140 g cm^{-2}

of the inner surface of the standing insulating ring and spread out with the pipette. After allowing the solvent to evaporate, the ring was manually rotated slightly, and the next section of the inner surface was coated in the same way. The remaining solution was then applied using a soaked clean room tissue with a polishing movement (moving in circles), completing two full rotations of the ring as shown in Figure 4.7.

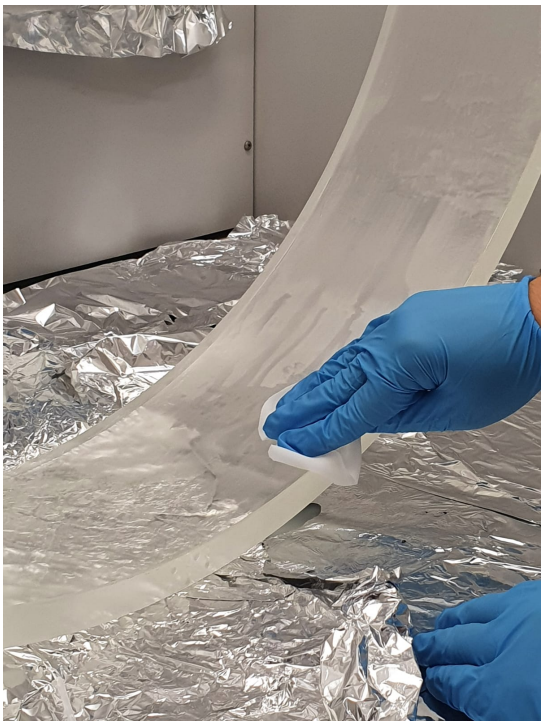

FIGURE 4.7: Picture of the coating process using the "brushing" technique for the insulating rings for the n2EDM precession chamber. The clean room tissue, specified in Footnote 6, is soaked in a deuterated toluene dPS solution. The solution is applied by a polishing movement.

The insulating ring I was coated with 2.60 g of dPS dissolved in 200 mL deuterated toluene. In this coating attempt, the solution was heated to approximately 70 °C, and three rotations of the ring were performed using a clean room tissue with a back-and-forth movement instead of a circular movement. As the UCN storage performance of insulating ring I was significantly worse than that of insulating ring II, as shown in Figure 4.8, a third coating was applied. For the third coating of the insulating ring, 2.60 g of dPS was dissolved in 200 mL non-deuterated toluene, as no deuterated toluene was available on short notice. For this attempt, the solution was applied at room temperature using a clean room tissue with a polishing movement. The coating was applied in six rotations of the ring. Roughly 15 mL of the solution was spilled and therefore not applied in the coating process. The results of these measurements are shown in Figure 4.8. The insulating ring II with the first dPS coating was not measured in this exact setup, as it was established that the storage performance of the insulating rings was similar

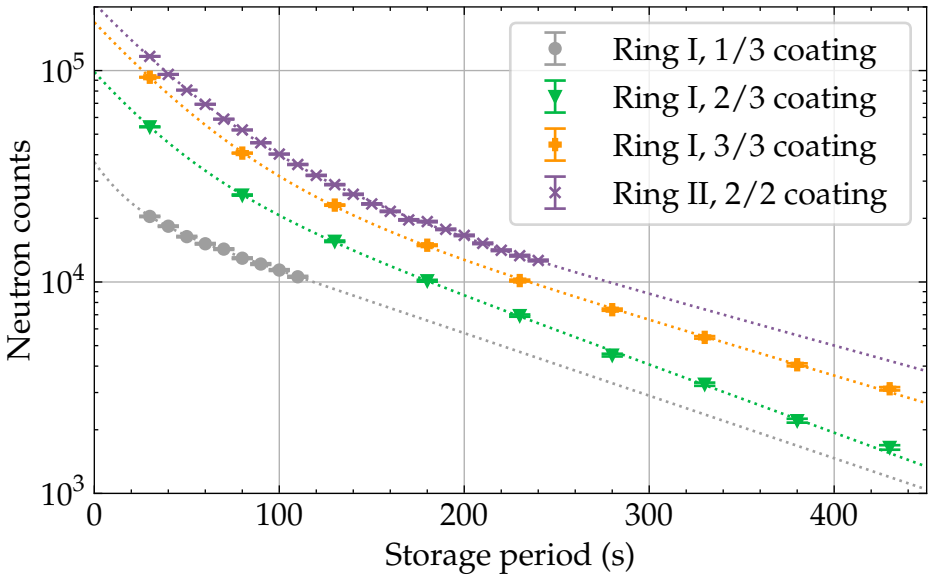

FIGURE 4.8: Comparison of the different coating attempts of the insulating rings for the n2EDM precession chamber to each other with the setup shown in Figure 4.5 and polarized UCNs. Data from runs 3198 – 3251 of the n2EDM experiment, with optimized filling times, were used. The dotted lines indicate the double exponential fits. The fit parameters are summarized in Table 4.4.

after the first coating. In Figure 4.8, it is clearly visible that the recoating improved the UCN storage properties of the insulating ring, especially for short storage periods. However, the coating process does not appear to be entirely reproducible. For instance, one recoating was sufficient for insulating ring II, while even after two recoating attempts, insulating ring I still exhibits worse storage performance than insulating ring II. From these measurements, it is also unclear if the insulating rings are now entirely coated in dPS or if there are still exposed Rexolite 1422 surfaces. The data were fitted using Equation (4.1) and the results of the fits are summarized in Table 4.4. The drastic

TABLE 4.4: Overview of the parameters for fitting the n2EDM storage curve data shown in Figure 4.8 using Equation (4.1).

Ring	coating	N_1	τ_1 s	N_2	τ_2 s	χ^2/ndf
I	1	15 000(1000)	16(8)	22 000(2000)	150(20)	1.6
I	2	61 000(3000)	32(3)	38 000(2000)	135(3)	4.0
I	3	130 000(3000)	39(2)	40 000(2000)	166(5)	4.0
II	2	162 000(3000)	40(2)	40 000(5000)	180(20)	6.4

performance increase at short storage times, which tapers off for longer storage periods, indicates that there are still uncoated areas. As smaller, uncoated

areas take longer for UCNs to encounter, this results in losses occurring only at longer storage periods.

4.5 Energy spectrum of stored UCNs in n2EDM precession chamber with recoated insulating rings

To verify that the recoating of the insulating rings improved the energy acceptance of the n2EDM precession chamber, the same measurements described in Section 4.2 were performed for the recoated insulating rings. The measurement results are shown in Figure 4.9.

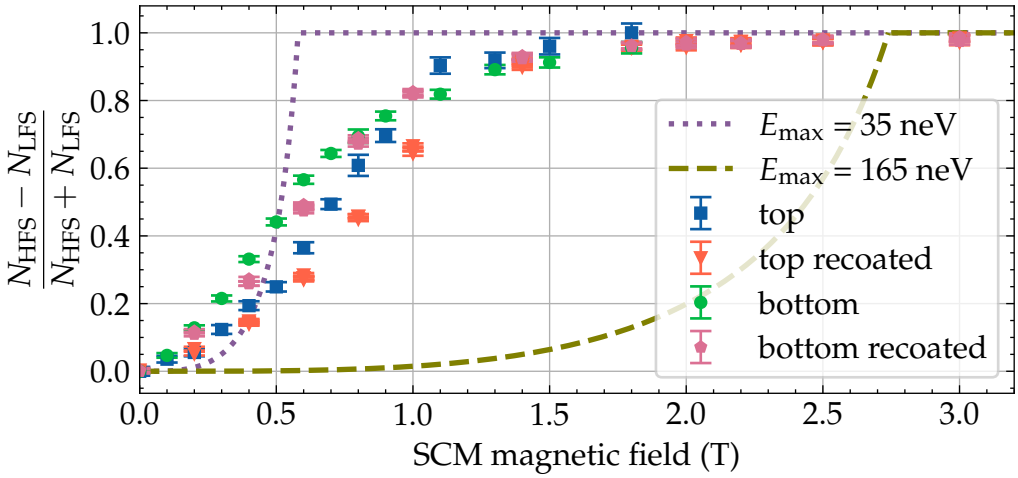

FIGURE 4.9: Measurements with 120 s storage period with different field strength of the SCM. Runs 2904 – 2944 and 3290 – 3314 of n2EDM were used. The counts were scaled so the minimum would be at an asymmetry of 0 and the maximum at a asymmetry of 1. The two lines indicate the calculated asymmetry for an UCN source spectrum scaling with $N(E) \propto E^{2.5}$ assuming the momenta of the UCNs is perpendicular to the magnetic field of the SCM and without considering gravity.

For low magnetic fields, a lower asymmetry is measured than before the recoating of the insulating rings, indicating a shift in the stored UCN spectrum to higher energies. As the average storable UCN energy in the chamber increased, more LFS neutrons can pass the magnetic potential of the magnetic field created by the SCM. This results in lower measured asymmetries for low magnetic fields. For higher magnetic fields, this effect vanishes, especially in comparison with the line for a maximum storable energy of 165 neV. This suggests that the coating is still not perfect and improvements are possible. This was also confirmed by Monte Carlo UCN simulations performed by Geza Zsigmond.

4.6 Storage measurements with recoated insulating rings

A storage curve for the recoated insulating rings is shown in Figure 4.10, with the fit parameters summarized in the Table 4.5.

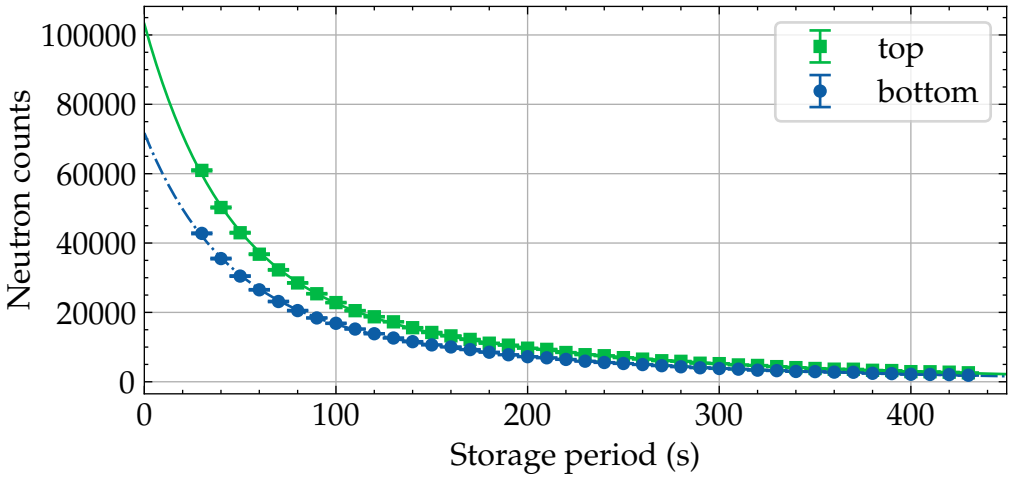

FIGURE 4.10: Storage curve for the top and bottom precession chambers with the recoated insulating rings with polarized UCNs. Data from run 3480 of the n2EDM experiment with a filling time of 30 s were used.

TABLE 4.5: Overview of the parameters used to fit the n2EDM storage curve data measured with the recoated insulating rings (Ring I 3/3 coating, Ring II 2/2 coating) with polarized UCNs shown in Figure 4.10 using Equation (4.1).

Chamber	N_1	τ_1 s	N_2	τ_2 s	χ^2/ndf
top	74 000(700)	41(1)	29 100(500)	174(2)	4
bottom	73 300(800)	38(1)	31 200(500)	178(2)	4

This measurement demonstrates a clear increase in storable UCNs for short storage periods compared to the first measured storage curve (Figure 4.1 , with $N_{1,\text{top}} + N_{2,\text{top}} = 21700(500)$ and $N_{1,\text{bottom}} + N_{2,\text{bottom}} = 14300(500)$). While the short storage time constant τ_1 is comparable with the one extracted from the first storage curve, the long τ_2 storage time constant is smaller. This finding aligns with the observation in Section 4.5 that the average energy in the chamber for short storage periods is higher. However, with longer storage periods, these neutrons encounter the still uncoated surface on the insulating rings and escape from the precession chamber lowering the long τ_2 storage time constant.

These curves represent the status at the end of 2023 for the n2EDM experiment, no newer data was used in this thesis. Although substantial advancements have been made, continued efforts will be required to refine the

coating process and increase the amount of stored UCNs in the n2EDM experiment. Ultimately, this will lead to a more sensitive measurement of the neutron's electric dipole moment as described in Equation (2.13).

Chapter 5

UCN storage in the τSPECT experiment

5.1 Feasibility of neutron lifetime measurement with τSPECT

The UCNτ collaboration has reported the most accurate measurement of the neutron lifetime to date, measuring a total of about 38×10^6 neutrons after storage periods ranging from 20 s–1550 s, as detailed in Ref. [UCN+21]. To achieve competitive results, the τSPECT experiment needs to measure a comparable number of neutrons after storage.

In Ref. [Aul+23] it is shown that the τSPECT experiment at the research reactor TRIGA Mainz stores approximately 700 – 100 UCNs for storage periods between 50 s – 1500 s respectively. Therefore, to measure a neutron lifetime competitive with the one published by the UCNτ collaboration, the τSPECT experiment would need to conduct $\approx 10^5$ measurement cycles at the research reactor TRIGA Mainz. The research reactor TRIGA Mainz is available for $\approx$ 700 h per year for UCN production, with UCNs produced in reactor pulses every 12 min. With some measurement cycles extending beyond this duration, the average time for a measurement cycle during data collection is $\approx$ 20 min. This results in an estimated 30 years of data collection under the conditions reported in Ref. [Aul+23], which is not feasible.

Thus, an increase in the number of stored neutrons per measurement or a higher number of measurements per year is necessary to achieve a neutron lifetime measurement with the τSPECT experiment that has a statistical uncertainty comparable to that reported in Ref. [UCN+21].

5.2 Improving the UCN source at the beam port D of the research reactor TRIGA Mainz

The objective of this study was to enhance the performance of the UCN source at the TRIGA research reactor Mainz to enable a feasible and competitive neutron lifetime measurement using the τSPECT experiment. Efforts focused on optimizing the UCN source to increase the number of stored neutrons per measurement and decrease the setup time of the UCN source

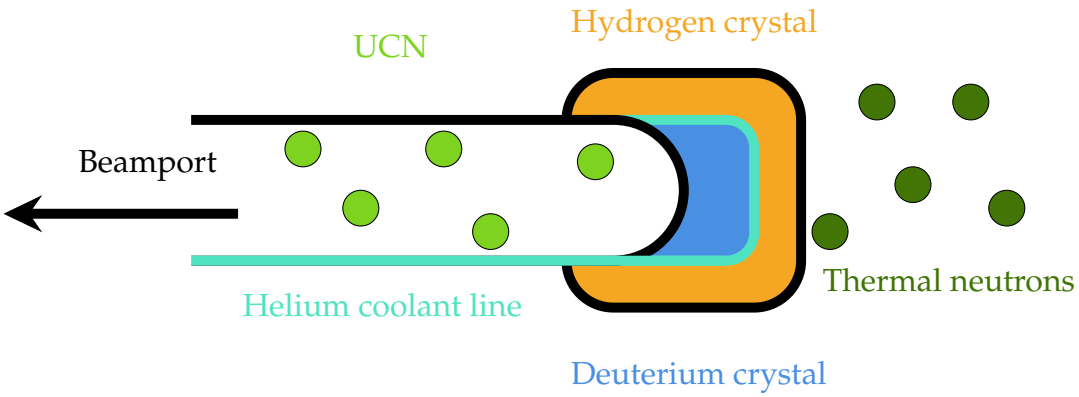

FIGURE 5.1: Schematic drawing of the UCN source at beam port D of the research reactor TRIGA Mainz, showing the positions of the deuterium and hydrogen crystals, as well as the liquid helium coolant line.

for beam times. This aims to increase the available measurement time for τSPECT experiment.

To increase the number of UCNs guided to the experiments and to enhance the availability of the UCN source at the research reactor TRIGA Mainz, the freeze-out process and post freeze-out treatment of the deuterium and hydrogen crystals was investigated. This work was conducted under the guidance of Simon Kaufmann, the UCN source coordinator at the research reactor TRIGA Mainz.

A detailed study on growing deuterium crystals for UCN production is available in Ref. [Kor+22]. The temperature and growth rate of the deuterium crystal significantly affect its shape, surface, and density, all of which influence UCN production and extraction. Temperature-dependent effects for the hydrogen premoderator crystal and the deuterium converter crystal, shown in Figure 5.1, have been discussed in Ref. [Kah+17] and Ref. [Kah20] for the UCN source at the research reactor TRIGA Mainz. In these references, it is concluded that the number of UCNs produced per measurement cycle increases with the number of previous measurement cycles for the same crystal.

It is suggested that the brief thermal load on the crystals during a reactor pulse heats the surface of the crystals causing them to melt, with the hydrogen/deuterium evaporating partially, coincidentally can be measured as a pressure increase of 1 mbar – 30 mbar within the beam tube. As soon as the thermal load from the reactor pulse decreases, the hydrogen/deuterium freezes again, which results in a higher density or better surface for UCN production and extraction. A better surface would be smooth rather than having solid deuterium powder on top. This ensures that neutrons moving out of the crystal to the beam port are not reflected by the powder layer back into the crystal. This goes hand in hand with an observed decrease of deuterium evaporation in the following UCN production cycles, indicating an improved cooling efficiency of the crystal.

However, if the improvement in UCN production is caused by repetitive thermal load on the crystals, this can theoretically be enhanced by reducing

cooling during the freeze-out process, during the first pulses of a beamtime, or during periods when no UCNs are produced, such as overnight. This could lead to a higher and more stable UCN output from the source at research reactor TRIGA Mainz.

The coolant (liquid helium) flow to the deuterium and hydrogen crystals can be controlled by a needle valve[7], and reducing the flow rate (by closing the valve) might optimize the crystal conditions through temporarily increasing the temperature. The standard setting for the needle valve during normal operation is 10.4 mm; decreasing this value reduces the flow rate and consequently increases the temperature. To test this hypothesis, measure-

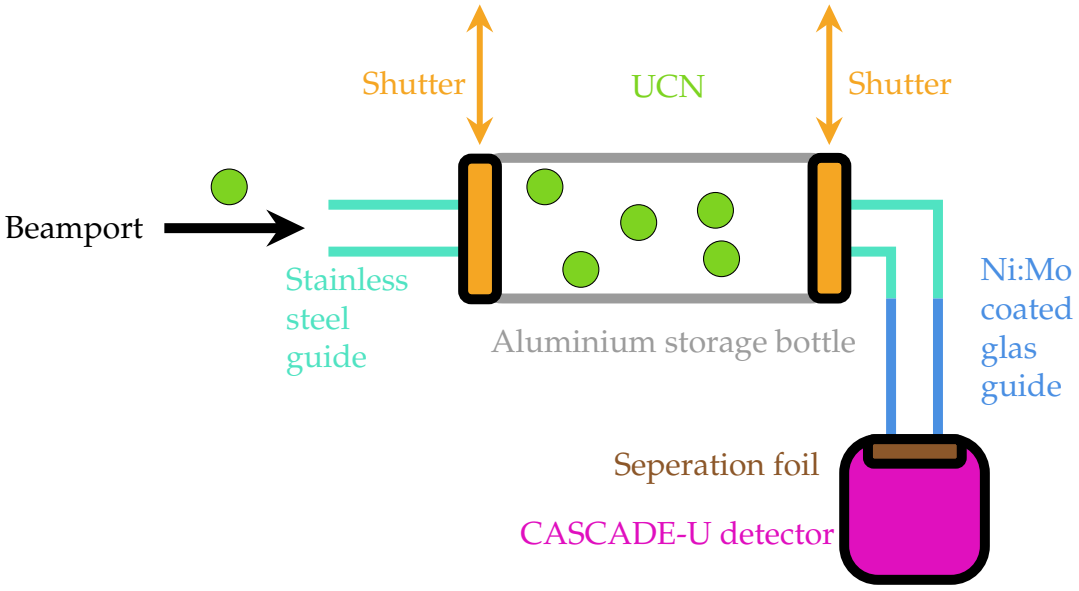

FIGURE 5.2: Schematic drawing of a aluminum storage bottle setup used to compare UCN source performance under different conditions.

ments were conducted using an aluminum UCN storage bottle with a Fermi pseudo-potential of 54 neV and a volume of approximately 9696(16) cm^3. The bottle was closed by two stainless steel shutters with a Fermi pseudo-potential of 180 neV. The setup is shown in Figure 5.2 and Figure 5.3. The needle valve settings were varied to reduce the helium coolant flow during the UCN production to increase the maximum temperature at the crystal during reactor operation.

The advantage of using a storage bottle lies in its relatively simple setup, which ensures good reproducibility between beam times. Additionally, this setup is far more convenient to measure at different UCN sources compared to relocating an entire experiment like the τSPECT experiment.

The neutrons were guided to the bottle using stainless steel guides with an inner diameter of 66 mm and a Fermi pseudo-potential of 180 neV. Additionally, two ^{58}Ni:Mo (85:15) reflective surfaces with a Fermi pseudo-potential of 305 neV were used to direct the UCNs through two 90° angles to

[7]Manufacturer: Oerlikon Leybold Hereaus, type: 283 30 B, serial number: 15407

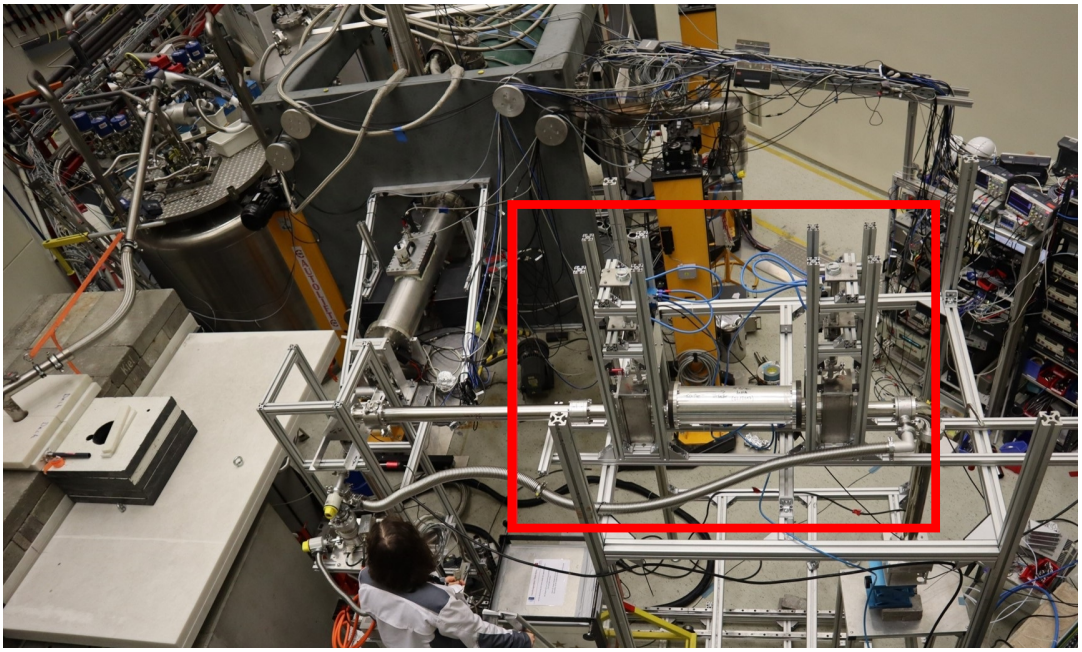

FIGURE 5.3: Picture of the aluminum storage bottle setup to monitor the source performance at beam port D of the research reactor TRIGA Mainz. This setup was used to compare the Mainz UCN source and PSI UCN source for neutron lifetime experiments at research reactor TRIGA Mainz. The storage bottle is highlighted by the red rectangle.

the height of 1525 mm from the center of the bottle to the center of the beamport for the measurements. The neutrons were detected with a commercially available UCN detector called CASCADE-U. The CASCADE-U detector utilizes gas electron multiplier cells (see Ref. [Sau97]) with an argon-carbon dioxide mixture (82:18) as the counting gas. To separate the counting gas from the experimental vacuum, the CASCADE-U detector employs a 100 µm thick separation foil made of aluminum with 3 % magnesium, resulting in a Fermi pseudo-potential of approximately 54 neV. Neutrons with kinetic energies below 54 neV are not transmitted through the foil. To overcome the Fermi pseudo-potential of the foil, a stainless steel 90° elbow piece with Fermi pseudo-potential of 180 neV with an 87 cm long vertical Ni:Mo (85:15) coated glass guide with an inner diameter of 66 mm and a Fermi pseudo-potential of 225 neV was mounted behind the bottle. This setup accelerates the neutrons through gravity, enabling neutrons with initial kinetic energies below 54 neV to pass through the separation foil.

The first measurement series was conducted after freezing out the crystal, with the goal of demonstrating that reducing the coolant flow during a UCN production cycle affects the crystals and determining which coolant flows are sustainable during pulses without melting the entire crystals.

After optimizing the filling time (grey area in Figure 5.4), measurements with a 5.5 s filling time for the aluminum bottle and a storage period of 20 s were taken. The data was normalized to the pulse energy of research reactor TRIGA Mainz during UCN production. During the UCN production

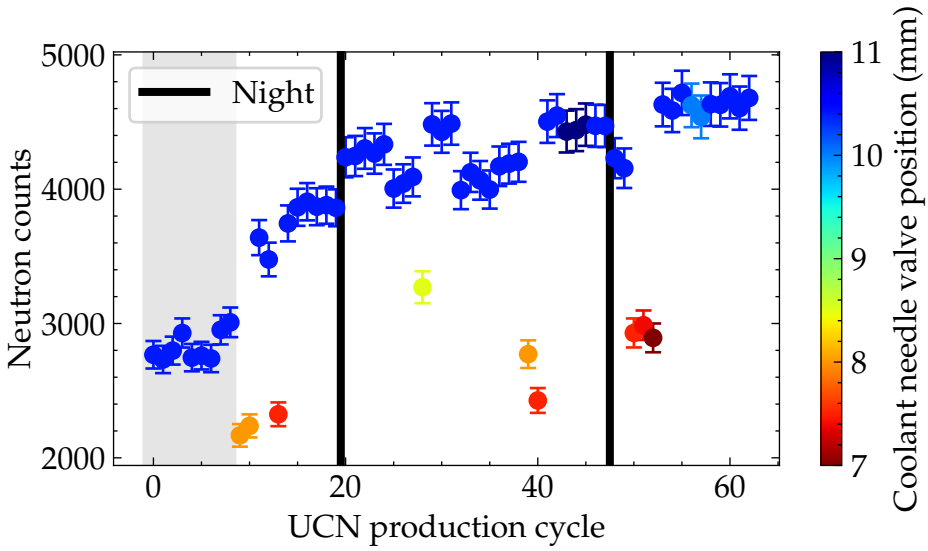

FIGURE 5.4: UCN counts for test of UCN production at research reactor TRIGA Mainz with increased temperature of the UCN source by reducing the coolant flow during a UCN production cycle via lowering the position of the coolant needle valve (colorbar). Data taken with an aluminum storage bottle, a storage time of 20 s, and a filling time of 5.5 s. Data points in the gray shaded area were used for the filling time optimization.

cycle with reduced coolant flow, neutron counts dropped drastically, implying that parts of the premoderator or converter crystal had melted, leaving less solid hydrogen/deuterium to moderate/convert the neutrons. In subsequent UCN production cycles following this reduction of coolant flow and partial melting of the crystal, an increase in the number of neutron counts was observed. Slight increases in coolant flow during operation did not significantly raise the number of storable UCNs. The lowest coolant needle valve setting determined by Simon Kaufmann to be sustainable without a high likelihood of losing the crystals was 7.5 mm.

Following these measurements, hydrogen and deuterium of the crystal were evaporated and then frozen-out again, but due to time restraints, the flow rate of the deuterium from storage to the growing crystal was slightly increased, from $0.30(5)\,\mathrm{L\,min^{-1}}$ to $0.50(5)\,\mathrm{L\,min^{-1}}$.Using a flow controller from MKS Instruments.[8] Then with the same storage bottle setup, tests were conducted to determine if reducing the helium coolant flow to the lowest sustainable coolant needle valve setting (7.5 mm) could achieve a stable and high UCN output from the UCN source without stepwise adjustments (Figure 5.5), as previously done (Figure 5.4). The baseline performance of the new crystal was first established with UCN production cycles. These already yielded an improved UCN production to the last measurement shown in Figure 5.4 of initially 5000 neutrons, probably caused by the increased deuterium flow rate during freeze-out, which will be investigated further in the next paragraph. To ensure the transferability of the needle valve settings

[8] type: 1640A-362, serial number: 016418123, MKS PR4000 readout

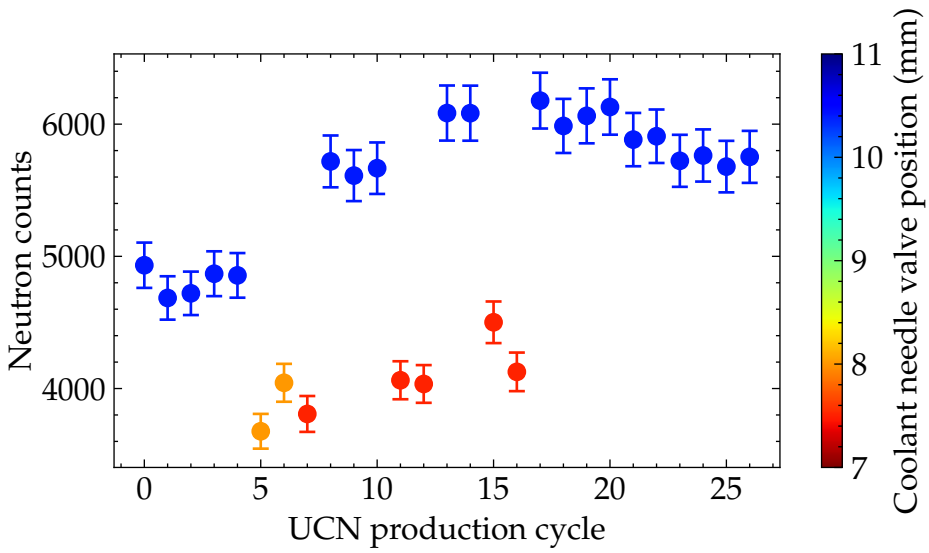

FIGURE 5.5: UCN counts for optimized procedure to enhance UCN production at research reactor TRIGA Mainz through increased temperature of the UCN source by reducing coolant flow via adjustment of the coolant needle valve position (colorbar). Data were acquired using an aluminum storage bottle with a storage time of 20 s and a filling time of 5.5 s.

and to avoid immediately melting of the crystal, two test production cycles were conducted with a slightly less extreme needle valve setting of 8.0 mm. After confirming that the crystal would likely withstand the reduced coolant flow at a needle valve setting of 7.5 mm, multiple sequences were performed. These sequences involved reducing the coolant flow to 7.5 mm and then measuring the UCN performance with the needle valve set back to 10.4 mm.

From the measurements shown in Figure 5.5, it is evident that the procedure of reducing the coolant flow by setting the needle valve to a lower flow rate reproducibly increases the UCN output of the UCN source at the research reactor TRIGA Mainz after a new freeze-out of the deuterium and hydrogen crystals. This method accelerates the process of reaching a stable plateau and ensures that more UCNs are available for longer periods of operation. Without the thermal treatment of the crystals, it would take multiple days for the source to achieve a stable high UCN output as shown in Ref. [Kah20].

As it was shown that thermal treatment of the deuterium and hydrogen crystals can increase the UCN output of the source at the research reactor TRIGA Mainz, the freeze-out process of the crystals was also investigated. This process can significantly alter the properties of the crystals, as described in Ref. [Kor+22]. For the freeze-out process, instead of adjusting the coolant valve settings, the flow rate of deuterium into the cryostat was increased as much as possible, limited only by the available cooling power. This approach has the additional benefit of accelerating the freeze-out process, thereby reducing the time needed to prepare the UCN source at TRIGA Mainz and increasing the available measurement time. In theory, the freeze-out would occur at higher temperatures because more deuterium needs to be cooled per

unit of time with the same cooling power as before. Therefore, the deuterium flow rate for the freeze-out was increased from 0.3 L min^{-1} to 0.8 L min^{-1} for the formation of a new deuterium crystal.

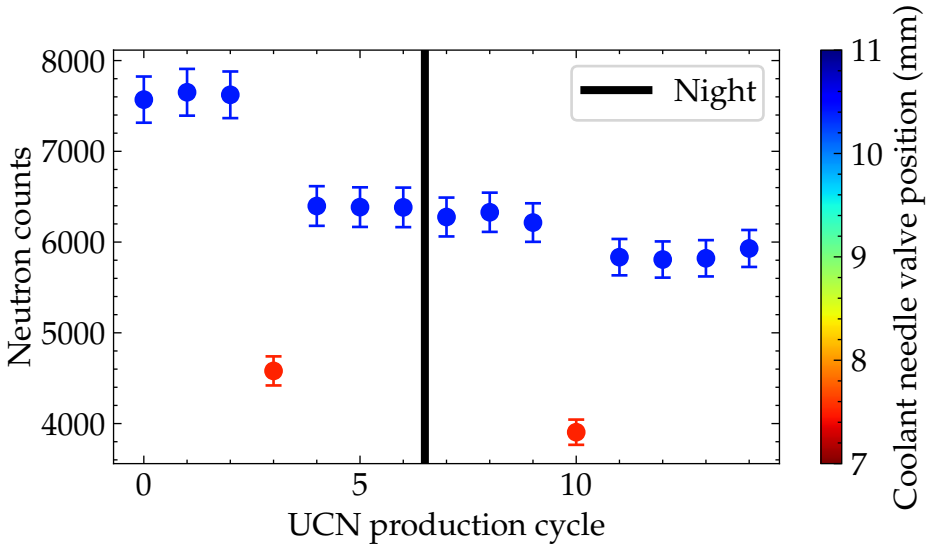

FIGURE 5.6: UCN counts for a faster freeze-out of the deuterium crystal (to enhance UCN production at research reactor TRIGA Mainz) and increased temperature of the UCN source by reducing coolant flow via adjustment of the coolant needle valve position (colorbar) after freeze-out. Data were acquired using an aluminum storage bottle with a storage time of 20 s and a filling time of 5.5 s.

After the freeze-out with the increased deuterium flow rate, which reduced the time required for the freeze-out by a factor of $\approx \frac{1}{2}$, it was tested whether the source performance could be further increased by increasing the temperature of the crystals, as shown in Figure 5.6.

The new freeze-out technique led to the highest UCN output among the three measurements presented in this chapter, increasing the number of neutrons available at the start of the beamtime by approximately a factor of 2. However, additionaly increasing the temperature after the freeze-out, which typically increases the neutron counts for a standard freeze-out with a deuterium flow rate of 0.3 L min^{-1} as shown in Figure 5.4 and Figure 5.5, decreased the UCN output for a crystal with a faster freeze-out.

These measurements indicate that additional heating of the crystal is not always beneficial for the UCN performance of the UCN source at research reactor TRIGA Mainz. Depending on the underlying reason why increased temperature of the UCN source increases the neutron counts, which is not fully understood, two possibilities arise. Either the freeze-out results in the optimal surfaces of the crystals, which then degrade due to heating and reformation, or the ideal position/shape of the crystal has a bistable maximum, dropping to less ideal positions/shapes at both lower and higher temperatures.

However, it was demonstrated that increased temperature of the UCN source at research reactor TRIGA Mainz can significantly enhance both the

production and stability of the UCN output. The new freeze-out technique has proven to be superior to thermal treatment of the crystals after their formation during UCN production cycles. With these findings, the freeze-out time for the deuterium crystal can be reduced from 2 days to 1 day, thereby increasing the available data collection time for experiments at the research reactor TRIGA Mainz. Additionally, this technique has increased the number of neutrons available per production cycle. While these improvements will benefit future UCN experiments at the research reactor TRIGA Mainz, they are still insufficient to achieve a competitive neutron lifetime measurement with the τSPECT experiment. This highlights the need to relocate the τSPECT experiment to a UCN source capable of producing higher UCN densities and providing more measurement time than the source at research reactor TRIGA Mainz to measure a neutron lifetime competitive with Ref. [UCN+21].

5.3 Comparison of UCN source performances for τSPECT

The UCN source performance of different UCN sources worldwide has already been compared in Ref. [Rie16] and Ref. [Bis+17]. The comparison was conducted using a UCN storage bottle with a Fermi pseudo-potential of 180 neV and a volume of approximately 32 044(164) cm^3. While these are typical parameters for experiments searching for the neutron's electric dipole moment, the current generation of neutron lifetime experiments, particularly the τSPECT experiment, focuses on storing lower energy neutrons in a smaller volume.

The energy range stored with the τSPECT experiment depends on the position during filling of the spin flipping unit and the way the spin flipping unit is operated. Using only the innermost spin flipper, the energy acceptance of the τSPECT experiment is depending on the position of the spin flipping unit is approximately 0 neV – 20 neV for UCNs at experiment height as described in Ref. [Aul+23]. To estimate the storable UCNs per measurement for the τSPECT experiment, another measurement series was required. As one of the sources with highest UCN densities in Ref. [Rie16] and Ref. [Bis+17] a comparison between the PSI and research reactor TRIGA Mainz for neutron lifetime experiments, was conducted. The measurements at beamport West-1 at PSI involved Martin Engler, Bernhard Lauss, Niklas Pfeifer, Ingo Rienäcker, Dieter Ries, Mauro Schaufelbühl, and myself.

Due to the Fermi pseudo-potential of the deuterium crystal (V_f = 104 neV), UCNs produced in a deuterium crystal and exiting to the vacuum of the beamline receive a kinetic energy boost of 104 neV. At the Mainz UCN source, this boost ensures that all UCNs have enough kinetic energy to travel through the 100 µm thick vacuum separation foil, which is made of aluminum with 3 % magnesium (V_f = 54 neV) and positioned at the same height as the crystals and the beamport. As a result, the energy spectrum

of UCNs at beamport height at the research reactor TRIGA Mainz starts at 104 neV. In contrast, at the PSI UCN source, UCNs are produced 1300 mm below the beamport in a vessel with a 500 µm thick lid made of aluminum with 3 % magnesium ($V_f = 54$ neV). Consequently, at beamport height at PSI, the UCN energy is shifted by 133 neV. To exit the beamport, UCNs must travel through a 100 µm thick vacuum separation foil made of aluminum with 3 % magnesium ($V_f = 54$ neV), which results in the UCN energy spectrum at PSI beamport starting at 54 neV. Additionally, the production time window for UCNs at the TRIGA Mainz research reactor is in the order of milliseconds. In contrast, at the PSI UCN source, the production time is typically 8 s. For the

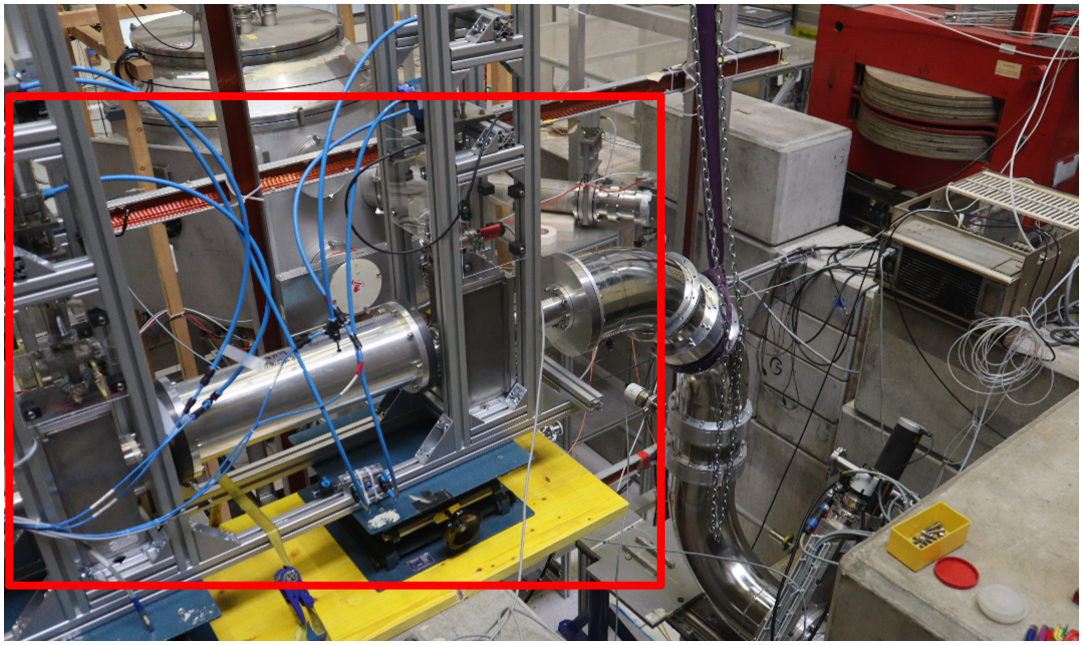

FIGURE 5.7: Picture at PSI Villigen of the aluminum storage bottle setup to compare the UCN source at research reactor Mainz and the UCN source at PSI for neutron lifetime experiments. The storage bottle is highlighted by the red rectangle.

comparison measurement, an aluminum UCN storage bottle with a Fermi pseudo-potential of 54 neV and a volume of 9696(16) cm^3 (Ref. [Kah20]) was used, closely matching the maximum storable energy (47 neV) and volume (10 700 cm^3) of the τSPECT experiment, shown in Figure 5.3.

To establish a baseline for the performance of the research reactor TRIGA Mainz, UCN storage curves were measured with the bottle at a height of 1525 mm from the center of the bottle to the center of the beamport, comparable to a typical operational height for the τSPECT experiment.

For the baseline at PSI, storage curves at different heights were measured, as the UCN spectrum changes due to the reduced kinetic energy of UCNs moving up in the gravitational field of the Earth (102 neV/m), as described in Subsection 2.1.3. At PSI, the beamline consists of stainless steel tubes with an inner diameter of 200 mm and a Fermi pseudo-potential of 180 neV. To connect the aluminum storage bottle with the beamline, an adapter flange was

used to reduce the beamline diameter to 66 mm in front of the bottle shown in Figure 5.7. While in Mainz the same beamline as described in Subsection 5.2 was used with an inner diameter of 66 mm and a Fermi pseudo-potential of 180 neV. The neutrons were guided to the storage using bent stainless steel tubes. To connect the bottle at different heights, small adjustments to the beamline were necessary. The height for the PSI setup was measured from beamport exit to the center of entrance guide of the bottle.

At both PSI and Mainz, the neutrons were detected using the same CASCADE-U detector, as described in Subsection 5.2. At PSI, two stor-

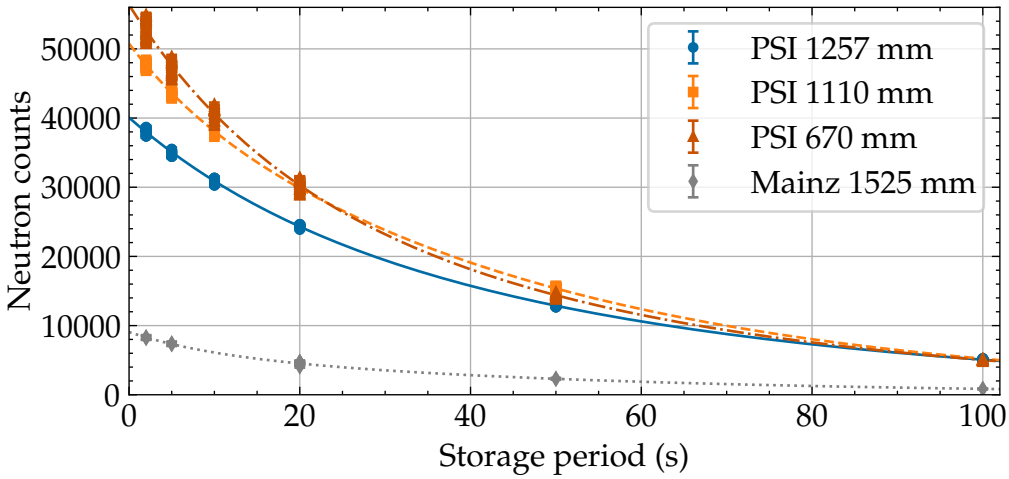

FIGURE 5.8: Storage curve for the aluminum storage bottle, comparing measurement conditions for neutron lifetime experiments at the UCN sources at PSI and the research reactor TRIGA Mainz. The labels indicate the different measurement heights, and the lines the double exponential fits of the data points using Equation (4.1).

TABLE 5.1: Overview of the parameters used to fit the storage curve data measured with an aluminum storage bottle at PSI and research reactor TRIGA Mainz. Data points in Figure 5.8 and Figure 5.9 were fitted using Equation (4.1).

Location	Height mm	Delay s	N_1 k	τ_1 s	N_2 k	τ_2 s	χ^2/ndf
PSI	1257	0	11(1)	19(2)	30(1)	57(2)	1.5
PSI	1257	35	3(3)	26(13)	10(3)	61(10)	0.7
PSI	1110	0	6(1)	8(2)	45(1)	46(1)	2.7
PSI	1110	35	6(3)	20(8)	15(3)	55(7)	3.3
PSI	670	0	20(2)	16(2)	37(2)	50(2)	19.3
PSI	670	35	9(1)	16(2)	17(1)	50(2)	0.9
Mainz	1575	0	3.0(5)	10(3)	6.1(6)	51(3)	1.2

age curves for each height with optimized filling times were measured. One

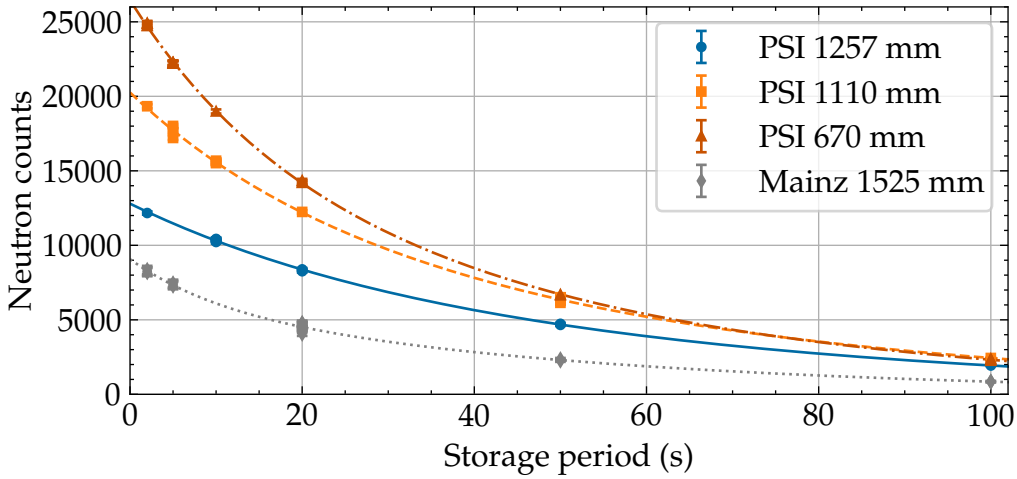

FIGURE 5.9: Storage curve for the aluminum storage bottle comparing measurement conditions for neutron lifetime experiments at the UCN sources at PSI and the research reactor TRIGA Mainz with 35 s delay after UCN production for the PSI measurement. This was done to mimic a filling of the n2EDM experiment before a measurement with the τSPECT experiment. The labels indicate the different measurement heights, and the lines the double exponential fits of the data points using Equation (4.1).

set of measurements assumed the τSPECT experiment as the sole user of the UCN source. The other set simulated conditions where neutrons were first extracted from another beamport to imitate the filling of the n2EDM experiment for 35 s before filling the bottle (or later the τSPECT experiment). The setups are shown in Figure 5.3 and Figure 5.7 the storage curves are shown in Figure 5.8 and Figure 5.9 and the parameter of the fits are summarized in Table 5.1.

These measurements show that at any given height, even with a delayed filling of 35 s, more UCNs were stored in the storage bottle at PSI compared to the research reactor TRIGA Mainz. This results in an increase in the number of initially filled neutrons in the storage bottle per measurement, with an approximate gain of 5 without a delay in filling and 3 with a 35 s delay for filling the storage bottle at a height of 670 mm.

It should be noted that there is a trend for shorter storage time constants at lower heights, which can be interpreted as the filled neutrons at these lower heights having higher mean energy. This is plausible since the energy spectrum is less decelerated by gravity at lower heights. The χ^2/ndf for the fit at 670 mm without a delayed filling significantly deviates from one, indicating that the fit model probably does not accurately describe the data points. This might be because separating the UCNs into just two energy groups may not accurately describe the stored UCNs for this measurement. At this low height, even more high-energy neutrons are stored without a delay in filling, indicating a more complex energy distribution. To enable better comparison with the other results, it was decided to retain the double exponential fit for this measurement series.

As the energy acceptance of the aluminum bottle (0 neV–54 neV) and the τSPECT experiment (0 neV–20 neV) for UCNs differ, these measurements cannot be directly translated to determine the optimal height for the τSPECT experiment nor provide an exact estimation of the storable neutrons at PSI with the τSPECT experiment. Nevertheless, these measurements can be used to gain insights into the UCN energy spectrum at PSI and can be utilized for estimations or simulations to compare the Mainz and PSI UCN sources for neutron lifetime experiments.

The UCN source at PSI is typically in operation from the start of May to the end of December, 24 hours a day, 7 days a week, with occasional breaks for infrastructure maintenance. Therefore, not only is the number of neutrons per measurement higher at PSI, but the available time for UCN production is also significantly larger, with approximately 3500 h per year compared to 700 h per year at the research reactor TRIGA Mainz. Additionally, UCN production is available every 5 min, which will reduce the average measurement duration compared to the 12 min intervals at the research reactor TRIGA Mainz. As a result, measurements with shorter storage periods can be conducted in less than 12 min, further enhancing the efficiency of data collection at PSI UCN source compared to the research reactor TRIGA Mainz.

From this measurement and considering the extended operation time of the UCN source at PSI, one can deduce that, in the best-case scenario the UCNs per measurement are increased by a factor of 5. This allows the measurement time in years to be reduced by at least a factor of 25, considering the 5 times greater available measurement time per year. Even in the worst-case scenario, the UCNs per measurement are increased by a factor of 3 a reduction factor of 15 is still realistic. Thus, a competitive neutron lifetime measurement with the τSPECT experiment at the PSI UCN source is achievable within approximately 2 years, making it a feasible and practical time frame for a neutron lifetime measurement.

5.4 First measurements of τSPECT at the PSI UCN source

From Section 5.3 it is clear that relocating the τSPECT experiment from the research reactor TRIGA Mainz to the PSI UCN source is essential to achieve a competitive neutron lifetime measurement with the experiment.

Therefore, the τSPECT experiment was moved from the research reactor TRIGA Mainz to PSI Villigen. After reassembling the experiment and conducting initial test measurements and troubleshooting, the storage curve shown in Figure 5.11 was measured in December 2023. A photograph of the τSPECT experiment at the West-1 beamport of the PSI UCN source can be seen in Figure 5.10.

The storage curve was measured at 1065 mm, which is the distance between the middle of the beamport exit and the middle of the τSPECT entrance, using stainless steel guides with an inner diameter of 66 mm and a

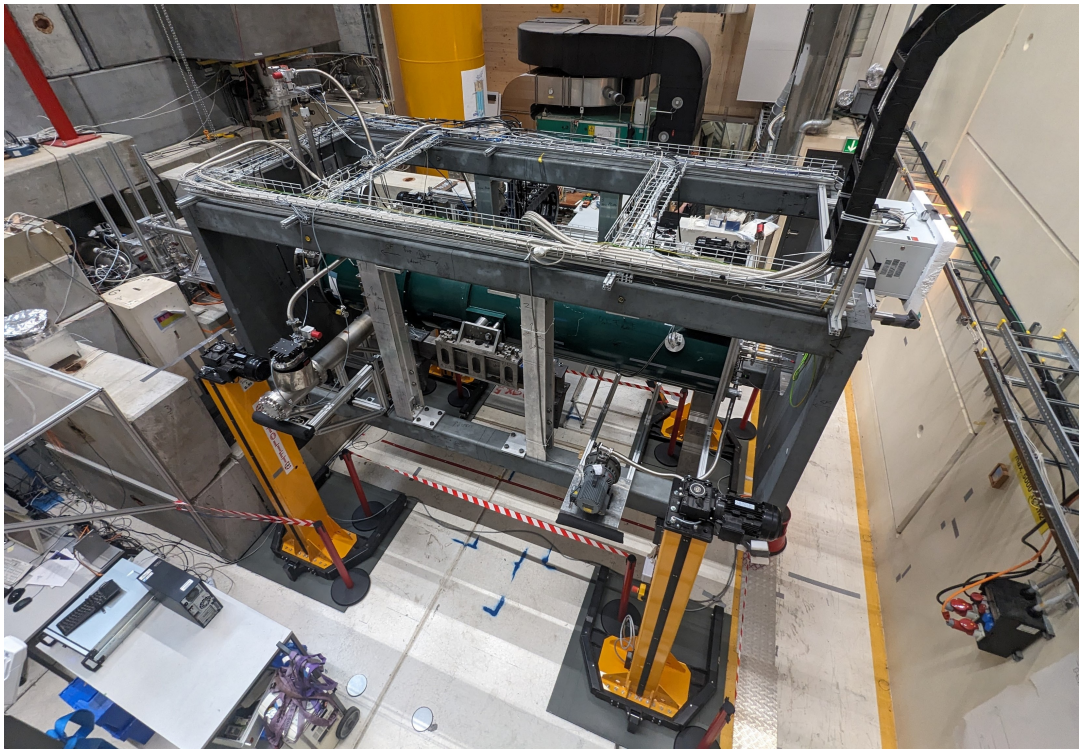

FIGURE 5.10: The τSPECT neutron lifetime experiment after its relocation from TRIGA research reactor, Mainz to PSI Villigen.

Fermi pseudo-potential of 180 neV. Additionally, two ^{58}Ni (85:15) reflective surfaces with a Fermi pseudo-potential of 305 neV were used to direct the UCNs through two 90° angles.

For the storage curve, an filling time of 30 s was used. This was done without delaying the filling due to the n2EDM experiment, but with simultaneous filling of the n2EDM and τSPECT experiments. The filling time is significant longer than the reported 6 s in Ref. [Aul+23]. This difference is expected because, at PSI, neutrons are first accumulated in the source volume for the duration of UCN production (8 s), during which their momenta are mixed before being guided to the experiments. In contrast, at Mainz, neutrons are directly extracted after production and accelerated towards the beam port due to the boost in kinetic energy from transitioning out of the deuterium crystal to the vacuum.

Only the innermost spin flipper was used. The frequency and position of the spin flipping unit were also optimized. The position of the spin flipping unit (970 mm) and the frequency of the spin flipper (5.9 MHz) are comparable to the values used in Ref. [Aul+23]. The duration (200 s) and position (1850 mm) where the detector enters the trap volume before the storage period are designed to remove the highest-energy neutrons from the trap. This ensures that only storable neutrons remain in the trap, as described in Subsection 2.2.2. These values are comparable with those reported in Ref. [Aul+23]. The data is not normalized, which can be seen in the spread of the data points, likely due to drifts in UCN source performance as the storage

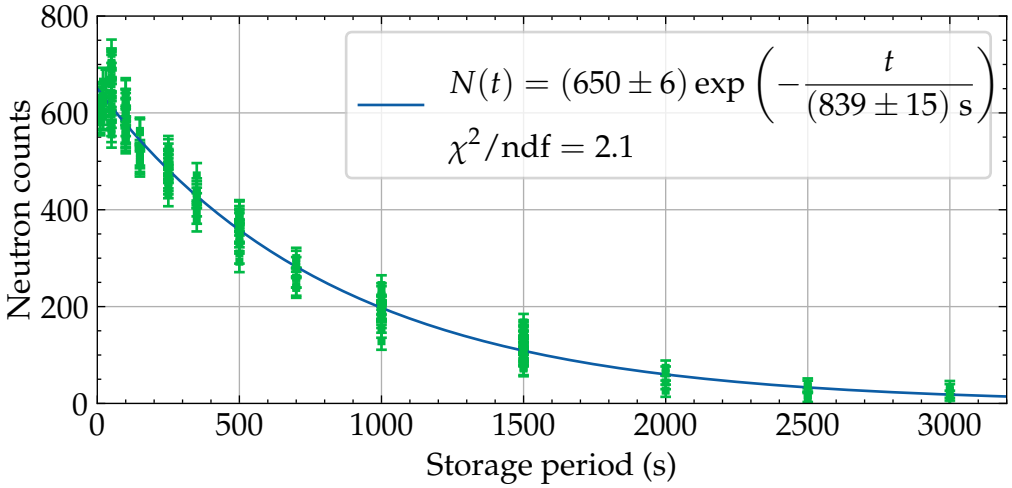

FIGURE 5.11: Storage curve measured at PSI with the τSPECT experiment in December 2023. The storage time constant was extracted using a single exponential fit. This should not be confused with a measurement of the free neutron lifetime.

curve was measured over multiple days. The normalization is highly challenging because the UCN energy spectrum may vary with each measurement cycle, necessitating normalization to UCNs in the same energy range stored in the τSPECT experiment. This motivates the ongoing work on normalizing the UCN storage counts to the produced UCNs per measurement cycle. Similar counting and background intervals were used as in Ref. [Aul+23]. Keeping the same background intervals as in Mainz is not ideal as the τSPECT experiment is not the sole user of the UCN sources and there might be UCN production during measurements. Even though the shutters are closed, these production intervals yield an increased count rate in the τSPECT detector from gamma radiation. This results in a higher count rate for some storage periods in the counting or background intervals, leading to either an overestimation or underestimation of the background counts for certain storage periods. This issue was only identified in hindsight and is a recent development that the collaboration is now actively working to resolve. However, if we compare Figure 5.11 with the storage curve shown in Ref. [Aul+23], as illustrated in Figure 5.12, there is no gain in the neutron counts per measurement at the same storage period. Additionally, the standard deviation for the measurements at the TRIGA Mainz research reactor is larger than that of the PSI measurements, indicating more fluctuations in UCN production at the TRIGA Mainz source during the measurement period. The non-observation of a gain for neutron counts per measurement at the same storage period is in disagreement with the measurements presented in Subsection 5.3. Several possible reasons could explain this discrepancy. As mentioned in Subsection 5.3, the UCN energy spectrum stored in the aluminum bottle is not the same as the one stored in the τSPECT experiment. If the better performance of the aluminum storage bottle is due to neutrons with kinetic energies ranging from 20 neV–54 neV, which are not storable in the τSPECT experiment but are in the aluminum storage bottle, the spectrum could be adjusted. This

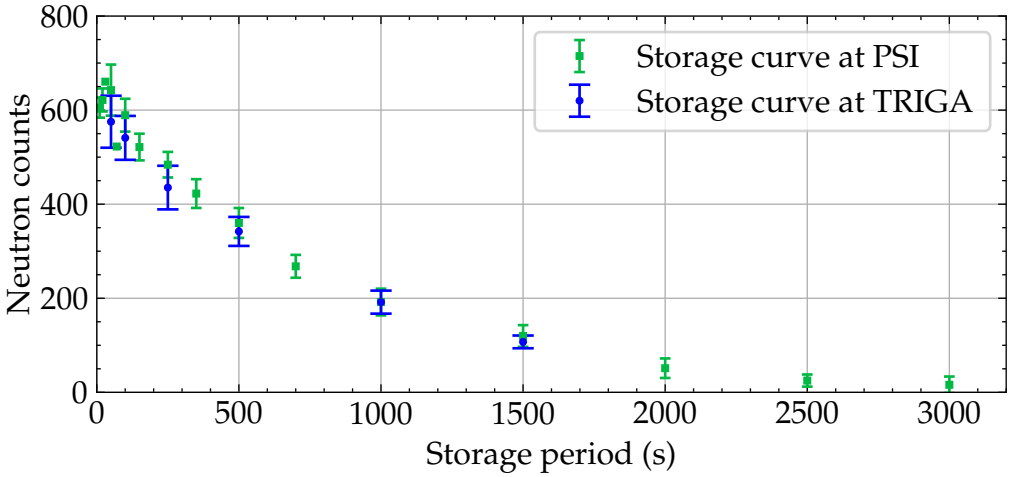

FIGURE 5.12: Storage curve measured at PSI with the τSPECT experiment in December 2023 compared to the data from Ref. [Aul+23] measured at research reactor TRIGA Mainz. The mean values of the measurements were taken to facilitate easier comparison of the data points, with error bars representing the standard deviation to indicate the spread of the data.

can be achieved by altering the height to reduce the kinetic energies of the neutrons with gravity, potentially improving the storage efficiency for the τSPECT experiment. Although some measurements were conducted at different heights, a full height optimization is still pending. Since the beamline has to be adjusted and reconstructed for each height, in 2023 the measurement time was better spent verifying that the setup is running properly and determining which upgrades need to be done in time without neutrons, rather than conducting a height optimization. Another reason for the discrepancy in the measurements could be position of the reduction flange for the beamline inner diameter to the τSPECT experiment compared to the aluminum storage bottle measurement. For the τSPECT experiment the inner diameter was reduced from 200 mm to 66 mm at the beamport for τSPECT, which reduces the number of neutrons guided to the entrance of the experiment. In contrast, for the aluminum storage bottle, the reduction occurred right in front of the bottle.

There are many potential reasons for the lack of increased counts per measurement observed after moving the τSPECT experiment from the UCN source at the research reactor TRIGA Mainz to the PSI UCN source. These need to be investigated further in the future. However, it is realistic to expect an increase in the number of storable neutrons per measurement with future optimizations, aligning more closely with the estimations made using the aluminum bottle. The move of the τSPECT experiment to PSI is already a success. With the additional operation time of the UCN source at PSI compared to the Mainz TRIGA reactor, the measurement time in years for a competitive neutron lifetime measurement has been reduced by approximately a factor of 5. With further optimizations, it is likely to reach the estimated 2 years, as discussed in Section 5.3.

Chapter 6

Summary and Outlook

6.1 UCN source at research reactor TRIGA Mainz

Efforts in this thesis have been focused on the UCN extraction and stability of the UCN production as well as increasing the measurement time per beam time for experiments of the UCN source at research reactor TRIGA Mainz.

By investigating the freeze-out processes of deuterium and hydrogen crystals, as well as exploring thermal treatments after the freeze-out process, significant improvements in UCN extraction were achieved. These optimizations not only increased the number of neutrons available for experiments but also reduced the setup time, thus enhancing the overall efficiency and productivity of the UCN source. Unfortunately, due to high radiation at the freeze-out point of the crystals, it is not possible to get precise temperature data, making it hard to understand the exact mechanisms underlying these improvements. Long-term stability measurements have to show how stable the UCN production is after the freeze-out with increased deuterium/hydrogen flow rates. Further research is needed to determine whether the observed behavior is unique to the UCN source at the research reactor TRIGA Mainz or if UCN sources worldwide could benefit from similar procedures.

However, this enhancement of the UCN source at the research reactor TRIGA Mainz solidifies its position as a pivotal training ground for young researchers and an attractive setup for new UCN experiments in the development phase.

6.2 τSPECT

However, despite these advancements of the UCN source, the UCN density at research reactor TRIGA Mainz was insufficient for a competitive neutron lifetime measurement. Consequently, relocating the τSPECT experiment to a facility with a higher UCN density became necessary.

A successful comparison between the UCN sources at the research reactor TRIGA Mainz and PSI was conducted, focusing on a energy range and a volume similar to that used in the τSPECT experiment. This comparison motivated and justified the move of the τSPECT experiment to the UCN source

at PSI. After relocating and upgrading the experiment, initial test measurements were performed. Although an increase in neutrons stored per measurement cycle was not observed—contrary to the results of the bottle comparison measurement—a substantial gain in statistical sensitivity per year for a neutron lifetime measurement with the τSPECT experiment was achieved due to the increased measurement time available at PSI compared to the research reactor TRIGA Mainz. Further investigations, including simulations, are required to understand the discrepancy between the gain observed with the aluminum bottle and the lack of gain in the τSPECT experiment.

However, improvements can be made to enhance the number of neutrons per measurement cycle in the τSPECT experiment, including a height scan and increasing the beamline diameter. Additionally, further work is needed to study systematic effects, understand background signals, and improve data normalization at PSI before a precise neutron lifetime can be measured with the τSPECT experiment. However, given the significant increase in statistical sensitivity from relocating the experiment to PSI, these measurements can be conducted more efficiently and swiftly.

The successful move and the subsequent improvements mark a milestone towards measuring a competitive neutron lifetime with the τSPECT experiment at PSI and thus contributing to the worldwide effort to clarify the neutron lifetime discrepancy.

6.3 n2EDM

A first set of insulating rings for the n2EDM experiment was produced, coated, and thoroughly characterized. These insulating rings were utilized for the initial measurements with the n2EDM apparatus. With the insulating rings, neutron operation, data acquisition, slow control of the experiment, mercury magnetometer test measurements, and high voltage tests were successfully established. However, the UCN densities in the experiment were significantly lower than expected. A series of measurements established that there was an issue with the coating of the insulating rings and electrodes. Additional layers of coating did not result in the predicted number of stored neutrons. However, they did increase the storable UCN densities in the n2EDM experiment, providing further insight into neutron storage and the coatings of the n2EDM experiment.

Despite this, the rings remained usable and were employed during the setup phase of the experiment. To reach the sensitivity goal of the experiment described in Ref. [Ayr+21], insulating rings with a higher Fermi pseudopotential are required. The production of such insulating rings is ongoing, and an alternative solution with quartz rings employing deuterated paraffin coatings as partially proposed in this thesis is under investigation. Quartz glass can withstand higher temperatures than Rexolite 1422, enabling the use of different coating techniques to apply the deuterated paraffin coatings presented in Ref. [Yaz20]. The foundation of characterization measurements for the new insulating rings has been laid with this thesis. Consequently, the

characterization of the new insulating rings should be relatively swift. The new development measurements and setups will enable effective testing of the new set of insulating rings.

Furthermore, the energy measurement through the ramping of the SCM enables an interesting way of studying energy-dependent systematic effects and allows also for investigation of the source spectrum. Combining this with other measurement techniques like spin echo spectroscopy will offer unique possibilities for understanding the neutron energy spectrum in the n2EDM experiment.

With a new set of insulating rings and the methods developed and improved in this thesis, the n2EDM experiment is ready to measure the neutron electric dipole moment with utmost precision.

Appendix A

Technical drawing insulating rings

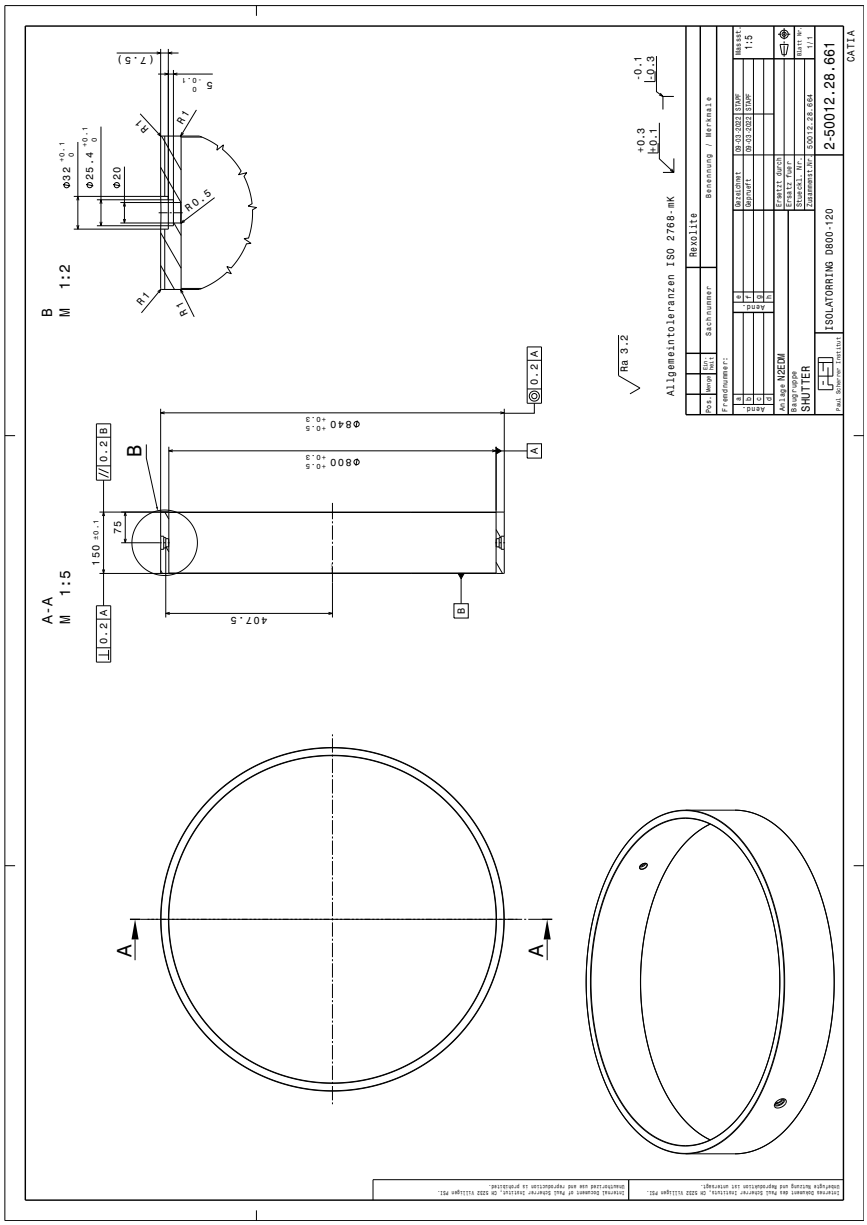

Created by Dieter Ries and Michael Meier.

Appendix B

Measurement report dimensions of insulating rings for the n2EDM precession chamber

Physikalisch-Technische Bundesanstalt
Nationales Metrologieinstitut

Bundesallee 100
38116 Braunschweig
DEUTSCHLAND

Abbestraße 2-12
10587 Berlin
DEUTSCHLAND

Messbericht Isolatorring I1

Messgegenstand

Ein Ring bestehend aus dem Kunststoff REXOLITE mit den nominalen Maßen:
Außendurchmesser von 840 mm, Innendurchmesser von 800 mm
und einer Höhe von 150 mm.

Abbildung 1: Isolatorring auf Koordinatenmessgerät

Messverfahren

Die Messungen wurden auf einem rückgeführten Koordinatenmessgerät vom Typ LEITZ Infinity durchgeführt. Der Ring lag plan auf dem Messtisch und war seitlich gegen verrutschen fixiert. Mit einem Taster von 180 mm Länge und einem Tastkugeldurchmesser von 10 mm wurde die Referenzfläche und die Messtischfläche mit je 72 Einzelpunkten gemessen, um den Abstand und die Parallelität der Stirnflächen zu ermitteln. Bezogen auf die Referenzfläche wurde in den Abständen von 130, 110, 90, 70, 50, 30 und 5 mm jeweils die Innendurchmesser und die Außendurchmesser mit je 72 einzelnen Antastpunkten mit demselben Taster gemessen. Die Querbohrungen sind mit jeweils einem horizontalen Taster von 33 mm Länge und einem Tastkugeldurchmesser von 3 mm mit je 16 einzelnen Antastpunkten gemessen worden. Die gemessenen Durchmesser und deren Formabweichungen sind nach der Methode der kleinsten Abstandsquadrate „Ausgleichkreis nach Gauss“ berechnet worden. Die Markierung auf der Stirnfläche, bezeichnet die Querbohrung 2.

Physikalisch-Technische Bundesanstalt
Nationales Metrologieinstitut

Bundesallee 100
38116 Braunschweig
DEUTSCHLAND

Abbestraße 2-12
10587 Berlin
DEUTSCHLAND

Umgebungsbedingungen

Die mittlere Temperatur betrug während der Messungen 20,2 °C. Die Ergebnisse sind auf 20 °C bezogen. Zur Korrektur wurde der thermische Ausdehnungskoeffizient $70{,}0*10^{-6}$ K^{-1} verwendet.

Ergebnisse

Die aus fünf Wiederholungsmessungen gemittelten Ergebnisse, sind in der Tabelle auf der folgenden Seite aufgeführt.

Messunsicherheit

Die Ermittlung der Messunsicherheit erfolgte gemäß dem „Guide to the Expression of Uncertainty in Measurement (GUM), Supplement 1“ (JCGM101:2008) und ISO/TS 15530-4:2008 „Evaluating task-specific measurement uncertainty using simulation“ unter Anwendung des Verfahrens Virtuelles Koordinatenmessgerät (VCMM).

Angegeben ist die erweiterte Messunsicherheit, die sich aus der Standardmessunsicherheit durch Multiplikation mit dem Erweiterungsfaktor *k* ergibt. Der Wert der Messgröße liegt im Regelfall mit einer Wahrscheinlichkeit von 95 % im zugeordneten Überdeckungsintervall.

Physikalisch-Technische Bundesanstalt
Nationales Metrologieinstitut

Bundesallee 100
38116 Braunschweig
DEUTSCHLAND

Abbestraße 2-12
10587 Berlin
DEUTSCHLAND

Messergebnisse Isolatorring I1 in mm

		Messunsicherheiten in µm
Form Stirnseite oben	0,045	1,3
Form Messtisch	0,006	1,1
Abstand Stirnseiten	150,001	0,7
Rechtwinkligkeit	0,192	5,7
Parallelität Stirnseiten	0,000	0,0
Konzentrizität	0,074	3,0

Querbohrung 1

Form Bohrung 20	0,035	1,0
DM Bohrung 20	20,026	1,8
Form Bohrung 25	0,018	0,9
DM Bohrung 25	25,459	1,8
Form Bohrung 32	0,015	1,0
DM Bohrung 32	32,061	1,7

Querbohrung 2 markiert

Form Bohrung 20	0,011	1,0
DM Bohrung 20	20,022	1,6
Form Bohrung 25	0,015	1,0
DM Bohrung 25	25,461	1,6
Form Bohrung 32	0,015	1,1
DM Bohrung 32	32,065	1,6

Abstand zur Bezugsebene	Innendurchmesser	
130 mm	799,960	5,0
110 mm	799,972	5,0
90 mm	800,006	5,0
70 mm	800,013	5,0
50 mm	800,009	5,0
30 mm	800,019	5,0
5 mm	800,173	5,0
Mittlerer Durchmesser	800,022	5,0

Abstand zur Bezugsebene	Außendurchmesser	
130 mm	840,258	6,0
110 mm	840,200	6,0
90 mm	840,192	6,0
70 mm	840,187	6,0
50 mm	840,181	6,0
30 mm	840,175	6,0
5 mm	840,134	6,0
Mittlerer Durchmesser	840,190	6,0

Arbeitsgruppe 3D-Kalibrierungen, 27.01.2023

Physikalisch-Technische Bundesanstalt
Nationales Metrologieinstitut

Bundesallee 100
38116 Braunschweig
DEUTSCHLAND

Abbestraße 2-12
10587 Berlin
DEUTSCHLAND

Messbericht Isolatorring I2

Messgegenstand

Ein Ring bestehend aus dem Kunststoff REXOLITE mit den nominalen Maßen:
Außendurchmesser von 840 mm, Innendurchmesser von 800 mm
und einer Höhe von 150 mm.

Abbildung 1: Isolatorring auf Koordinatenmessgerät

Messverfahren

Die Messungen wurden auf einem rückgeführten Koordinatenmessgerät vom Typ LEITZ Infinity durchgeführt. Der Ring lag plan auf dem Messtisch und war seitlich gegen verrutschen fixiert. Mit einem Taster von 180 mm Länge und einem Tastkugeldurchmesser von 10 mm wurde die Referenzfläche und die Messtischfläche mit je 72 Einzelpunkten gemessen, um den Abstand und die Parallelität der Stirnflächen zu ermitteln. Bezogen auf die Referenzfläche wurde in den Abständen von 130, 110, 90, 70, 50, 30 und 5 mm jeweils die Innendurchmesser und die Außendurchmesser mit je 72 einzelnen Antastpunkten mit demselben Taster gemessen. Die Querbohrungen sind mit jeweils einem horizontalen Taster von 33 mm Länge und einem Tastkugeldurchmesser von 3 mm mit je 16 einzelnen Antastpunkten gemessen worden. Die gemessenen Durchmesser und deren Formabweichungen sind nach der Methode der kleinsten Abstandsquadrate „Ausgleichkreis nach Gauss“ berechnet worden. Die Markierung auf der Stirnfläche, bezeichnet die Querbohrung 2.

Physikalisch-Technische Bundesanstalt
Nationales Metrologieinstitut

Bundesallee 100
38116 Braunschweig
DEUTSCHLAND

Abbestraße 2-12
10587 Berlin
DEUTSCHLAND

Umgebungsbedingungen

Die mittlere Temperatur betrug während der Messungen 20,2 °C. Die Ergebnisse sind auf 20 °C bezogen. Zur Korrektur wurde der thermische Ausdehnungskoeffizient $70{,}0 * 10^{-6}\ K^{-1}$ verwendet.

Ergebnisse

Die aus fünf Wiederholungsmessungen gemittelten Ergebnisse, sind in der Tabelle auf der folgenden Seite aufgeführt.

Messunsicherheit

Die Ermittlung der Messunsicherheit erfolgte gemäß dem „Guide to the Expression of Uncertainty in Measurement (GUM), Supplement 1“ (JCGM101:2008) und ISO/TS 15530-4:2008 „Evaluating task-specific measurement uncertainty using simulation“ unter Anwendung des Verfahrens Virtuelles Koordinatenmessgerät (VCMM).

Angegeben ist die erweiterte Messunsicherheit, die sich aus der Standardmessunsicherheit durch Multiplikation mit dem Erweiterungsfaktor *k* ergibt. Der Wert der Messgröße liegt im Regelfall mit einer Wahrscheinlichkeit von 95 % im zugeordneten Überdeckungsintervall.

Physikalisch-Technische Bundesanstalt
Nationales Metrologieinstitut

Bundesallee 100
38116 Braunschweig
DEUTSCHLAND

Abbestraße 2-12
10587 Berlin
DEUTSCHLAND

Messergebnisse Isolatorring I2 in mm

		Messunsicherheiten in µm
Form Stirnseite oben	0,049	1,3
Form Messtisch	0,005	1,1
Abstand Stirnseiten	150,004	0,7
Rechtwinkligkeit	0,190	5,7
Parallelität Stirnseiten	0,001	0,0
Konzentrizität	0,047	3,0

Querbohrung 1

Form Bohrung 20	0,012	1,0
DM Bohrung 20	20,028	1,8
Form Bohrung 25	0,016	0,9
DM Bohrung 25	25,468	1,8
Form Bohrung 32	0,014	1,0
DM Bohrung 32	32,073	1,7

Querbohrung 2 markiert

Form Bohrung 20	0,014	1,0
DM Bohrung 20	20,026	1,6
Form Bohrung 25	0,017	1,0
DM Bohrung 25	25,467	1,6
Form Bohrung 32	0,016	1,1
DM Bohrung 32	32,071	1,6

Abstand zur Bezugsebene	Innendurchmesser	
130 mm	800,024	5,0
110 mm	800,034	5.0
90 mm	800,051	5,0
70 mm	800,071	5,0
50 mm	800,085	5,0
30 mm	800,086	5,0
5 mm	800,138	5,0
Mittlerer Durchmesser	800,070	5,0

Abstand zur Bezugsebene	Außendurchmesser	
130 mm	840,277	6,0
110 mm	840,221	6,0
90 mm	840,208	6,0
70 mm	840,204	6,0
50 mm	840,204	6,0
30 mm	840,198	6,0
5 mm	840,165	6,0
Mittlerer Durchmesser	840,211	6,0

Arbeitsgruppe 3D-Kalibrierungen, 27.01.2023

Created by Konrad Hierse and Jürgen Hirsch.

Appendix C

Specification of the chemicals used for the coating of the first set of insulating rings of the n2EDM experiment

TABLE C.1: The specification of the chemicals used for the coating of the first set of insulating rings of the n2EDM experiment.

chemical	usage	seller	specification	CAS	Batch
dPS (styrene-d8 polymerized)	coating insulating ring	AMAR Chemicals	>98 % atom D	19361-62-7	17143
benzene-d6	coating insulating ring	Deutero	>99.5 %	1076-43-3	25207
toluene-d8	coating insulating ring	Deutero	>99.0 %	2037-26-5	25445
toluene-d8	second coating insulating ring	Thermo scientific	>99.5 % atom	2037-26-5	A5451957
toluene	coating insulating ring	Carl Roth GmbH	>99.5 % p.a.	108-88-3	110292973
toluene	coating insulating ring	Fisher Scientific	>99.8 %	108-88-3	2233957
Propanol-2	cleaning insulating ring	Fisher Scientific	>99.8 %	67-63-0	2227290
dPE (polyethylen-d4)	coating mercury window	AMAR Chemicals	>98 % atom D	25549-98-8	D-738A
o-xylene-d10	coating mercury window	Sigma Aldrich	>99 % atom D	56004-61-6	05301EAV
1,2–xylene-d10	coating mercury window	AMAR	>99.5 % atom D	56004-61-6	1429

Appendix D

Specification of copper sheet for n2EDM test measurments

thyssenkrupp

Werkstoffdatenblatt

Reinkupfer

Materials Services
Materials Germany
Technischer Verkauf

Werkstoffbezeichnung:	EN-Werkstoff-Nr.	DIN-Werkstoff-Nr.
	CW004A [Cu-ETP]	2.0065

Geltungsbereich

Dieses Datenblatt gilt für Flach- und Langprodukte aus dem Reinkupferwerkstoff CW004A.

Anwendung

Der Werkstoff CW004A weist niedrige Festigkeitswerte auf und ist nur bedingt schweißbar. Reinkupfer weist eine gute Korrosionsbeständigkeit in natürlicher Atmosphäre auf. Der Werkstoff weist eine sehr hohe elektrische Leitfähigkeit auf kann aber aufgrund des Sauerstoffgehaltes nur schwer geschweißt (Sauerstoffkrankheit) werden. Zusätzlich besitzt Reinkupfer eine sehr gute Umformbarkeit. Dieser Werkstoff findet Anwendung, wenn eine hohe elektrische Leitfähigkeit erforderlich ist (Elektrotechnik).

Chemische Zusammensetzung in %

Cu	Bi	O	Pb
≥99,90[a)]	≤0,0005	≤0,040	≤0,005

Sonstige Elemente[b)]: Insgesamt: max. 0,03 %

[a)] Einschließlich Silber bis max. 0,015 %

[b)] Die Summe von sonstigen Elementen (außer Kupfer) ist definiert als die Summe von Ag, As, Bi, Cd, Co, Cr, Fe, Mn, Ni, O, P, Pb, S, Sb, Se, Si, Sn, Te und Zn, wobei die einzeln angegebenen Elemente ausgeschlossen sind.

thyssenkrupp

Mechanische Eigenschaften bei Raumtemperatur (Stangen und Drähte) gem. EN 13601

Liefer-zustand	Maße			Härte		Zugfestigkeit	Dehngrenze	Bruchdehnung	
	Rund, quadra-tisch, sechseckig	rechteckig Dicke	rechteckig Breite	Brinell	Vickers	R_m	$R_{p0,2}$	$A_{100\,mm}$	A
	[mm]	[mm]	[mm]	HBW	HV	[N/mm²]	[N/mm²]	[%]	[%]
D	2-160	0,5-40	1-200	kalt gefertigt ohne festgelegte Eigenschaften					
H035[a)]	2-160	0,5-40	1-200	35-65	35-65	-	-	-	-
R200[a)]	2-160	1-40	5-200	-	-	≥200	120	≥25	≥35
H065	2-80	0,5-40	1-200	65-60	70-95	-	-	-	-
R250	2-10	1-10	5-200	-	-	≥250	≥200	≥8	≥12
R250	>10-140	>10-40	>10-200	-	-	≥250	≥180	-	≥15
R230	>30-80	>10-40	>10-200	-	-	≥230	≥160	-	≥18
H085	2-40	0,5-20	1-120	85-110	90-115	-	-	-	-
H075	>40-80	>20-40	>20-160	75-100	80-105	-	-	-	-
R300	2-20	1-10	5-120	-	-	≥300	≥260	≥5	≥8
R280	>20-60	>10-20	>10-160	-	-	≥280	≥240	-	≥10
R260	>40-60	>20-40	>20-160	-	-	≥260	≥220	-	≥12
H100	2-10	0,5-5	1-120	≥100	≥110	-	-	-	-
R350	2-10	1-5	5-120	-	-	≥350	≥320	≥3	≥5

[a)] geglüht

Mechanische Eigenschaften bei Raumtemperatur (Rohre) gem. EN 13600

Lieferzustand	Wanddicke t [mm]	Dehngrenze $R_{p0,2}$ [N/mm²]	Zugfestigkeit R_m [N/mm²]	Bruchdehnung $A_{100\,mm}$ [%]	Härte HBW	Härte HV
D	alle	kaltgezogen ohne festgelegte mechanische Eigenschaften				
H035	≤40	-	-	-	35-60	35-65
R200	≤40	≤120	200-250	≥35	-	-
H065	≤20	-	-	-	60-90	65-95
R250	≤20	≥150	250-300	≥15	-	-
H090	≤10	-	-	-	85-105	90-110
R290	≤10	≥250	290-360	≥5	-	-
H100	≤5	-	-	-	≥95	≥100
R360	≤5	≥320	≥360	(≥3)[a)]	-	-

[a)] Die Zahl in Klammer ist keine Anforderung der Norm, sondern ist nur zur Information angegeben

thyssenkrupp

Mechanische Eigenschaften bei Raumtemperatur (Bleche, Bände und Platten) gem. EN 13599

Lieferzustand	Dicke t [mm]	Dehngrenze $R_{p0,2}$ [N/mm²]	Zugfestigkeit R_m [N/mm²]	Bruchdehnung $A_{50\,mm}$ für Dicken von 0,1 mm bis 2,5 mm [%]	$A_{50\,mm}$ für Dicken > 2,5 mm [%]	Härte HV
M	10-25	wie gefertigt				
H035	0,10-5	-	-	-	-	40-65
R220		(≤140)	220-260	≥33	≥42	-
H040	0,20-10	-	-	-	-	40-65
R200		(≤100)	200-250	-	≥42	-
H065	0,10-10	-	-	-	-	65-95
R240		≥180	240-300	≥8	≥15	-
H090	0,10-10	-	-	-	-	90-110
R290		≥250	290-360	≥4	≥6	-
H110	0,10-2	-	-	-	-	≥110
R360		≥320	≥360	≥2	-	

Anhaltsangaben für einige physikalische Eigenschaften

Dichte bei 20 °C [kg/dm³]	Elektrische Leitfähigkeit [MS/m]	Wärmeleitfähigkeit [W/m•K]	Spezifische Wärmekapazität [J/Kg•K]	Elastizitätsmodul [MPa]	Schubmodul [MPa]
8,93	57,0	394	386	110000	-

Hinweise auf Temperaturen für die Wärmebehandlung

Weichglühen Temperatur	Entspannungsglühen Temperatur	Warmumformen Temperatur
250-500 °C	150-200 °C	750-950 °C

Verarbeitung/Schweißen

Der Werkstoff ist sehr gut kaltumformbar. Des Weiteren ist CW004A zum Schweißen und Hartlöten in reduzierender Atmosphäre nicht geeignet. Die Zerspanbarkeit dieses Werkstoffes wird mit mäßig bis schwer beurteilt. Mit steigender Festigkeit verbessert sich die Zerspanbarkeit.

Bemerkungen

Der Werkstoff ist RoHS- und REACH-konform.

thyssenkrupp

Herausgeber

thyssenkrupp Schulte GmbH
Technischer Verkauf
thyssenkrupp Allee 1
45143 Essen

Literaturhinweis

DIN EN 13599 : 2014-12 — Beuth Verlag GmbH, Postfach, D-10772 Berlin
DIN EN 13600 : 2013-09
DIN EN 13601 : 2019-09
Kupfer-Datenblätter — Deutsches Kupferinstitut Berufsverband e.V. D-40239 Düsseldorf

Wichtiger Hinweis

Appendix E

Use of AI-Tools for this thesis

TABLE E.1: Used AI tools for this work.

AI tool	Use case	Why	When
ChatGPT	spell-checking and grammar checking	improve readability	across the entire work
ChatGPT	LaTex formatting	make things look better	across the entire work
ChatGPT	Python and C++ code	improve code quality	across the entire work
ChatGPT	structuring	improve text apprehension	across the entire work
ChatGPT	reformulation of my draft texts	improve readability	across the entire work
DeepL	translation	access to research results	across the entire work
LanguageTool	spell-checking and grammar checking	improve readability	across the entire work
PyCharm AI Assistant	Python coding	improve code quality	across the entire work

Appendix F

Use of Python 3 packages for this thesis

TABLE F.1: Used Python 3 packages for this work.

Package Name	Version
ace_tools	0.0
anaconda-anon-usage	0.4.4
anaconda-client	1.12.3
anaconda-cloud-auth	0.5.1
anaconda-navigator	2.5.4
annotated-types	0.6.0
anyio	4.2.0
archspec	0.2.3
argon2-cffi	21.3.0
argon2-cffi-bindings	21.2.0
asttokens	2.0.5
async-lru	2.0.4
attrs	23.1.0
Babel	2.11.0
backcall	0.2.0
backports.functools-lru-cache	1.6.4
backports.tempfile	1.0
backports.weakref	1.0
beautifulsoup4	4.12.2
bleach	4.1.0
boltons	23.0.0
Brotli	1.0.9
certifi	2024.7.4
cffi	1.16.0
chardet	4.0.0
charset-normalizer	2.0.4
click	8.1.7
colorama	0.4.6
comm	0.2.1
conda	24.7.1

TABLE F.1: Used Python 3 packages for this work (continued).

Package Name	**Version**
conda-build	24.5.1
conda-content-trust	0.2.0
conda_index	0.4.0
conda-libmamba-solver	24.1.0
conda-package-handling	2.2.0
conda_package_streaming	0.9.0
conda-repo-cli	1.0.88
conda-token	0.4.0
conda-verify	3.4.2
contourpy	1.0.5
cryptography	42.0.5
cycler	0.11.0
debugpy	1.6.7
decorator	5.1.1
defusedxml	0.7.1
distro	1.9.0
exceptiongroup	1.2.0
executing	0.8.3
fastjsonschema	2.16.2
filelock	3.13.1
fonttools	4.51.0
frozendict	2.4.2
future	0.18.3
garth	0.4.44
gmpy2	2.1.2
idna	3.7
importlib-metadata	7.0.1
importlib-resources	6.1.1
ipykernel	6.28.0
ipython	8.12.2
ipywidgets	8.1.2
jaraco.classes	3.2.1
jedi	0.18.1
Jinja2	3.1.4
json5	0.9.6
jsonpatch	1.33
jsonpointer	2.1
jsonschema	4.19.2
jsonschema-specifications	2023.7.1
jupyter_client	8.6.0
jupyter_core	5.5.0
jupyter-events	0.8.0
jupyter-lsp	2.2.0

TABLE F.1: Used Python 3 packages for this work (continued).

Package Name	Version
jupyter_server	2.10.0
jupyter_server_terminals	0.4.4
jupyterlab	4.0.11
jupyterlab-pygments	0.1.2
jupyterlab_server	2.25.1
jupyterlab-widgets	3.0.10
keyring	24.3.1
kiwisolver	1.4.4
libarchive-c	2.9
libmambapy	1.5.8
lxml	5.2.1
MarkupSafe	2.1.3
matplotlib	3.5.3
matplotlib-inline	0.1.6
menuinst	2.1.0
mistune	2.0.4
mkl-fft	1.3.8
mkl-random	1.2.4
mkl-service	2.4.0
more-itertools	10.1.0
mpmath	1.3.0
navigator-updater	0.5.0
nbclient	0.8.0
nbconvert	7.10.0
nbformat	5.9.2
nest-asyncio	1.6.0
notebook_shim	0.2.3
numpy	1.24.3
oauthlib	3.2.2
overrides	7.4.0
packaging	23.2
pandas	2.0.3
pandocfilters	1.5.0
parso	0.8.3
pickleshare	0.7.5
pillow	10.3.0
pip	24.0
pkce	1.0.3
pkginfo	1.10.0
pkgutil_resolve_name	1.3.10
platformdirs	3.10.0
pluggy	1.0.0
ply	3.11

TABLE F.1: Used Python 3 packages for this work (continued).

Package Name	Version
pooch	1.7.0
prometheus-client	0.14.1
prompt-toolkit	3.0.43
psutil	5.9.0
PulseAnalysis	0.1
pure-eval	0.2.2
pycosat	0.6.6
pycparser	2.21
pydantic	2.5.3
pydantic_core	2.14.6
Pygments	2.15.1
PyJWT	2.8.0
pyparsing	3.0.9
PyQt5	5.15.10
PyQt5-sip	12.13.0
PySocks	1.7.1
python-dateutil	2.9.0
python-dotenv	0.21.0
python-json-logger	2.0.7
pytz	2024.1
pywin32	305.1
pywin32-ctypes	0.2.2
pywinpty	2.0.10
PyYAML	6.0.1
pyzmq	25.1.2
QtPy	2.4.1
referencing	0.30.2
requests	2.32.2
requests-oauthlib	1.4.0
requests-toolbelt	1.0.0
rfc3339-validator	0.1.4
rfc3986-validator	0.1.1
rpds-py	0.10.6
ruamel.yaml	0.17.21
ruamel.yaml.clib	0.2.6
SciencePlots	2.1.1
scipy	1.10.1
semver	3.0.2
Send2Trash	1.8.2
setuptools	69.5.1
sip	6.7.12
six	1.16.0
sniffio	1.3.0

TABLE F.1: Used Python 3 packages for this work (continued).

Package Name	**Version**
soupsieve	2.5
stack-data	0.2.0
sympy	1.12
tauConfig	1.0
terminado	0.17.1
tikzplotlib	0.10.1
tinycss2	1.2.1
tomli	2.0.1
tornado	6.3.3
tqdm	4.66.4
traitlets	5.7.1
typing_extensions	4.10.0
tzdata	2024.1
ujson	5.10.0
unicodedata2	15.1.0
urllib3	2.2.1
wcwidth	0.2.5
webcolors	1.13
webencodings	0.5.1
websocket-client	1.8.0
wheel	0.43.0
widgetsnbextension	4.0.10
win-inet-pton	1.1.0
zipp	3.17.0
zstandard	0.22.0

Bibliography

[Abe+20] C. Abel et al. "Measurement of the Permanent Electric Dipole Moment of the Neutron". In: *Physical Review Letters* 124.8 (Feb. 28, 2020), p. 081803. DOI: 10.1103/PhysRevLett.124.081803. URL: https://link.aps.org/doi/10.1103/PhysRevLett.124.081803 (visited on 01/17/2024).

[Ade+16] P. a. R. Ade et al. "Planck 2015 results - XIII. Cosmological parameters". In: *Astronomy & Astrophysics* 594 (Oct. 1, 2016), A13. ISSN: 0004-6361, 1432-0746. DOI: 10.1051/0004-6361/201525830. URL: https://www.aanda.org/articles/aa/abs/2016/10/aa25830-15/aa25830-15.html (visited on 05/20/2024).

[Afa+15] S. Afach et al. "A device for simultaneous spin analysis of ultracold neutrons". In: *Eur. Phys. J.* A51.11 (2015). _eprint: 1502.06876, p. 143. DOI: 10.1140/epja/i2015-15143-7.

[Alt+08] I. Altarev et al. "Neutron velocity distribution from a superthermal solid sD2 ultracold neutron source". In: *The European Physical Journal A - Hadrons and Nuclei* 37.1 (2008). Publisher: Springer Berlin / Heidelberg, pp. 9–14. ISSN: 1434-6001. URL: http://dx.doi.org/10.1140/epja/i2008-10604-8.

[Ani+05] D. Anicic et al. "A fast kicker magnet for the PSI 600 MeV proton beam to the PSI ultra-cold neutron source". In: *Nuclear Instruments and Methods in Physics Research A* 541 (Apr. 2005), pp. 598–609. DOI: 10.1016/j.nima.2004.12.032.

[Arz+12] S. S. Arzumanov et al. "Analysis and correction of the measurement of the neutron lifetime". In: *JETP Letters* 95.5 (2012), pp. 224–228. ISSN: 1090-6487. DOI: 10.1134/S0021364012050025.

[Ass09] US EPA National Center for Environmental Assessment. *CRC handbook of chemistry and physics*. Mar. 15, 2009. URL: https://hero.epa.gov/hero/index.cfm/reference/details/reference_id/4731459 (visited on 07/22/2024).

[Atc+05] F. Atchison et al. "Measured Total Cross Sections of Slow Neutrons Scattered by Solid Deuterium and Implications for Ultracold Neutron Sources". In: *Phys. Rev. Lett.* 95 (2005). Publisher: American Physical Society, p. 182502. DOI: 10.1103/PhysRevLett.95.182502. URL: http://link.aps.org/doi/10.1103/PhysRevLett.95.182502.

[Atc+07a] F. Atchison et al. "Cold Neutron Energy Dependent Production of Ultracold Neutrons in Solid Deuterium". In: *Phys. Rev. Lett.* 99.26 (Dec. 2007). Publisher: American Physical Society, p. 262502. DOI: 10.1103/PhysRevLett.99.262502. URL: http://link.aps.org/doi/10.1103/PhysRevLett.99.262502.

[Atc+07b] F. Atchison et al. "Measurement of the Fermi potential of diamond-like carbon and other materials". In: *Nuclear Instruments and Methods in Physics Research Section B: Beam Interactions with Materials and Atoms* 260.2 (2007), pp. 647–656. ISSN: 0168-583X. DOI: http://dx.doi.org/10.1016/j.nimb.2007.04.253.

[Aul+23] J. Auler et al. *tauSPECT: A spin-flip loaded magnetic ultracold neutron trap for a determination of the neutron lifetime*. Oct. 25, 2023. DOI: 10.48550/arXiv.2311.00712. arXiv: 2311.00712[nucl-ex,physics:physics]. URL: http://arxiv.org/abs/2311.00712 (visited on 07/19/2024).

[Ayr+21] N. J. Ayres et al. "The design of the n2EDM experiment". In: *The European Physical Journal C* 81.6 (June 12, 2021), p. 512. ISSN: 1434-6052. DOI: 10.1140/epjc/s10052-021-09298-z. URL: https://doi.org/10.1140/epjc/s10052-021-09298-z (visited on 01/19/2024).

[Bae+11] Stefan Baessler et al. "The GRANIT spectrometer". In: *Comptes Rendus Physique* 12.8 (2011), pp. 707–728. ISSN: 1631-0705. DOI: http://dx.doi.org/10.1016/j.crhy.2011.04.010.

[Bak+11] C. A. Baker et al. "The search for the neutron electric dipole moment at the Paul Scherrer Institute". In: *Physics Procedia* 17.0 (2011), pp. 159–167. ISSN: 1875-3892.

[Bak+14] C. A. Baker et al. "Apparatus for measurement of the electric dipole moment of the neutron using a cohabiting atomic-mercury magnetometer". In: *Nuclear Instruments and Methods in Physics Research Section A: Accelerators, Spectrometers, Detectors and Associated Equipment* 736 (2014), pp. 184–203. ISSN: 0168-9002. DOI: http://dx.doi.org/10.1016/j.nima.2013.10.005.

[Bak06] Baker, C.A., Doyle, D.D., Geltenbort, P., Green, K., van der Grinten, M.G.D. and others. "An Improved experimental limit on the electric dipole moment of the neutron". In: *Phys.Rev.Lett.* 97 (2006). _eprint: hep-ex/0602020, p. 131801. DOI: 10.1103/PhysRevLett.97.131801.

[Bec+15] H. Becker et al. "Neutron production and thermal moderation at the PSI UCN source". In: *Nuclear Instruments and Methods in Physics Research Section A* 777.0 (2015), pp. 20–27. ISSN: 0168-9002. DOI: 10.1016/j.nima.2014.12.091.

[Bis+17] G. Bison et al. “Comparison of ultracold neutron sources for fundamental physics measurements”. In: *Physical Review C* 95.4 (Apr. 28, 2017), p. 045503. DOI: 10.1103/PhysRevC.95.045503. URL: https://link.aps.org/doi/10.1103/PhysRevC.95.045503 (visited on 07/08/2024).

[Bis08] Caterina Biscari. “Engines of Discovery: A Century of Particle Accelerators”. In: *Physics Today* 61.9 (Sept. 1, 2008), pp. 68–69. ISSN: 0031-9228. DOI: 10.1063/1.2982128. URL: https://doi.org/10.1063/1.2982128 (visited on 07/29/2024).

[Bor00] J Bork. “The 8-layered magnetically shielded room of the PTB: Design and construction”. In: Proceedings of the 12th International Conferenc on Biomagnetism (2000), pp. 970–973.

[Bou23] Thomas Bouillaud. “The internal magnetic field of the n2EDM experiment to probe CP symmetry : calculation of the magic field and control of non-uniformities”. PhD thesis. Université Grenoble Alpes [2020-....], Nov. 20, 2023. URL: https://theses.hal.science/tel-04543374 (visited on 06/19/2024).

[Bro+13] Leah Broussard et al. “UCNB: The Neutrino Asymmetry in Polarized Ultracold Neutron Decay”. In: *11TH CONFERENCE ON THE INTERSECTIONS OF PARTICLE AND NUCLEAR PHYSICS (CIPANP 2012)*. Ed. by Fleming, B. Vol. 1560. AIP Conference Proceedings. ISSN: 0094-243X Type: Proceedings Paper. AMER INST PHYSICS, 2013, pp. 149–151. ISBN: 978-0-7354-1188-3. DOI: 10.1063/1.4826741.

[Bro24] Louis de Broglie. “Recherches sur la théorie des Quanta”. PhD thesis. Migration - université en cours d’affectation, Nov. 25, 1924. URL: https://theses.hal.science/tel-00006807 (visited on 07/22/2024).

[Bry07] T. Brys. “Extraction of ultracold neutrons from a solid deuterium source”. PhD thesis. ETH Zürich, No.17350, 2007.

[Bur+04] M. Burghoff et al. “dc Magnetoencephalography: Direct measurement in a magnetically extremely-well shielded room”. In: *Applied Physics Letters* 85.25 (Dec. 20, 2004), pp. 6278–6280. ISSN: 0003-6951. DOI: 10.1063/1.1836869. URL: https://doi.org/10.1063/1.1836869 (visited on 07/22/2024).

[CF20] Fabrice Cousin and Giulia Fadda. “An introduction to neutron reflectometry”. In: *EPJ Web of Conferences* 236 (2020). Publisher: EDP Sciences, p. 04001. ISSN: 2100-014X. DOI: 10.1051/epjconf/202023604001. URL: https://www.epj-conferences.org/articles/epjconf/abs/2020/12/epjconf_jdn24_04001/epjconf_jdn24_04001.html (visited on 07/26/2024).

[Cha32] J. Chadwick. "Possible Existence of a Neutron". In: *Nature* 129.3252 (Feb. 1932). Publisher: Nature Publishing Group, pp. 312–312. ISSN: 1476-4687. DOI: 10.1038/129312a0. URL: https://www.nature.com/articles/129312a0 (visited on 07/29/2024).

[Col+22] PIONEER Collaboration et al. *PIONEER: Studies of Rare Pion Decays*. Mar. 7, 2022. DOI: 10.48550/arXiv.2203.01981. arXiv: 2203.01981[hep-ex,physics:hep-ph,physics:physics]. URL: http://arxiv.org/abs/2203.01981 (visited on 07/22/2024).

[CR15] Timothy Chupp and Michael Ramsey-Musolf. "Electric dipole moments: A global analysis". In: *Phys. Rev. C* 91.3 (Mar. 2015). Publisher: American Physical Society, p. 035502. DOI: 10.1103/PhysRevC.91.035502.

[Cyb+16] Richard H. Cyburt et al. "Big bang nucleosynthesis: Present status". In: *Reviews of Modern Physics* 88.1 (Feb. 23, 2016). Publisher: American Physical Society, p. 015004. DOI: 10.1103/RevModPhys.88.015004. URL: https://link.aps.org/doi/10.1103/RevModPhys.88.015004 (visited on 07/22/2024).

[Dha+23] K. Dhanmeher et al. "BRAND—A detection system for beta-decay correlation measurement". In: *Nuclear Instruments and Methods in Physics Research Section A: Accelerators, Spectrometers, Detectors and Associated Equipment* 1048 (Mar. 1, 2023), p. 167955. ISSN: 0168-9002. DOI: 10.1016/j.nima.2022.167955. URL: https://www.sciencedirect.com/science/article/pii/S0168900222012475 (visited on 01/28/2024).

[ERK13] Jonathan Engel, Michael J. Ramsey-Musolf, and U. van Kolck. "Electric dipole moments of nucleons, nuclei, and atoms: The Standard Model and beyond". In: *Progress in Particle and Nuclear Physics* 71 (2013), pp. 21–74. ISSN: 0146-6410. DOI: http://dx.doi.org/10.1016/j.ppnp.2013.03.003. URL: http://www.sciencedirect.com/science/article/pii/S0146641013000227.

[Ezh+14] V. F. Ezhov et al. "Measurement of the neutron lifetime with ultra-cold neutrons stored in a magneto-gravitational trap". In: (2014). _eprint: 1412.7434.

[Fer+46] E. Fermi et al. *Reflection of neutrons on mirrors*. United States. Atomic Energy Commission. MDDC ;56. Oak Ridge, Tenn.: Manhattan District, 1946. 4 pp. URL: https://catalog.hathitrust.org/Record/007841265 (visited on 04/02/2024).

[Fer13] Martin Fertl. "A laser based mercury co-magnetometer for the neutron electric dipole moment search". Accepted: 2017-10-03T10:12:46Z. Doctoral Thesis. ETH Zurich, 2013. DOI: 10.3929/ethz-a-010049897. URL: https://www.research-collection.ethz.ch/handle/20.500.11850/77320 (visited on 08/04/2024).

[Fra+09] A. I. Frank et al. "New test of the weak equivalence principle for neutrons". In: *Nuclear Instruments and Methods in Physics Research Section A: Accelerators, Spectrometers, Detectors and Associated Equipment* 611.2 (2009), pp. 314–317. ISSN: 0168-9002. DOI: http://dx.doi.org/10.1016/j.nima.2009.07.088.

[Fra13] Allan Franklin. *Shifting Standards: Experiments in Particle Physics in the Twentieth Century*. University of Pittsburgh Press, 2013. ISBN: 978-0-8229-4430-0. DOI: 10.2307/j.ctv80c9p7. URL: https://www.jstor.org/stable/j.ctv80c9p7 (visited on 07/29/2024).

[GB83] R. Golub and K. Böning. "New type of low temperature source of Ultra-cold neutrons and production of continous beams of UCN". In: *Zeitschrift für Physik B Condensed Matter* 51.2 (June 1, 1983), pp. 95–98. ISSN: 1431-584X. DOI: 10.1007/BF01308763. URL: https://doi.org/10.1007/BF01308763 (visited on 04/02/2024).

[Göl+13] L. Göltl et al. "An endoscopic detector for ultracold neutrons". In: *The European Physical Journal A* 49.1 (2013), pp. 1–9. ISSN: 1434-601X. DOI: 10.1140/epja/i2013-13009-8.

[Göl08] L. Göltl. "Measurements and procedures for the construction and characterization of ultra-cold neutron guides". Master's Thesis (Diplomarbeit). University of Heidelberg and University of Mainz, 2008.

[Göl12] L. Göltl. "Characterization of the PSI ultra-cold neutron source". PhD thesis. ETH Zürich, No.20350, 2012.

[Gol91] Golub, R. and Richardson, D. and Lamoreaux, S.K. *Ultra-Cold Neutrons*. Adam Hilger, 1991.

[Gri+13] J. Grillenberger et al. "Status and further development of the PSI high intensity proton facility". In: *Proceedings of Cyclotrons2013, Vancouver, BC, Canada* MOPPT004 (2013), p. 1.

[GS23] Mikhail Gorchtein and Chien-Yeah Seng. "The Standard Model Theory of Neutron Beta Decay". In: *Universe* 9.9 (Sept. 2023). Number: 9 Publisher: Multidisciplinary Digital Publishing Institute, p. 422. ISSN: 2218-1997. DOI: 10.3390/universe9090422. URL: https://www.mdpi.com/2218-1997/9/9/422 (visited on 07/25/2024).

[GS24] Mikhail Gorchtein and Chien-Yeah Seng. "Superallowed Nuclear Beta Decays and Precision Tests of the Standard Model". In: (Apr. 17, 2024). Publisher: Annual Reviews. DOI: 10.1146/annurev-nucl-102622-020726. URL: https://www.annualreviews.org/content/journals/10.1146/annurev-nucl-102622-020726 (visited on 07/25/2024).

[Hal80] K. Halbach. "Design of permanent multipole magnets with oriented rare earth cobalt material". In: *Nuclear Instruments and Methods* 169.1 (Feb. 1, 1980), pp. 1–10. ISSN: 0029-554X. DOI: 10.1016/0029-554X(80)90094-4. URL: https://www.sciencedirect.com/science/article/pii/0029554X80900944 (visited on 07/22/2024).

[HS39] O. Hahn and F. Strassmann. "Über den Nachweis und das Verhalten der bei der Bestrahlung des Urans mittels Neutronen entstehenden Erdalkalimetalle". In: *Naturwissenschaften* 27.1 (1939), pp. 11–15. ISSN: 1432-1904. DOI: 10.1007/BF01488241. URL: http://dx.doi.org/10.1007/BF01488241.

[Hua14] Zhu De Hua. "The Total Scattering Cross Section of Ultracold Neutrons in Gaseous Deuterium". Master's Thesis. ETH Zürich, 2014.

[Ito07] Takeyasu M. Ito. "Plans for a Neutron EDM Experiment at SNS". In: *Journal of Physics: Conference Series* 69.1 (2007), p. 012037. URL: http://stacks.iop.org/1742-6596/69/i=1/a=012037.

[Jen+11] Tobias Jenke et al. "Realization of a gravity-resonance-spectroscopy technique". In: *Nat Phys* 7.6 (June 2011). Publisher: Nature Publishing Group, pp. 468–472. ISSN: 1745-2473. DOI: 10.1038/nphys1970.

[Jen+14] T. Jenke et al. "Gravity Resonance Spectroscopy Constrains Dark Energy and Dark Matter Scenarios". In: *Phys. Rev. Lett.* 112.15 (Apr. 2014). Publisher: American Physical Society, p. 151105. DOI: 10.1103/PhysRevLett.112.151105.

[Kah+17] J. Kahlenberg et al. "Upgrade of the ultracold neutron source at the pulsed reactor TRIGA Mainz". In: *The European Physical Journal A* 53.11 (Nov. 28, 2017), p. 226. ISSN: 1434-601X. DOI: 10.1140/epja/i2017-12428-9. URL: https://doi.org/10.1140/epja/i2017-12428-9 (visited on 01/28/2024).

[Kah20] Jan Kahlenberg. "First full-magnetic storage of ultracold neutrons in the tSPECT experiment for measuring the neutron lifetime". PhD thesis. Johannes Gutenberg-Universität Mainz, 2020. DOI: 10.25358/OPENSCIENCE-5455. URL: https://openscience.ub.uni-mainz.de/handle/20.500.12030/5459 (visited on 07/16/2024).

[Kar+14] J. Karch et al. "Performance of the solid deuterium ultra-cold neutron source at the pulsed reactor TRIGA Mainz". In: *Eur. Phys. J. A* 50.4 (2014), p. 78. DOI: 10.1140/epja/i2014-14078-9.

[KM73] Makoto Kobayashi and Toshihide Maskawa. "CP-Violation in the Renormalizable Theory of Weak Interaction". In: *Progress of Theoretical Physics* 49.2 (Feb. 1, 1973), pp. 652–657. ISSN: 0033-068X. DOI: 10.1143/PTP.49.652. URL: https://doi.org/10.1143/PTP.49.652 (visited on 04/22/2024).

[Kom12] S. Komposch. "Untersuchungen zur Charakterisierung der Quelle fuer ultrakalte Neutronen am Paul Scherrer Institut". Master's Thesis (Diplomarbeit). Johannes Gutenberg Universitaet Mainz, 2012.

[Kor+22] Ekaterina Korobkina et al. "Growing solid deuterium for UCN production". In: *Journal of Neutron Research* 24.2 (Jan. 1, 2022), pp. 179–191. ISSN: 1023-8166. DOI: 10.3233/JNR-220010. URL: https://content.iospress.com/articles/journal-of-neutron-research/jnr220010 (visited on 07/16/2024).

[Kuz08] Marcin Kuzniak. "The neutron electric dipole moment experiment: Research and development for the new spectrometer". In: *These de l'université de Cracovie* (2008). URL: https://www.psi.ch/sites/default/files/import/ltp-ucn-physics/PapersThesesEN/kuzniak_thesis.pdf (visited on 06/05/2024).

[LG09] S. K. Lamoreaux and R. Golub. "Experimental searches for the neutron electric dipole moment". In: *Journal of Physics G: Nuclear and Particle Physics* 36.10 (2009), p. 104002. DOI: 10.1088/0954-3899/36/10/104002.

[Lus+69] V. I. Lushikov et al. "Observation of Ultracold Neutrons". In: *JETP Letters* 9 (1969), pp. 23–26. URL: http://www.jetpletters.ac.ru/ps/1639/article_25024.shtml.

[LZ13] Th. Lauer and Th. Zechlau. "A prospective pulsed source of ultracold neutrons for experiments in fundamental neutron physics". In: *The European Physical Journal A* 49.8 (2013), pp. 1–6. ISSN: 1434-601X. DOI: 10.1140/epja/i2013-13104-x.

[Mar20] J.W. Martin. "Current status of neutron electric dipole moment experiments". In: *Journal of Physics: Conference Series* 1643.1 (Dec. 1, 2020), p. 012002. ISSN: 1742-6588, 1742-6596. DOI: 10.1088/1742-6596/1643/1/012002. URL: https://iopscience.iop.org/article/10.1088/1742-6596/1643/1/012002 (visited on 01/17/2024).

[Mat+09] S. Materne et al. "PENeLOPE—on the way towards a new neutron lifetime experiment with magnetic storage of ultracold neutrons and proton extraction". In: *Nuclear Instruments and Methods in Physics Research Section A: Accelerators, Spectrometers, Detectors and Associated Equipment*. Particle Physics with Slow Neutrons 611.2 (Dec. 1, 2009), pp. 176–180. ISSN: 0168-9002. DOI: 10.1016/j.nima.2009.07.055. URL: https://www.sciencedirect.com/science/article/pii/S0168900209015204 (visited on 01/28/2024).

[Men+13] M. P. Mendenhall et al. "Precision measurement of the neutron \ensuremath\beta-decay asymmetry". In: *Phys. Rev. C* 87.3 (Mar. 2013). Publisher: American Physical Society, p. 032501. DOI: 10.1103/PhysRevC.87.032501.

[MF39] Lise Meitner and O. R. Frisch. "Disintegration of Uranium by Neutrons: a New Type of Nuclear Reaction". In: *Nature* 143.3615 (Feb. 11, 1939), pp. 239–240. DOI: 10.1038/143239a0.

[Mor+02] C. L. Morris et al. "Measurements of Ultracold-Neutron Lifetimes in Solid Deuterium". In: *Phys. Rev. Lett.* 89.27 (Dec. 2002). Publisher: American Physical Society, p. 272501. DOI: 10.1103/PhysRevLett.89.272501.

[MS06] William J. Marciano and Alberto Sirlin. "Improved Calculation of Electroweak Radiative Corrections and the Value of V_ud". In: *Phys. Rev. Lett.* 96.3 (Jan. 2006). Publisher: American Physical Society, p. 032002. DOI: 10.1103/PhysRevLett.96.032002.

[NAR] NARZISS. *NARZISS: Polarised Neutron Reflectometer \textbar BL: SINQ/NARZISS \textbar PSI*. URL: https://www.psi.ch/en/sinq/narziss (visited on 06/18/2024).

[Nes+02] Valery V. Nesvizhevsky et al. "Quantum states of neutrons in the Earth's gravitational field". In: *Nature* 415.6869 (Jan. 17, 2002), pp. 297–299. ISSN: 0028-0836. DOI: 10.1038/415297a.

[Par+22] Particle Data Group et al. "Review of Particle Physics". In: *Progress of Theoretical and Experimental Physics* 2022.8 (Aug. 8, 2022), p. 083C01. ISSN: 2050-3911. DOI: 10.1093/ptep/ptac097. URL: https://doi.org/10.1093/ptep/ptac097 (visited on 01/19/2024).

[Pau09] Stephan Paul. "The Puzzle of Neutron Lifetime". In: *Nuclear Instruments and Methods in Physics Research Section A: Accelerators, Spectrometers, Detectors and Associated Equipment* 611.2 (Dec. 2009), pp. 157–166. ISSN: 01689002. DOI: 10.1016/j.nima.2009.07.095. arXiv: 0902.0169[hep-ex,physics:nucl-ex]. URL: http://arxiv.org/abs/0902.0169 (visited on 04/11/2024).

[Pen+15] J. M. Pendlebury et al. "Revised experimental upper limit on the electric dipole moment of the neutron". In: *Phys. Rev. D* 92.9 (Nov. 2015). Publisher: American Physical Society, p. 092003. DOI: 10.1103/PhysRevD.92.092003.

[Pic+10] A. Pichlmaier et al. "Neutron lifetime measurement with the {UCN} trap-in-trap {MAMBO} {II}". In: *Physics Letters B* 693.3 (2010), pp. 221–226. ISSN: 0370-2693. DOI: http://dx.doi.org/10.1016/j.physletb.2010.08.032.

[PP12] Florian M. Piegsa and Guillaume Pignol. "Limits on the Axial Coupling Constant of New Light Bosons". In: *Physical Review Letters* 108.18 (May 1, 2012). Publisher: American Physical Society, p. 181801. DOI: 10.1103/PhysRevLett.108.181801. URL: https://link.aps.org/doi/10.1103/PhysRevLett.108.181801 (visited on 07/26/2024).

[Ram50] Norman F. Ramsey. "A Molecular Beam Resonance Method with Separated Oscillating Fields". In: *Physical Review* 78.6 (June 15, 1950), pp. 695–699. DOI: 10.1103/PhysRev.78.695. URL: https://link.aps.org/doi/10.1103/PhysRev.78.695 (visited on 01/17/2024).

[Ram55] Ramsey, N. F. "Resonance Transitions Induced by Perturbations at Two or More Different Frequencies". In: *Phys. Rev.* 100.4 (Nov. 1955). Publisher: American Physical Society, pp. 1191–1194. DOI: 10.1103/PhysRev.100.1191. URL: http://link.aps.org/doi/10.1103/PhysRev.100.1191.

[Ram82] N. F. Ramsey. "Electric-dipole moments of particles". In: *Annual Review of Nuclear and Particle Science* 32.1 (1982). Publisher: Annual Reviews 4139 El Camino Way, PO Box 10139, Palo Alto, CA 94303-0139, USA, pp. 211–233. DOI: 10.1146/annurev.ns.32.120182.001235.

[Rie16] Dieter Achim Ries. "The Source for Ultracold Neutrons at the Paul Scherrer Institute - Characterisation, Optimisation, and International Comparison". Doctoral Thesis. ETH Zurich, 2016. DOI: 10.3929/ethz-a-010795050. URL: https://www.research-collection.ethz.ch/handle/20.500.11850/123070 (visited on 07/08/2024).

[Roß21] Kim Ulrike Roß. "Towards a high precision measurement of the free neutron lifetime with tauSPECT". PhD thesis. [object Object], 2021. DOI: 10.25358/OPENSCIENCE-6540. URL: https://openscience.ub.uni-mainz.de/handle/20.500.12030/6550 (visited on 04/11/2024).

[SA17] Masayoshi Satoh and Samir Aboulroos, eds. *Irrigated Agriculture in Egypt: Past, Present and Future*. Cham: Springer International Publishing, 2017. ISBN: 978-3-319-30215-7. DOI: 10.1007/978-3-319-30216-4. URL: https://link.springer.com/10.1007/978-3-319-30216-4 (visited on 07/29/2024).

[Sak67] A. D. Sakharov. "Violation of CP Invariance, C asymmetry, and baryon asymmetry of the universe". In: *Pisma Zh. Eksp. Teor. Fiz.* 5 (1967), pp. 32–35. DOI: 10.1070/PU1991v034n05ABEH002497.

[Sal+14] D. J. Salvat et al. "Storage of ultracold neutrons in the magneto-gravitational trap of the \mathrmUCN\ensuremath\tau experiment". In: *Phys. Rev. C* 89.5 (May 2014). Publisher: American Physical Society, p. 052501. DOI: 10.1103/PhysRevC.89.052501.

[Sau+13] A. Saunders et al. "Performance of the Los Alamos National Laboratory spallation-driven solid-deuterium ultra-cold neutron source". In: *Review of Scientific Instruments* 84.1 (2013). DOI: 10.1063/1.4770063.

[Sau97] F. Sauli. "GEM: A new concept for electron amplification in gas detectors". In: *Nuclear Instruments and Methods in Physics Research Section A: Accelerators, Spectrometers, Detectors and Associated Equipment* 386.2 (Feb. 21, 1997), pp. 531–534. ISSN: 0168-9002. DOI: 10.1016/S0168-9002(96)01172-2. URL: https://www.sciencedirect.com/science/article/pii/S0168900296011722 (visited on 07/21/2024).

[Sea37] G. T. Seaborg. "The interaction of fast neutrons with lead". PhD thesis. University of California, Berkeley, USA, 1937.

[Sei70] W.-D. Seiffert. "Messung der Streuquerschnitte von flüssigem und festem Wasserstoff, Deuterium und Deuteriumhydrid für thermische Neutronen". In: *Euratom Report NO. EUR 4455d* (1970).

[Sen+18] Chien-Yeah Seng et al. "Reduced Hadronic Uncertainty in the Determination of {V}_{ud}". In: *Physical Review Letters* 121.24 (Dec. 14, 2018), p. 241804. DOI: 10.1103/PhysRevLett.121.241804. URL: https://link.aps.org/doi/10.1103/PhysRevLett.121.241804 (visited on 01/19/2024).

[Ser+05] A. Serebrov et al. "Measurement of the neutron lifetime using a gravitational trap and a low-temperature Fomblin coating". In: *Physics Letters B* 605.1 (2005), pp. 72–78. ISSN: 0370-2693. DOI: http://dx.doi.org/10.1016/j.physletb.2004.11.013.

[Ser+15] A. P. Serebrov et al. "New measurements of the neutron electric dipole moment with the Petersburg Nuclear Physics Institute double-chamber electric dipole moment spectrometer". In: *Physics of Particles and Nuclei Letters* 12.2 (2015), pp. 286–296. ISSN: 1531-8567. DOI: 10.1134/S1547477115020193.

[Sha68] F. L. Shapiro. "ELECTRIC DIPOLE MOMENTS OF ELEMENTARY PARTICLES". In: *Soviet Physics Uspekhi* 11.3 (1968), p. 345. DOI: 10.1070/PU1968v011n03ABEH003840. URL: http://stacks.iop.org/0038-5670/11/i=3/a=A11.

[Sou86] P. C. Souers. *Hydrogen properties for fusion research*. Univ. of California Press, Berkeley-Los Angeles-London, 1986.

[Ste+86] A. Steyerl et al. "A new source of cold and ultracold neutrons". In: *Physics Letters A* 116.7 (1986), pp. 347–352. ISSN: 0375-9601. DOI: 10.1016/0375-9601(86)90587-6.

[Str09] Giorgio Strano. "Galileo's telescope: history, scientific analysis, and replicated observations". In: *Experimental Astronomy* 25.1 (Aug. 1, 2009), pp. 17–31. ISSN: 1572-9508. DOI: 10.1007/s10686-009-9142-0. URL: https://doi.org/10.1007/s10686-009-9142-0 (visited on 07/29/2024).

[Tan23] Wanpeng Tan. "Neutron Lifetime Anomaly and Mirror Matter Theory". In: *Universe* 9.4 (Apr. 2023), p. 180. ISSN: 2218-1997. DOI: 10.3390/universe9040180. URL: https://www.mdpi.com/2218-1997/9/4/180 (visited on 04/22/2024).

[UCN+21] UCNtau Collaboration et al. "Improved Neutron Lifetime Measurement with UCNtau". In: *Physical Review Letters* 127.16 (Oct. 13, 2021), p. 162501. DOI: 10.1103/PhysRevLett.127.162501. URL: https://link.aps.org/doi/10.1103/PhysRevLett.127.162501 (visited on 01/17/2024).

[VD09] Guido Van Rossum and Fred L. Drake. *Python 3 Reference Manual*. Scotts Valley, CA: CreateSpace, Feb. 2009. 242 pp. ISBN: 978-1-4414-1269-0.

[Wan+15] Zhehui Wang et al. "A multilayer surface detector for ultracold neutrons". In: *Nuclear Instruments and Methods in Physics Research Section A: Accelerators, Spectrometers, Detectors and Associated Equipment* 798 (2015), pp. 30–35. ISSN: 0168-9002. DOI: http://dx.doi.org/10.1016/j.nima.2015.07.010.

[Wan+19] Xiangzun Wang et al. "Design of the magnet system of the neutron decay facility PERC". In: *EPJ Web of Conferences* 219 (2019). Publisher: EDP Sciences, p. 04007. ISSN: 2100-014X. DOI: 10.1051/epjconf/201921904007. URL: https://www.epj-conferences.org/articles/epjconf/abs/2019/24/epjconf-ppns2019_04007/epjconf-ppns2019_04007.html (visited on 07/25/2024).

[WH06] M. Wohlmuther and G. Heidenreich. "The spallation target of the ultra-cold neutron source UCN at PSI". In: *Nuclear Instruments and Methods A* 564 (2006), p. 51.

[Won+23] D. K. -T. Wong et al. "Characterization of the new Ultracold Neutron beamline at the LANL UCN facility". In: *Nuclear Instruments and Methods in Physics Research Section A: Accelerators, Spectrometers, Detectors and Associated Equipment* 1050 (May 1, 2023), p. 168105. ISSN: 0168-9002. DOI: 10.1016/j.nima.2023.168105. URL: https://www.sciencedirect.com/science/article/pii/S0168900223000955 (visited on 07/28/2024).

[Yaz20] Noah Yazdandoost. "Deuterated polymer coatings for experiments with ultracold neutrons". Master's Thesis. Mainz: Johannes Gutenberg-Universität Mainz, Apr. 2020.

[YK64] J. A. Young and J. U. Koppel. "Slow neutron scattering by molecular hydrogen and deuterium". In: *Phys. Rev.* 135 (1964). Publisher: American Physical Society, A603–A611.

[Yue+13] A. T. Yue et al. “Improved Determination of the Neutron Lifetime”. In: *Physical Review Letters* 111.22 (Nov. 27, 2013). Publisher: American Physical Society, p. 222501. DOI: 10.1103/PhysRevLett.111.222501. URL: https://link.aps.org/doi/10.1103/PhysRevLett.111.222501 (visited on 07/22/2024).

[Zel59] Zel’dovich, Z. B. “Storage of Cold Neutrons”. In: *Sov. Phys. JETP* 9 (1959), p. 1389. URL: http://www.jetp.ac.ru/cgi-bin/e/index/e/9/6/p1389?a=list.

[ZPI11] O. Zimmer, F.M. Piegsa, and S.N. Ivanov. “Superthermal Source of Ultracold Neutrons for Fundamental Physics Experiments”. In: *Phys. Rev. Lett.* 107.13 (Sept. 2011). Publisher: American Physical Society, p. 134801. DOI: 10.1103/PhysRevLett.107.134801.